university of groningen

University Medical Center Groningen

University of Groningen

How light intensity and colour impact nonvisual functions in humans

Woelders, Tom

IMPORTANT NOTE: You are advised to consult the publisher's version (publisher's PDF) if you wish to cite from it. Please check the document version below.

Document Version
Publisher's PDF, also known as Version of record

Publication date:
2018

Link to publication in University of Groningen/UMCG research database

Citation for published version (APA):
Woelders, T. (2018). *How light intensity and colour impact nonvisual functions in humans: Effects of light on entrainment, sleep and pupil constriction*. University of Groningen.

Copyright
Other than for strictly personal use, it is not permitted to download or to forward/distribute the text or part of it without the consent of the author(s) and/or copyright holder(s), unless the work is under an open content license (like Creative Commons).

The publication may also be distributed here under the terms of Article 25fa of the Dutch Copyright Act, indicated by the "Taverne" license. More information can be found on the University of Groningen website: https://www.rug.nl/library/open-access/self-archiving-pure/taverne-amendment.

Take-down policy
If you believe that this document breaches copyright please contact us providing details, and we will remove access to the work immediately and investigate your claim.

Downloaded from the University of Groningen/UMCG research database (Pure): http://www.rug.nl/research/portal. For technical reasons the number of authors shown on this cover page is limited to 10 maximum.

Download date: 05-05-2023

How light intensity and colour impact nonvisual functions in humans

Effects of light on entrainment, sleep and pupil constriction

Tom Woelders

How light intensity and colour impact nonvisual functions in humans. Effects of light on entrainment, sleep and pupil constriction. Woelders, T., November 2018.

PhD thesis, University of Groningen, The Netherlands.

The work presented in this thesis was conducted at the Department of Neurobiology, Groningen Institute for Evolutionary Life Sciences, University of Groningen, The Netherlands.

This work was founded by the Technology foundation STW Grant 10.13039/501100003958 (project 12187).

ISBN (print): 978-94-034-1119-4
ISBN (online): 978-94-034-1118-7

Cover & Layout: Iliana Boshoven-Gkini, www.AgileColor.com
Printing by: Ridderprint BV, www.ridderprint.nl

Copyright © by Tom Woelders

All rights reserved. No part of this thesis may be reproduced or transmitted in any form or by any means without prior permission of the author.

university of groningen

How light intensity and colour impact nonvisual functions in humans

Effects of light on entrainment, sleep and pupil constriction

PhD thesis

to obtain the degree of PhD at the
University of Groningen
on the authority of the
Rector Magnificus Prof. E. Sterken
and in accordance with
the decision by the College of Deans.

This thesis will be defended in public on
Friday 23 November 2018 at 16.15 hours

by

Tom Woelders

born on 3 May 1986
in Enschede

Supervisors
Prof. R.A. Hut
Prof. D.G.M. Beersma

Co-supervisors
Dr. M.C.M. Gordijn
Dr. E.J. Wams

Assessment committee
Prof. N.M. Jansonius
Prof. R.J. Lucas
Prof. E.J.W. van Someren

Dit proefschrift is geschreven in dankbare herinnering aan mijn lieve moeder,
Margriet Woelders-Eman

Table of contents

Chapter 1

General introduction

Tom Woelders

This thesis is inspired by my belief that there is a prominent role reserved for biological sciences to understand the impact of human-induced environmental changes, and at the same time to provide society with possible strategies in coping with any health-related effects that may consequently emerge. The access to light at any time of day, with artificial light replacing the absence of light during solar darkness, is considered an influential and biologically relevant by-product of industrialisation for nature, including humans. Indeed, we have moved away from a situation where our light-dark cycle is solely determined by the forces of nature, as we are capable of constructing our light environment ourselves. Over the past decades, it has become clear that light fulfils many more biological purposes than solely allowing us to consciously perceive our surroundings through vision. Light affects a number of other biological functions, such as alertness[1–6], hormone secretion[7,8], and our biological clocks[9–11]. Some of these functions are severely affected by the introduction of artificial light into society, with accumulating evidence that our wellbeing and health may suffer as well[12]. My contribution to society and science that I hope to achieve with the work I present in this thesis is therefore to improve our understanding of the nonvisual effects of light in humans, with an emphasis on our biological clocks.

Biological clocks

Many biological functions have evolved to anticipate predictable environmental changes. A good example is provided by Pavlov's conditioning experiments in which he elegantly showed how the body prepares its digestive system for feeding behaviour whenever environmental stimuli indicate that food will soon become available. For other biological functions, it is more beneficial to adopt a less stimulus-driven approach, to help the body anticipate events that typically occur at a certain time of day without directly requiring external stimuli, such as for example the event of waking up. Such clock function is beneficial for any species, because the body can be efficiently prepared for activity before actually waking up. Also, the time we wake up can be consistently timed to coincide with our preferred temporal niche of activity: daytime. Such time-oriented organisation and anticipatory behaviour requires an internal time reference, for which an internal oscillator is a perfect tool that can act as a clock. Not only does an internal clock allow for proper timing of behaviour with respect to recurrent changes in our environment such as temperature or light availability, but also for optimal timing of rhythmic bodily functions with respect to one another. This allows for an efficient distribution of energy among bodily functions whenever the time is right to adopt a physiological state that is required for a certain type of behaviour. For humans, it would for example be a waste of energy to maintain our digestive system in an active state during the night where we typically do not eat, or to sustain an elevated blood flow irrespective of our typical temporal niche of activity. Indeed, the biological clock is now known to regulate these processes with a 24h rhythm through specific influences on the autonomic nervous system[13].

Over the course of the 20th century, many scientists have pioneered elucidating the presence of biological clocks that fulfil exactly this function of an internal time reference. Biological clocks are now known to be conserved over a wide range of species including plants, bacteria and mammals[14]. In mammalian species, such as ourselves, the main anatomical substrate of the biological clock is a network of cells comprising the suprachiasmatic nucleus (SCN) of the hypothalamus. These cells display a rhythmic activity pattern of approximately 24 hours (i.e. circadian), and orchestrate the timing of many rhythmic downstream peripheral processes[15]. The optimal time to sleep, for example, is indicated by our circadian clocks[16], at least partially via interactions with the sleep-promoting neurons in the ventrolateral preoptic nucleus (VPLO)[17]. In humans, several parameters that are mainly under direct circadian clock control, such as the core-body temperature (CBT) rhythm or the rhythmic secretion of the hormone melatonin, are widely used as proxies of the internal time as indicated by our body clocks[18], which is also known as our internal circadian time.

How light affects biological clocks

Virtually all biological clocks in the animal kingdom respond to light. The importance of having a biological clock that is sensitive to light is perhaps best demonstrated by drawing the analogy with mechanical clocks that are incorporated in our everyday lives. These clocks are of course designed to fulfil two purposes: 1) to synchronise our society and 2) to provide an indication of time that bears relationship with environmental changes as a consequence of a rotating earth (e.g. the light-dark cycle). Our mechanical clocks, however, rarely cycle with a period of exactly 24 hours; some may be slightly faster whereas others may be slower, depending on the exact machinery and imperfections of the individual clockworks. The two purposes that clocks are supposed to serve can therefore only be fulfilled when we manually reset our mechanical clocks from time to time to keep them synchronized with the rotation of the earth and the consequential light-dark cycle. If we would not do this, our mechanical clocks would gradually desynchronise, both with respect to one another and with respect to the solar light-dark cycle. It would be impractical when my 9 AM would be different than that of my professor, or when noon would occur during day time in one week, and during night time a few weeks later. Thus, although we use mechanical clocks to time our daily schedules, it is crucial that all clocks are synchronised to a common reference, in our case the 24-hours axial rotation of our planet.

Our biological clocks can be regarded as the biological equivalent of the mechanical clocks humans have designed, with the same flaws and purposes. Just like mechanical clocks, biological clocks rarely cycle with an intrinsic period of exactly 24 hours when isolated from environmental influences. To function as a reliable time reference, a stable phase relationship between the biological clock rhythm and a biologically relevant rhythm that serves as a reliable time reference is required. The most reliable and predictable indication of time ("*Zeitgeber*") for biological clocks is the light-dark cycle. Biological

clocks have evolved a phase-locking mechanism of its rhythmic activity with the recurrent light-dark cycle. In the field of chronobiology, this process is called entrainment; a phenomenon first experimentally demonstrated by Christian Huygens, describing how two oscillators with different cycling periods automatically assume a common period when a strong enough coupling exists between them (at the time described as 'odd sympathy')[19]. In other words, entrainment allows biological clocks to adopt the 24-hour rhythmicity of the solar light-dark cycle, instead of following the period that is dictated by their intrinsic machinery which may deviate from 24 hours. The mammalian biological clock is sensitive to light through retinal input[20], which ensures a coupling between the solar light-dark cycle and the biological clock.

Light exposure affects the cycling rate of the clock in a circadian phase-dependent manner[10]. This relationship between the timing of light exposure and the response of the biological clock can be illustrated by creating a phase response curve (PRC), which shows how the phase shifting effect of light on the clock depends on the circadian time at which light is perceived. For example, it can be appreciated from the human PRC in Figure 1 that when a pulse of light is perceived 3 hours before or after the occurrence of the CBT minimum, that same CBT minimum is approximately delayed by 3 or advanced by 2 hours respectively the following day.

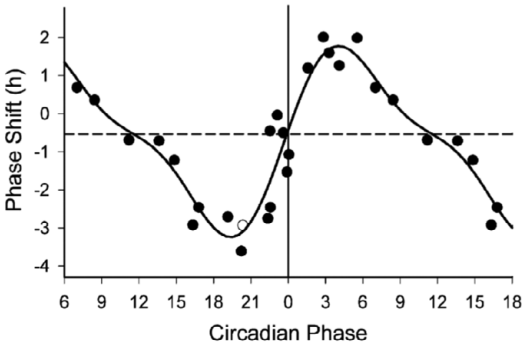

Figure 1. Human phase response curve from Khalsa and colleagues (2003)[10]. Phase-shifts of the human circadian system are plotted as a function of the midpoint of a 6-hour light pulse of 9500 lux, relative to the occurrence of CBT_{min} (phase 0). Negative and positive values indicate phase-delays and phase-advances respectively.

In humans, CBT minimum occurs approximately 2-3 hours before sleep offset, such that light in the evening (~12 to 0 hours before CBT_{min}) temporarily decelerates the clock and light in the morning (~0 to 12 hours after CBT_{min}) temporarily accelerates it[10]. In nature, humans are not exposed to pulses of light, but experience a light intensity profile over the course of the day, where light continuously affects the cycling rate of the circadian clock[21]. The process of entrainment ensures that the phase of the circadian cycle automatically adjusts itself relative to the solar cycle. This phase adjustment continues until the integrated advancing and delaying effects of light over the course of a day make

up for the difference that exists between the 24-hour light-dark cycle and the intrinsic period of an individual's circadian clock (τ)[22]. When this relationship holds, the biological clock is said to be stably entrained to the light-dark cycle, where the phase difference between these two oscillations is known as the phase angle of entrainment. With an average intrinsic period of 24.2 hours[9], the circadian clock of the average human being therefore reaches a stable phase of entrainment when the integrated net effect of light exposure over a day results on average in an acceleration of 0.2 hours. When for any reason, the biological clock is a little slower than 24.2 hours on one day, that portion of the circadian cycle where light normally elicits delays is postponed into solar darkness. As part of the delay zone then becomes shielded from light exposure, the result is a relative advance as compared to the days before. Additionally, the slower clock will automatically postpone the advance portion of the PRC from the end of the night into the morning light, which will complementarily lead to an acceleration of the clock. By these effects, the rhythm of the circadian clock shifts back towards its stably entrained phase. This process leads to stable entrainment over days and biological clocks have thus evolved to use sunlight as an external time reference where, in chronobiological terms, sunlight has been the most influential '*Zeitgeber*' for life on earth over the course of evolution. By its phase-dependent light sensitivity, our clocks are thus buffered against small day-to-day deviations in their cycling rate, ensuring a stable phase relationship between the light-dark cycle and the biological clock rhythm. Where we used to adjust our mechanical clocks manually to achieve a stable phase relationship with the solar light-dark cycle, evolution has found an elegant way of light integration to synchronise biological clocks with the axial rotation of the earth.

Individual clock differences: the phase-period rule of entrainment

Just like mechanical clocks, our biological clock may display quite different characteristics, not in the last place due to individual differences in the intrinsic cycling period (τ) of our circadian clocks. As explained previously, our clocks adjust their phase relative to the light-dark cycle to ensure that the effect of light makes up for the difference that exists between the 24-hour light-dark cycle and τ. The result is that an individual with a very slow (e.g. 24.5 hours) clock entrains at a relatively late phase where the majority of the delaying clock phase is postponed into the dark phase, and the accelerating phase occurs in the beginning of the light phase. On the other side of the spectrum, individuals with fast clocks expose a significant portion of the delaying phase to light and the advance portion of their PRC to darkness; a condition that is met when the clock has an early phase of entrainment relative to the light-dark cycle. More specifically, phase of entrainment is defined as the time difference between a phase marker of the circadian rhythm (e.g. the onset of melatonin secretion in dim-light conditions; DLMO, or CBT minimum) and a phase-marker of the light-dark cycle (e.g. lights off). The relation between phase angle of entrainment and internal circadian period (τ), depends on the (local) slope and time integration properties of the PRC. In healthy humans, a one-hour difference in τ has been

shown to be related to a four-hour difference in phase of entrainment[23]. In individuals with a τ of 23.5 or 24.5 hours, DLMO occurs approximately five hours or one hour before lights off respectively[23]. The time between DLMO and the onset of darkness thus depends on the τ of an individual.

The impact of electrical light on circadian organisation

For simplicity, I assumed up to this point that the far majority of light we are exposed to on a daily basis originates from the sun. It is clear that in modern-day society this has dramatically changed. Humans typically expose themselves to artificial light in the evening hours to be able to see. This involves ordinary room light, but also light emitted from our electronic devices. Our biological clocks, unfortunately, do not discriminate between electrical light or daylight, and as a consequence, our circadian organisation is influenced by artificial light on a daily basis. At the same time, we often sleep with closed curtains, effectively shifting our light-dark cycle to a later phase with respect to the solar light-dark cycle. Although we expose ourselves to light in the evening, our constructed delayed light-dark cycle still follows a period of 24 hours because we like to be active during the day, and our employers typically expect from us that we show up at work at an agreed-upon time. The phase angle of entrainment that allows our clock cycle to retain a 24-hour period under these constructed light-dark cycles, is however different from when our species was solely exposed to daylight[24,25]. Because we delay our light-dark cycle, our clocks accommodate this by delaying their phase as well, resulting in a human phase of entrainment in modern-day society that is much later than it was under pre-industrialized conditions, with a much wider distribution[26]. Problems occur when the clock cycle becomes so late, relative to the solar cycle, that the resulting phase of entrainment interferes with societal demands. Where humans consistently woke up close to dawn when their circadian systems were mainly affected by daylight[25], many humans are now forced to wake themselves up in the morning with alarm clocks, at circadian times where the clock is still promoting sleep. The consequence is thus not per se that our clocks are not entrained, as they may very well be even under modern-day conditions (although see[27], who show that individuals with slow clocks may have difficulty entraining when exposed to too much evening light), but that we are delaying its phase, resulting in overruling its sleep-promoting signals in the evening and as a result subsequently also in the morning. Particularly those individuals that feel the most sleep deprived during week days and find themselves sleeping in during the weekends, spend a substantial part of their lives being awake when their circadian clocks are still promoting sleep. As displaying an activity pattern that conflicts with our biological clock rhythm is so reminiscent of constantly living with a jetlag, it is not surprising that this phenomenon is widely known as ‘social jetlag’ in the field of chronobiology[28]. A chronic phenotype of social jetlag has now been related to numerous health and performance issues, including depression[29], the tendency to smoke[28], increased body-mass index[30], cardiovascular risk factors[31] and decreased academic performance[32].

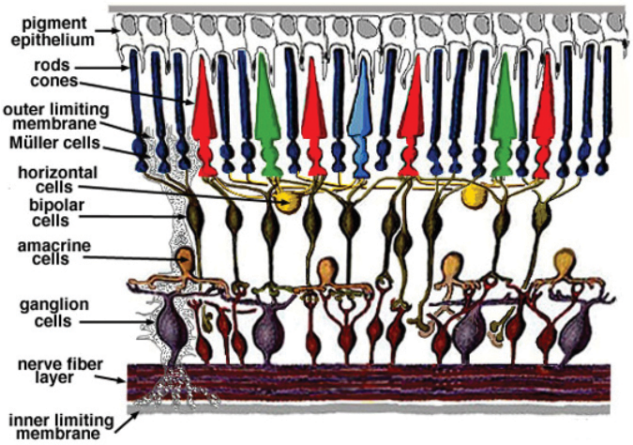

Figure 2. Schematic overview of the human retina from Kolb (1995)[34]. Light enters the eye from below (through the inner limiting membrane) and passes a number of neuronal layers before the light reaches the photoreceptor layer containing rods and cones. Rods and cones indirectly signal to the ganglion cells via rod and cone bipolar cells. The ganglion cells finally relay light information to the brain.

How light information is processed in the (primate) retina

When we, as scientists, want to fulfil our role in society in suggesting means of coping with these light-induced problems, a clear understanding on how our eyes process light information is crucial. After all, a vast amount of light information processing occurs already in the retina, whether we are considering visual or nonvisual functions. A thorough understanding of our retinal organisation may potentially be exploited to minimise unwanted nonvisual effects of light, or to design lighting conditions that are tuned to be optimal for an individual's preferred behaviour (e.g. shift-workers, frequent travellers experiencing jet lag or individuals with sleep problems). As much of my work focusses on light processing in the retina, a brief description of our current knowledge on retinal organisation with respect to both visual and nonvisual functions is warranted (see[33] for a complete overview of mammalian visual and nonvisual photoreception). A schematic overview of the human retina is provided in Figure 2.

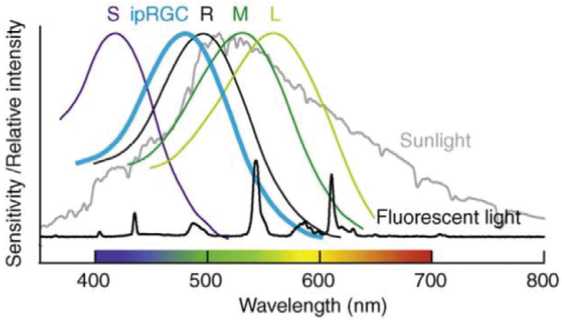

Figure 3. Overview of spectral sensitivities of primate photoreceptors plotted relative to their peak sensitivity, overlaid with representative light spectra for sunlight and a fluorescent light source, from Panda & Hatori (2010)[38].

Photoreceptors. The processing of light in the retina starts with light-sensitive cells known as photoreceptors. Humans express at least five distinct types of photoreceptors: rods, short-, middle- and long-wavelength sensitive cones and intrinsically photosensitive retinal ganglion cells (ipRGCs). What these cells have in common, is the expression of opsin proteins that undergo a conformational change with the absorption of a photon, eventually leading to hyper- (rods and cones) or depolarization (ipRGCs) of the photoreceptor membrane. Different photoreceptor types are maximally sensitive to different parts of the visual light spectrum, depending on the spectral sensitivity of the opsins that are expressed in the receptor cells. Rods express the rod opsin, which has its peak spectral sensitivity at ~500 nm[35]. The S-, M- and L-cones express cyanolabe, chlorolabe and erythrolabe cone opsins respectively, which peak approximately at ~420, ~530 and ~560 nm[36]. The light-induced response of ipRGC cells is mediated by the melanopsin photopigment, with maximal spectral sensitivity at ~480 nm[37]. Photoreceptors become less sensitive at wavelengths that deviate from the wavelength of their maximal sensitivity, resulting in the spectral sensitivity curves displayed in Figure 3.

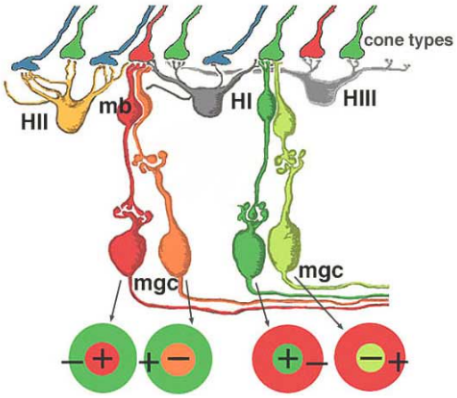

Figure 4. Retinal circuit underlying red-green colour coding in the primate retina, from Kolb (1995)[33]. The red and orange bipolar cells (mb) and ganglion cells (mgc) correspond to ON- and OFF-center circuits respectively, with an L-cone in the center. The dark and light green bipolar and ganglion cells correspond to ON- and OFF-center circuits respectively, with an M-cone in the center. The center-surround organisation of these circuits originates from lateral inhibition of central cones through horizontal cells (HI, HII and HIII). For each of the four circuits, the symbols illustrate whether the center/surround is sensitive to green or red, and whether activation of the center/surround inhibits (-) or excites (+) the ganglion cell. For example, the most left circuit is excited by red light in the center of its receptive field and inhibited by green light in the surround.

Colour-coding in the primate retina. Humans have trichromatic colour vision, meaning that all colours we perceive emerge from a relative comparison of the three photoreceptors that are sensitive to different parts of the visual spectrum: the cones. It is important to note that one photoreceptor is not sufficient to encode colour. For example, for the M-cone, two equally bright light sources of ~510 nm and ~550 nm would

elicit identical responses in the M-cone due to the bell shape of the M-cone spectral sensitivity curve with its peak at 530 nm. The M-cone response to the two stimuli would thus be identical. Similarly, a ~530 nm light source and a ~560 nm light source will elicit the same response in the M-cone when the latter is twice as bright as the former. One photoreceptor can therefore never tell whether a decreased activation is due to the stimulus being less bright, or the stimulus being further away from its peak spectral sensitivity wavelength. The reason we are in fact able to discriminate these wavelengths through their apparent colour is because our eyes compare the relative activation of the M- and L-cones to obtain an indication of colour on a red-green scale. In addition, our eyes compare the S-cone activation to the summed activation of (L+M) cones to obtain an indication of colour on a blue-yellow scale. Thus, the human retina extracts two principal components from any light spectrum, which can together account for the millions of colours we can discriminate. The first cells in the retina that contain information on the red-green colour scale are the cone-bipolar cells (Figure 2; *mb* in Figure 4). Each cone-bipolar cell is contacted by one cone only (either L or M) which forms the center of its receptive field (i.e. all photoreceptors that can modulate the activity of the bipolar cell). In these bipolar cells, the response mediated by the center cone is always opposed by the response mediated by the surrounding cones through lateral inhibition via horizontal cells. The result is that the receptive field of such a bipolar cell is organised in a center-surround ON-OFF or OFF-ON organisation, depending on whether the bipolar cell excites or inhibits the ganglion cell it signals to. For an ON-OFF bipolar cell with an L-cone at its center and a mixture of L- and M-cones in its surround, a green spot of light covering its entire receptive field results in less activation than a red spot of light, because in the former the inhibitory surround is heavily activated in comparison to the center, whereas in the latter the center receives relatively more activation than the surround. The ganglion cells that are contacted by these bipolar cells then relay this red-green colour information to the brain. For an excellent review on the pathways involved in primate red-green colour-coding, I refer to Kolb (1995)[39].

The retinal circuits involved in blue-yellow colour coding[40] are slightly more complex (Figure 5). The OFF-ON bipolar cell has a blue cone at its center which is inhibited by a surrounding mixture of L- and M-cones, much like how bipolar cells in red-green colour coding are organised (Figure 5, top). These bipolar cells thus excite the ganglion cells they project to in response to yellow light in their surround, and inhibit the ganglion cell in response to blue light in their center. These are therefore blue-OFF/yellow-ON bipolar and ganglion cells. Blue-ON/yellow-OFF colour coding is thought to be encoded at the level of the ganglion cell, not at the level of the bipolar cell as was the case in the circuitries discussed so far (Figure 5, bottom). These ganglion cells receive input from an ON-OFF blue/yellow bipolar, but also from an OFF-ON yellow-yellow bipolar. Because the first one has an OFF-surround and the second one has an ON-surround, the (yellow-sensitive) surrounds cancel out and what is relayed by the ganglion cell is the remaining ON-OFF blue/yellow signal originating from the centers of these bipolar cells (hence the center-surround organisation present in the two bipolar cells is lost at the level of the ganglion cell).

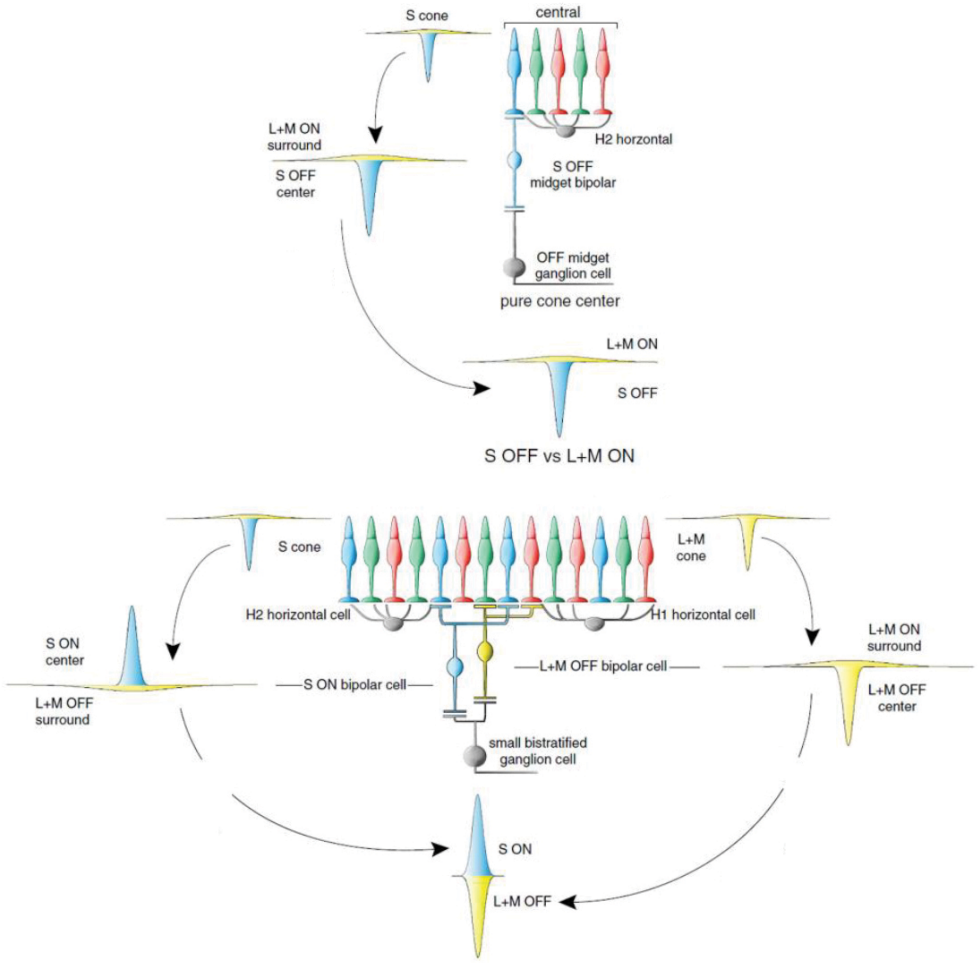

Figure 5. Retinal circuits thought to underly blue-yellow colour-coding in the primate retina, from Dacey and colleagues (2014)[40].

Achromatic contrast coding in the primate retina. The bipolar cells involved in the red-green and the S-OFF circuitries are part of the midget bipolar cell family, which are all contacted by one cone only that forms the center of their receptive fields. Another class of bipolar cells, the diffuse bipolar cells, are contacted by multiple cones (such as the L+M bipolar in the S-ON pathway)[41] and their centers are mediated by multiple cones. Diffuse bipolar cells do have a center-surround organisation, but because both the center and the surround are regulated by a mixture of M- and L-cones, these cells are not colour-sensitive but encode only local contrast in light intensity (luminance). A white light spot presented at its receptive field center (with darkness on its surround) will evoke a large response in a diffuse bipolar, while a uniform stimulation of both its surround and center will not result in a response due to cancellation between center and surround. The diffuse

bipolar cells send information to parasol ganglion cells, which convey information on luminance contrast to the brain[42].

Intrinsically photosensitive retinal ganglion cells. The circuits discussed so far all require input from the outer retina, where the rod and cone photoreceptors are expressed. There is, however, one distinct class of retinal ganglion cells that is light-sensitive[37] even in the absence of functional rods and cones[43], via the expression of the melanopsin photopigment[44,45]. This cell is of particular interest for the nonvisual effects of light, such as photoentrainment and the pupillary light response; genetic ablation of these cells severely disrupts these nonvisual light responses in mice[46]. Although there may be many subtypes of intrinsically photosensitive retinal ganglion cells, my main focus will be on the M1-subtype which is the main mediator of these two nonvisual light responses and is most relevant in the context of circadian photoentrainment[47]. IpRGCs are thought to be mainly involved in the encoding of absolute light levels (i.e. irradiance), and are capable of linearly encoding irradiance levels in the intact retina over a wide range of intensities (>6 log units)[48]. The dendrites of ipRGCs span large areas across the retina in comparison to the dendrites of midget or parasol ganglion cells[49], suggesting that ipRGC cells are relatively insensitive to local contrast and not particularly useful in encoding detailed visual information, but are perfectly suited to sample levels of irradiance over a wide surface of the retina. This is a feature that is of particular interest for a nonvisual function such as the pupillary light-response, which mediates (and should be responsive to) the overall illumination at the surface of the entire retina. Similarly, such irradiance-coding could provide SCN cells with a sinusoid-like entraining signal, corresponding to time of day. In the mouse retina, ipRGCs have been shown to receive synaptic input from mainly ON-center bipolar cells[50,51]. This bipolar input suggests these cells are in addition to their intrinsic melanopsin response sensitive to colour, which has indeed been demonstrated in mice[52] and, using electrophysiological measurements of ipRGC responses to colour modulations, also in the primate (macacque) retina[49]. In the primate retina, ipRGCs are excited by yellow light (demonstrated via L+M-cone selective increments), whereas blue light inhibits the activation of these cells (demonstrated via S-cone selective modulation)[49]. It might be that these ipRGCs therefore receive input exclusively from S-OFF bipolar cells with an (L+M)-ON surround. However, such an organisation would be accompanied by a center-surround organisation, which appears to be absent in these colour-sensitive ipRGCs[40]. One explanation for this absence may be that these cells receive input from multiple S-OFF bipolar cells. This may then cause overlapping receptive fields of all bipolar cells projecting to one ipRGC, blurring the center-surround organisation in the bipolar cells at the level of the ipRGC itself. Another explanation for the loss of center-surround organization in ipRGCs may be that ipRGCs encode colour on a blue-yellow axis in a similar way as the S-ON/(L+M)-OFF pathway presented in Figure 5. These cells lack a center-surround organization due to the cancellation of inhibitory (S-ON bipolar cell) and excitatory (diffuse bipolar cell) surrounds that are both sensitive to yellow. IpRGCs may for example receive input from

S-OFF midget bipolar cells (with yellow ON surround) and yellow-ON diffuse bipolar cells (with yellow OFF surround). Such an organization would lead to cancellation of the yellow surrounds of both bipolars, leaving only the blue-OFF and yellow-ON centers affecting the ipRGC response. Whatever the underlying circuitry mediating yellow-blue colour coding in these cells, it is important to note that Dacey and colleagues[49] have only modulated M- and L-cones in concert, but did not examine whether selective modulation of M- and L-cones affected the electrical response of these ipRGCS. The question thus remains as to whether these ipRGCs also receive input from bipolar cells involved in red-green colour-coding.

Thesis overview

At the level of the individual with an aberrant sleep phase, it is important to provide advice on how light exposure impacts the timing of sleep. For such advice, knowledge on individual clock characteristics may be important. For example, it has recently been suggested that individuals with slow circadian clocks (i.e. individuals with the longest τ) are more influenced by the delaying effects of light in the evening[27]. For these individuals, it may therefore be relatively important to minimize evening light exposure, as compared to individuals with slightly faster circadian clocks. Additionally, and alternatively, these individuals may benefit from any treatment that shortens τ, which is expected to decrease the delaying effects of evening light and to advance the optimal sleep phase. In both rodents and humans, τ has been shown to be affected by light[53,54], and in rodents it has been shown that specific dietary restrictions also impact τ[55]. In order for the scientific community to study how τ is most efficiently altered, tools that allow for the estimation of τ on an individual level may be of primary importance. However, such tools are at present not available, and the estimation of τ on an individual level still requires time-consuming and expensive laboratory protocols. To accommodate for this gap in our knowledge, I analysed individual 1-week light exposure data collected under ambulatory conditions, followed by one circadian phase assessment in the lab. This analysis allowed for the development of a method that may prove useful in estimating τ on an individual level, which is presented in **chapter 2**.

Such methods as described in chapter two rely on the integrity of the model that is used to simulate how a human SCN would respond to light. This model, however, completely lacks a module that accounts for the spectral composition of light; a feature that would make the model more reliable. One fundamental aspect of the human circadian system that therefore requires additional attention is how our circadian system, including the retina, processes light information. The pupillary control system in mammals receives major inputs from ipRGCs, and characterising colour sensitivity of the pupil response may provide important insight into the very first stages of nonvisual photoreception. Therefore, **chapter 3** describes how the pupil responds to selective activation and deactivation of one photoreceptor type only, while keeping a constant activation of the other types. The resulting information could be used to deduce what bipolar cell types

connect to M1 ipRGCs. In addition, predictions are formulated on the spectral sensitivity of the human circadian system, focussing not only on the sensitivity of melanopsin, but also on encoded colour via cones and bipolar cells.

Although not much is known on how human ipRGCs in fact do encode colour, it is of major importance to formulate hypotheses as to why our circadian system should be sensitive to colour modulations in the first place. One functional benefit of circadian colour-coding, at least over the course of evolution, is that cone input may minimize day-to-day variability in our phase of entrainment. In **chapter 4** I aim to provide a testable hypothesis that may prove useful in answering how a circadian system that is solely sensitive to irradiance (i.e. melanopsin activation) may become more stable when colour is concomitantly encoded. This hypothesis is based on an analysis of continuously collected (100 days) solar spectral data from the top of the Bernoulliborg; a 27 meters high academic building located on the Zernike campus of the University of Groningen.

Although the optimal timing of sleep is largely gated by our circadian clocks, the effects of light on sleep may not only work through the circadian system. From rodent studies, it is evident that the mammalian retina projects not only to the SCN, but also to other brain areas including the VLPO and the thalamus[56]. These brain areas are heavily involved in sleep-wake regulation and the generation of slow waves during NREM sleep[17,57]. As such brain areas receive direct input from the retina, it is possible that the sleep homeostat itself may be directly influenced by the light we are exposed to when we are awake. **Chapter 5** therefore describes a field study that was designed to gain knowledge on the relationship between light exposure during the day and the timing and architecture of subsequent sleep.

Thesis summary

The studies that are discussed in this thesis have led to a number of novel findings. In **chapter 2**, we discuss a novel method in estimating the intrinsic period of a human individual, solely by analysing 1 week of ambulatory-collected light exposure data followed by one clock phase assessment in the lab. Such methods are crucial in understanding circadian clocks on an individual level, and may in the future reduce the necessity of extensive laboratory protocols in determining this important characteristic of individual clocks. Such advances may prove useful in individually targeted chronotherapy, and may for example be used to predict how individual clocks respond to any given light exposure pattern.

Our analyses in **chapter 3** suggest that human ipRGCs that mediate pupil constriction (and most likely also circadian photoentrainment) are sensitive to colour. These ipRGCs appear to encode colour on both a red-green and yellow-blue axis, in a red-ON/green-OFF and yellow-ON/blue-OFF manner. Depending on the situation, it is important to have control over the amount of phase-shift a certain light spectrum will elicit. In case of countering jet lag, large shifts may be desired to quickly entrain to the new light-dark cycle, but for recreational use of LED screens such effects should be minimal to prevent

phase-shifting of the clock. Our data suggests that in addition to decreasing the intensity of a light source, changing the colour may provide a degree of flexibility in achieving these goals more efficiently.

As it is becoming clear that human ipRGCs encode colour, there is an increasing need for an explanation or hypothesis as to why such colour-coding would be beneficial for human circadian photoentrainment. In **chapter 4** I show that light intensity and colour together contain more information on solar time than light intensity alone. A combination of both factors is therefore the most stable *Zeitgeber* signal thinkable for a retina that is capable of extracting both intensity and colour information from daylight.

In **chapter 5**, we show that the intensity of light exposure during the day affects not only the timing of sleep, but also sleep architecture and quality itself. Such findings are important and could eventually be incorporated in models describing sleep, to predict not only the timing of sleep but also more qualitative aspects during sleep.

References

1. Van Der Lely, S., Frey, S., Garbazza, C., Wirz-Justice, A., Jenni, O. G., Steiner, R., Wolf, S., Cajochen, C., Bromundt, V. & Schmidt, C. Blue blocker glasses as a countermeasure for alerting effects of evening light-emitting diode screen exposure in male teenagers. *J. Adolesc. Heal.* **56,** 113–119 (2015).
2. Cajochen, C., Frey, S., Anders, D., Spati, J., Bues, M., Pross, A., Mager, R., Wirz-Justice, A. & Stefani, O. Evening exposure to a light-emitting diodes (LED)-backlit computer screen affects circadian physiology and cognitive performance. *J. Appl. Physiol.* **110,** 1432–1438 (2011).
3. Lockley, S. W., Brainard, G. C. & Czeisler, C. A. High Sensitivity of the Human Circadian Melatonin Rhythm to Resetting by Short Wavelength Light. *J. Clin. Endocrinol. Metab.* **88,** 4502–4502 (2003).
4. Najjar, R. P., Wolf, L., Taillard, J., Schlangen, L. J. M., Salam, A., Cajochen, C. & Gronfier, C. Chronic artificial blue-enriched white light is an effective countermeasure to delayed circadian phase and neurobehavioral decrements. *PLoS One* **9,** (2014).
5. Cajochen, C., Zeitzer, J. M., Czeisler, C. A. & Dijk, D.-J. J. Dose-response relationship for light intensity and ocular and electroencephalographic correlates of human alertness. *Behav. Brain Res.* **115,** 75–83 (2000).
6. Cajochen, C. Alerting effects of light. *Sleep Med. Rev.* **11,** 453–464 (2007).
7. Brainard, G. C., Hanifin, J. P., Greeson, J. M., Byrne, B., Glickman, G., Gerner, E. & Rollag, M. D. Action spectrum for melatonin regulation in humans: evidence for a novel circadian photoreceptor. *J. Neurosci.* **21,** 6405–6412 (2001).
8. Jung, C. M., Khalsa, S. B. S., Scheer, F. A. J. L., Cajochen, C., Lockley, S. W., Czeisler, C. A. & Wright, K. P. Acute Effects of Bright Light Exposure on Cortisol Levels. *J. Biol. Rhythms* **25,** 208–216 (2010).
9. Zeitzer, J. M., Dijk, D. J., Kronauer, R. E., Brown, E. N. & Czeisler, C. A. Sensitivity of the human circadian pacemaker to nocturnal light: melatonin phase resetting and suppression. *J. Physiol.* **526,** 695–702 (2000).
10. Khalsa, S. B. S., Jewett, M. E., Cajochen, C. & Czeisler, C. A. A phase response curve to single bright light pulses in human subjects. *J. Physiol.* **549,** 945–952 (2003).
11. Gooley, J. J., Rajaratnam, S. M. W., Brainard, G. C., Kronauer, R. E., Czeisler, C. A. & Lockley, S. W. Spectral Responses of the Human Circadian System Depend on the Irradiance and Duration of Exposure to Light. *Sci. Transl. Med.* **2,** 31ra33-31ra33 (2010).
12. Bonmati-Carrion, M. A., Arguelles-Prieto, R., Martinez-Madrid, M. J., Reiter, R., Hardeland, R., Rol, M. A. & Madrid, J. A. Protecting the melatonin rhythm through circadian healthy light exposure. *Int. J. Mol. Sci.* **15,** 23448–23500 (2014).
13. Kalsbeek, A., Perreau-Lenz, S. & Buijs, R. M. A network of (autonomic) clock outputs. *Chronobiol. Int.* **23,** 521–35 (2006).
14. Bhadra, U., Thakkar, N., Das, P. & Pal Bhadra, M. Evolution of circadian rhythms: from bacteria to human. *Sleep Med.* **35,** 49–61 (2017).
15. Hastings, M. H., Reddy, A. B. & Maywood, E. S. A clockwork web: circadian timing in brain and periphery, in health and disease. *Nat. Rev. Neurosci.* **4,** 649–661 (2003).
16. Daan, S., Beersma, D. G. M. & Borbély, A. A. Timing of human sleep: recovery process gated by a circadian pacemaker. *Am. J. Physiol.* **246,** R161–R183 (1984).
17. Saper, C. B., Scammell, T. E. & Lu, J. Hypothalamic regulation of sleep and circadian rhythms. *Nature* **437,** 1257–1263 (2005).
18. Benloucif, S., Guico, M. J., Reid, K. J., Wolfe, L. F., L'hermite-Balériaux, M. & Zee, P. C. Stability of melatonin and temperature as circadian phase markers and their relation to sleep times in humans. *J. Biol. Rhythm. Rhythm.* **20,** 178–188 (2005).

19. Huygens, C. Correspondance. in *Oeuvres complètes de Christiaan Huygens vol. V* 1664–1665 (La Societe Hollandaise des Sciences, 1893).
20. Hattar, S., Liao, H.-W. W., Takao, M., Berson, D. M. & Yau, K. W.-W. Melanopsin-containing retinal ganglion cells: architecture, projections, and intrinsic photosensitivity. *Science* **295,** 1065–1070 (2002).
21. Jewett, M., Rimmer, D., Duffy, J., Klerman, E., Kronauer, R. & Czeisler, C. Human circadian pacemaker is sensitive to light throughout subjective day without evidence of transients. *Am. J. Physiol.* **273,** R1800–R1809 (1997).
22. Roenneberg, T., Hut, R., Daan, S. & Merrow, M. Entrainment Concepts Revisited. *J. Biol. Rhythms* **25,** 329–339 (2010).
23. Wright Jr, K. P., Gronfier, C., Duffy, J.F., Czeisler, C. A. Intrinsic Period and Light Intensity Determine the Phase Relationship between Melatonin and Sleep in Humans. *J. Biol. Rhythms* **20,** 168–177 (2005).
24. Iglesia, H. O. De, Fernández-duque, E., Golombek, D. A., Lanza, N., Duffy, J. F., Czeisler, C. A. & Valeggia, C. R. Access to Electric Light Is Associated with Shorter Sleep Duration in a Traditionally Hunter-Gatherer Community. **30,** 342–350 (2015).
25. Yetish, G., Kaplan, H., Gurven, M., Wood, B., Pontzer, H., Manger, P. R., Wilson, C., McGregor, R. & Siegel, J. M. Natural Sleep and Its Seasonal Variations in Three Pre-industrial Societies. *Curr. Biol.* **25,** 2862–2868 (2015).
26. Wright, K. P., McHill, A. W., Birks, B. R., Griffin, B. R., Rusterholz, T. & Chinoy, E. D. Entrainment of the Human Circadian Clock to the Natural Light-Dark Cycle. *Curr. Biol.* **23,** 1554–1558 (2013).
27. Skeldon, A. C., Phillips, A. J. K. & Dijk, D.-J. The effects of self-selected light-dark cycles and social constraints on human sleep and circadian timing: a modeling approach. *Sci. Rep.* **7,** 45158 (2017).
28. Wittmann, M., Dinich, J., Merrow, M. & Roenneberg, T. Social jetlag: Misalignment of biological and social time. *Chronobiol. Int.* **23,** 497–509 (2006).
29. Levandovski, R., Dantas, G., Fernandes, L. C., Caumo, W., Torres, I., Roenneberg, T., Hidalgo, M. P. L. & Allebrandt, K. V. Depression Scores Associate With Chronotype and Social Jetlag in a Rural Population. *Chronobiol. Int.* **28,** 771–778 (2011).
30. Roenneberg, T., Allebrandt, K. V., Merrow, M. & Vetter, C. Social jetlag and obesity. *Curr. Biol.* **22,** 939–943 (2012).
31. Kantermann, T., Duboutay, F., Haubruge, D., Kerkhofs, M., Schmidt-Trucksäss, A. & Skene, D. J. Atherosclerotic risk and social jetlag in rotating shift-workers: First evidence from a pilot study. *Work* **46,** 273–282 (2013).
32. Haraszti, R. Á., Ella, K., Gyöngyösi, N., Roenneberg, T. & Káldi, K. Social jetlag negatively correlates with academic performance in undergraduates. *Chronobiol. Int.* **31,** 603–612 (2014).
33. Kolb, H., Fernandez, E. & Nelson, R. *Webvision: The Organization of the Retina and Visual System*. (1995).
34. Kolb, H. *Simple Anatomy of the Retina. Webvision: The Organization of the Retina and Visual System* (1995).
35. Bowmaker, J. K. & Dartnall, H. J. Visual pigments of rods and cones in a human retina. *J. Physiol.* **298,** 501–11 (1980).
36. Stockman, A. & Sharpe, L. T. The spectral sensitivities of the middle- and long-wavelength-sensitive cones derived from measurements in observers of known genotype. *Vision Res.* **40,** 1711–1737 (2000).
37. Berson, D. M., Dunn, F. A. & Takao, M. Phototransduction by retinal ganglion cells that set the circadian clock. *Science* **295,** 1070–3 (2002).
38. Hatori, M. & Panda, S. The emerging roles of melanopsin in behavioral adaptation to light. *Trends Mol. Med.* **16,** 435–446 (2010).
39. Kolb, H. *Midget pathways of the primate retina underlie resolution and red green color opponency. Webvision: The Organization of the Retina and Visual System* (1995).

40. Dacey, D. M., Crook, J. D. & Packer, O. S. Distinct synaptic mechanisms create parallel S-ON and S-OFF color opponent pathways in the primate retina. *Vis. Neurosci.* **31,** 139–151 (2014).
41. Nelson, R. & Connaughton, V. *Bipolar Cell Pathways in the Vertebrate Retina. Webvision: The Organization of the Retina and Visual System* (1995).
42. Marshak, D. W. Retinal Ganglion Cells: Anatomy. in *Encyclopedia of Neuroscience* 211–218 (Elsevier, 2009). doi:10.1016/B978-008045046-9.00897-4
43. Hattar, S., Lucas, R. J., Mrosovsky, N., Thompson, S., Douglas, R. H., Hankins, M. W., Lem, J., Biel, M., Hofmann, F., Foster, R. G. & Yau, K.-W. Melanopsin and rod-cone photoreceptive systems account for all major accessory visual functions in mice. *Nature* **424,** 76–81 (2003).
44. Provencio, I., Jiang, G., de Grip, W. J., Hayes, W. P. & Rollag, M. D. Melanopsin: An opsin in melanophores, brain, and eye. *Proc. Natl. Acad. Sci. U. S. A.* **95,** 340–345 (1998).
45. Provencio, I., Rodriguez, I. R., Jiang, G., Hayes, W. P., Moreira, E. F. & Rollag, M. D. A novel human opsin in the inner retina. *J. Neurosci.* **20,** 600–605 (2000).
46. Güler, A. D. *et al.* Melanopsin cells are the principal conduits for rod-cone input to non-image-forming vision. *Nature* **453,** 102–105 (2008).
47. Schmidt, T. M., Chen, S.-K. & Hattar, S. Intrinsically photosensitive retinal ganglion cells: many subtypes, diverse functions. *Trends Neurosci.* **34,** 572–580 (2011).
48. Wong, K. Y. A retinal ganglion cell that can signal irradiance continuously for 10 hours. *J. Neurosci.* **32,** 11478–11485 (2012).
49. Dacey, D. M., Liao, H.-W., Peterson, B. B., Robinson, F. R., Smith, V. C., Pokorny, J., Yau, K.-W. & Gamlin, P. D. Melanopsin-expressing ganglion cells in primate retina signal colour and irradiance and project to the LGN. *Nature* **433,** 749–754 (2005).
50. Belenky, M. A., Smeraski, C. A., Provencio, I., Sollars, P. J. & Pickard, G. E. Melanopsin retinal ganglion cells receive bipolar and amacrine cell synapses. *J. Comp. Neurol.* **460,** 380–393 (2003).
51. Wong, K. Y., Dunn, F. A., Graham, D. M. & Berson, D. M. Synaptic influences on rat ganglion-cell photoreceptors. *J. Physiol.* **582,** 279–296 (2007).
52. Walmsley, L., Hanna, L., Mouland, J., Martial, F., West, A., Smedley, A. R., Bechtold, D. a., Webb, A. R., Lucas, R. J. & Brown, T. M. Colour As a Signal for Entraining the Mammalian Circadian Clock. *PLOS Biol.* **13,** e1002127 (2015).
53. Pittendrigh, C. S. & Daan, S. A functional analysis of circadian pacemakers in nocturnal rodents I. The stability and lability of spontaneous frequency. *J. Comp. Physiol.* **106,** 223–252 (1976).
54. Scheer, F. A. J. L., Wright, K. P., Kronauer, R. E. & Czeisler, C. A. Plasticity of the intrinsic period of the human circadian timing system. *PLoS One* **2,** (2007).
55. Kohsaka, A., Laposky, A. D., Ramsey, K. M., Estrada, C., Joshu, C., Kobayashi, Y., Turek, F. W. & Bass, J. High-Fat Diet Disrupts Behavioral and Molecular Circadian Rhythms in Mice. *Cell Metab.* **6,** 414–421 (2007).
56. Hattar, S., Kumar, M., Park, A. & Tong, P. Central Projections of Melanopsin-Expressing Retinal Ganglion Cells in the Mouse. **497,** 326–349 (2006).
57. Crunelli, V., David, F., Lorincz, M. L. & Hughes, S. W. The thalamocortical network as a single slow wave-generating unit. *Curr. Opin. Neurobiol.* **31,** 72–80 (2015).

Chapter 2

Daily light exposure patterns reveal phase and period of the human circadian clock

Tom Woelders,
Domien G.M. Beersma,
Marijke C.M. Gordijn,
Roelof A. Hut
and Emma J. Wams

Journal of biological rhythms 32 (3), 274-286

Abstract

Light is the most potent time cue that synchronizes (entrains) the circadian pacemaker to the 24-hour solar cycle. This entrainment process is an interplay between an individual's daily light perception and intrinsic pacemaker period under free-running conditions. Establishing individual estimates of circadian phase and period can be time-consuming. We show that circadian phase can be accurately predicted (SD=1.1h for dim light melatonin onset, DLMO) using 9 days of ambulatory light and activity data as an input to Kronauer's limit-cycle model for the human circadian system. This approach also yields an estimated circadian period of 24.2h (SD=0.2h), with longer periods resulting in later DLMOs. A larger amount of daylight exposure resulted in an earlier DLMO. Individuals with a long circadian period also showed shorter intervals between DLMO and sleep timing. When validated under laboratory studies in a wide variety of individuals, the proposed methods may prove to be essential tools for individualized chronotherapy and light treatment for shift work and jetlag applications. These methods may improve our understanding of fundamental properties of human circadian rhythms under daily living conditions.

Humans possess a circadian pacemaker, located in the suprachiasmatic nucleus of the hypothalamus (SCN), which synchronizes many rhythmic processes such as hormone secretion, skin temperature, heart rate and the sleep-wake cycle (review: Schmidt et al., 2007). Light can phase shift the circadian pacemaker, which allows for synchronization of behavioral and physiological rhythms with the 24-hour solar cycle, a process called entrainment (review: Duffy & Wright Jr., 2005). Humans are unique in their light-exposure patterns due to the fact that this pattern can be altered with self-employed electrical lighting patterns. The individual regulation of light exposure seems to broaden the distribution of phase of entrainment in humans (Wright et al., 2013), as compared to other species. This exceptional broad distribution of entrainment has been related to numerous health problems (review: Bonmati-Carrion et al., 2014) and understanding the complexity of human light entrainment is therefore important.

Assessment of circadian phase typically requires relatively expensive laboratory hormone assessments (dim light melatonin onset; DLMO). To make circadian phase assessment more accessible for researchers and clinicians, less expensive alternatives are needed. Modeling the effect of light on the human circadian system may provide such an alternative as ambulatory (wrist-actigraph) light exposure data can be collected in a low-cost and noninvasive manner, without the need for subjects to change their daily living routines. Furthermore, such approaches may provide knowledge on human circadian organization in real life settings. One mathematical model that has been particularly accurate in modeling the circadian response to light is the limit-cycle oscillator model developed by Kronauer et al. (1990; 1999) with revised versions presented by Jewett et al. (1999) and St. Hilaire et al. (2007). This model describes a light-sensitive circadian pacemaker where the circadian phase of the pacemaker defines its sensitivity to light. Not only can this model be used to replicate phase-response curves reported in literature (e.g. Khalsa et al., 2003), it may also be a valuable tool to evaluate light exposure patterns in human entrainment.

Whether this model can reliably predict circadian phase in the field is unknown, as it was developed, refined and validated using only controlled laboratory studies on amplitude-suppressing and phase-shifting effects of light on the circadian pacemaker (Jewett et al., 1991, 1994; Khalsa et al., 1997; St. Hilaire et al., 2007). Here we will test whether Kronauer's model can be used to estimate circadian phase under daily living conditions by entering individually collected ambulatory light data into the model. By letting Kronauer's model entrain to the light data that were collected for each individual, the entrained phase of each individual (DLMO) can be directly compared to the entrained phase of the model. As intrinsic circadian period length (τ) will not be determined for the participants described here, the default value of 24.2 hours will initially be assumed for the model parameter describing τ. However, it is well known that humans differ considerably in intrinsic period length (Czeisler et al., 1999; Duffy et al., 2011; Hiddinga et al., 1997). This variation in intrinsic period may affect the phase angle of entrainment between the external light-dark cycle (sunlight and/or artificial light) and the entrained circadian rhythm in humans (Duffy et al., 2001; Wright Jr et al., 2005; Gronfier et al., 2007; Eastman et al., 2015; Hasan et al., 2012) as has been observed in other species

(e.g. Pittendrigh & Daan, 1976; Merrow et al., 2006). After determining the amount of variance in circadian phase attributable to ambulatory light exposure, we assumed that τ is the dominant factor in explaining individual differences in the timing of DLMO, and that the remaining unexplained variance will be mainly attributable to individual differences in intrinsic period. Minimizing this unexplained variance through iterative tuning of individual τ, we present the possibility that Kronauer's model can be used as a tool to predict not only circadian phase, but also human intrinsic period.

Methods

Participants included 20 healthy male (n=9) and female (n=11) subjects, aged 20-27 (average 23.2 ± 1.7 (±SD)). Chronotype was assessed via the Munich Chronotype Questionnaire (MCTQ; Roenneberg et al., 2003). A broad distribution of chronotypes was achieved by including only very early (MSF 2.75-3.79), intermediate (MSF 4.63-4.83) and very late chronotypes (MSF 7.04-7.75). The cut-off values used for classification of chronotype groups were determined by analyzing the distribution of chronotypes available in the MCTQ Dutch database (updated from Zavada et al., 2005), containing 4132 individuals within the age range of 20-30 (very early, intermediate and very late types fell within the lowest, middle and highest 10% of this distribution respectively). The dataset contained 8 very early (MSF 3.5 ± 0.3 (Mean ± SD)), 9 intermediate (MSF 4.7 ± 0.1 (Mean ±SD) and 3 very late (MSF 7.3 ± 0.4 (Mean ± SD)) chronotypes.

Exclusion criteria were the presence of moderate sleep disturbances assessed with the Pittsburgh Sleep Quality Index (PSQI; > 9 (average 3.52 ± 1.71; ±SD, 2 individuals scored > 5); Buysse et al., 1989), tendencies for anxiety and/or depression, determined via the Beck Depression Inventory (BDI; > 7; Beck et al., 1996) and Hospital Anxiety and Depression Scale (HADS; > 7; Zigmond & Snaith, 1983) and color-blindness, indicated by the inability of completing an Ishihara color blindness test (Clark, 1924) without errors. All participants completed an in-house developed general health questionnaire, which was assessed to exclude participants from the study when reporting chronic medical conditions or the need for medication use, previous head injury, epilepsy, smoking, excessive use of alcohol or caffeine (> 3 and > 8 consumptions per day, respectively) the use of recreational drugs during the last year, a BMI outside the range of 18-27, a body weight of less than 36 kg or having a history of shift work and/or having travelled across more than one time-zone in the last month prior to the experiment.

From a total of 23 participants enrolled into the study, one dropped out and two participants were excluded from analysis because of malfunctioning of the equipment, leaving a total of 20 participants for analysis.

The study procedures were approved by the Medical Ethical Research Committee of the University Medical Centre Groningen (NL48468.042.14), Netherlands and are in accordance with the Declaration of Helsinki (2013). All participants gave written informed consent.

Study procedures

The procedures described here are part of a 3-week field study protocol in which ambulatory data were collected for the assessment of human biological rhythms in the field. Only the first nine days are relevant for the current study. All measurements were conducted in the Groningen Area (the Netherlands), between November 2014 and January 2016.

Light-intensity and activity were continuously monitored from Friday evening (day 0) until Sunday afternoon (day 9) using actigraph devices (MotionWatch 8™, MW8™, CamNTech. Ltd.), containing an accelerometer and a broadband light sensor. On day 8, a laboratory session was scheduled to assess circadian clock phase under dim light conditions (< 10 lux in the angle of gaze; dim-light melatonin onset; DLMO). Participants entered the lab 9 hours before habitual sleep onset. For each participant, 8 hourly saliva samples were obtained with the last sample scheduled at the time of habitual sleep onset. Participants remained in a posture-controlled position for 15 min preceding saliva sampling. Participants needed to attend the lab for device changes twice during the week for less than 30 minutes each time, at a time of choice that was not restrictive to their sleep-wake schedule. No further interventions were applied during these 9 days of data collection.

Measurements

Data were collected throughout the year, but not within one week after daylight savings time transitions (end of March and end of October). For all data collected under daylight savings time, one hour was subtracted from the time values, such that all time values were expressed as GMT+1 for the time zone of the Netherlands.

Actigraphy. Activity was measured using a MotionWatch 8™ (MW8™, CamNTech. Ltd.), which returns activity counts per one-minute epoch as the cumulative sum of motion, as recorded by a tri-axial accelerometer. The average activity acrophase was estimated by fitting a single sine wave harmonic with a period of 24 hours to the available 9 days of actigraphy data (CircWave, version1.4, Roelof A. Hut, University of Groningen, NL).

Light intensity. Light intensity (in lux) was measured per second and recorded as 1 min averages. The light data that were used for all analyses were the per-minute averages as returned by the MotionWatch 8™. The sensor accurately describes light intensity in the 0 – 64000 lux range, which we validated using a photo spectrometer (SpecBos 1211 LAN UV, JETI Technische Instrumente GmbH). A distribution of light intensities measured for each participant over the course of the 9-day protocol is presented in Figure S2. Furthermore, an estimation of the amount of daylight each participant was exposed to was calculated as the percentage of lux values > 615 for each individual separately. This threshold was chosen as 99% of all light intensities measured during solar darkness did not exceed 615 lux (Figure S3), which means that any values > 615 lux must have been

collected during daytime. For one participant, the device measured 7 hours of aberrant high light intensities. As no concomitant activity was measured during this time window, these deviating lux-values were marked as an artifact and were set to 0 accordingly (analysis was performed with and without this artifact correction, and it was found not to affect the results).

Sleep timing. Sleep timing parameters (onset and offset) were calculated from the activity and light data using Sleep analysis software (version 7, CamNTech Ltd.). Sleep offset was calculated as the time when activity and light intensity showed an increase compared to preceding values, and maintained at that increased level for at least 10 minutes. Sleep onset was calculated as the time when the reverse was true.

Core-body temperature. Participants were asked to swallow a core body temperature (CBT) measuring pill (CorTempTM, HQ Inc.) at the afternoon of day 1 (Saturday) and day 5 (Wednesday). A belt worn receiver at the abdomen collected the data emitted by the pill until it was excreted from the body after 24-32 hours. For each participant, CBT data were smoothed by locally weighted scatterplot smoothing (R function *loess*, after Cleveland et al., 1992), using a 10-h smoothing span. The smoothed data were used to determine CBT minimum (CBT_{min}) for each night.

DLMO assessment. Salivary melatonin was collected using Salivette® (Sarstedt™ Ltd., Germany). Samples were centrifuged and stored overnight at ~4 °C and then stored in a -80 °C freezer. To assess melatonin concentration, a double-antibody radioimmunoassay (RIA; intra-assay variation coefficient of 13.97% and 9.11% for low and high concentration controls respectively, inter-assay variation coefficient of 13.99% and 14.64% for low and high concentration controls respectively) was performed (Bühlmann Direct Saliva Melatonin kit, Bühlmann Laboratories AG, Switzerland) after termination of the study. DLMO was marked as the first time where linear interpolated melatonin concentrations exceeded the 4 pg/ml threshold.

Modeling the circadian response to ambulatory light data

For each participant, 9 days of light data were available (average lux value per minute from Friday evening until the next Sunday afternoon). Light data was cut to start at the time of the first estimated CBT_{min} (estimated as measured DLMO + 7h; based on e.g. Brown et al., 1997; Benloucif et al., 2005) and to end at the Sunday afternoon. As the first estimated CBT_{min} always occurred during the early Saturday morning, the final dataset that was processed by the model consisted of ~8 days of data (from Saturday morning until the Sunday afternoon). As each individual light profile was cut to start at (DLMO – 7), the clock time associated with the onset of each light profile was different for each individual profile. Kronauer's model was implemented in R (R Core Team, 2015; version: 3.2.3), based on the most recent formulas and parameter values described in (St. Hilaire et al., 2007).

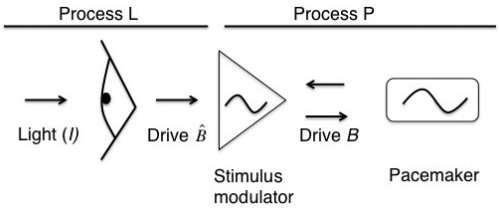

Figure 1. Graphical overview of information flow at each model iteration. On a per-minute basis, Kronauer's model evaluates the effect of light (in lux) on the circadian pacemaker. When light is presented to the model, process L generates a drive , which is influenced both by the current intensity of light and state of adaptation. This drive $\hat{B}$ is then altered by a stimulus modulator, based on the current phase and amplitude of the pacemaker, resulting in a modulated drive *B*. Drive *B* in turn affects the speed and amplitude with which the pacemaker oscillates.

Kronauer's limit cycle oscillator for the human circadian pacemaker. To model individual circadian responses to the ambulatory light data, the revised limit cycle oscillator model of the human circadian pacemaker was implemented, which is explained in detail in Jewett et al. (1999) with minor revisions proposed in St. Hilaire et al. (2007). The model consists of a pacemaker that, in the absence of light, oscillates in a circular fashion (the limit cycle) with a period of 24.2 hours and amplitude normalized to 1. Light has the potential to push the oscillator away from the limit cycle, effectively influencing both the amplitude of the cycle and the speed at which the pacemaker traverses through this cycle. The effect of light on speed and amplitude depend on the phase of the circadian pacemaker, such that light is most efficient in influencing these parameters when the pacemaker phase is close to the CBT_{min}. When light is perceived before the critical phase (close to CBT_{min}), the speed of the pacemaker is slowed down, resulting in a phase-delay. This phase delay gradually changes into a phase advance when light is perceived after the critical phase. Light and dark adaptation is incorporated in the model, such that the efficiency of light to affect the pacemaker gradually decreases during prolonged light exposure, whereas the opposite occurs during prolonged darkness. This adaptation mechanism is modeled by a pool of photosensitive elements in the light-sensitive module that can either be in the "used" (variable n) state or the "ready" (fraction 1 - n) state, which is analogous to the effect of light on retinal photo pigments: the photon-induced conformational change of a photo pigment molecule renders it insensitive to light until it is recycled. A graphical representation of the processes described above is presented in Figure 1. As an example, a simulated phase-delay is presented in Figure 2. A complete overview of the model parameters and formulas are presented in Table S1. No modifications to the core model components were applied. Slight alterations to initial variable values (values that are required to describe the baseline state of the model when the first lux value in a light profile is evaluated) are described below when the ambulatory light data modeling is discussed.

Core-body temperature minimum as a phase marker. As a circadian phase marker, the time of CBT_{min} can be calculated from the relationship between state variables x_c and x (see Figure 2; May et al., 2002; St. Hilaire et al., 2007) such that CBT_{min} equals (time when $atan(x_c, x) = -2.98 + \varphi_{ref}$, where $\varphi_{ref} = 0.97$ hours). Typically, CBT_{min} occurs approximately 1 hour after the occurrence of x_{min}. Although St. Hilaire et al. (2007) provide a method to use predicted melatonin synthesis onset as a phase marker of Kronauer's model, we have decided to use the time of predicted CBT_{min} as the model output. As the time interval between CBT_{min} and DLMO has consistently been reported to approximate 7 hours (e.g. Brown et al., 1997; Benloucif et al., 2005), the time of the model-predicted CBT_{min} is easily converted into a model-predicted DLMO by subtracting 7 hours from predicted CBT_{min}.

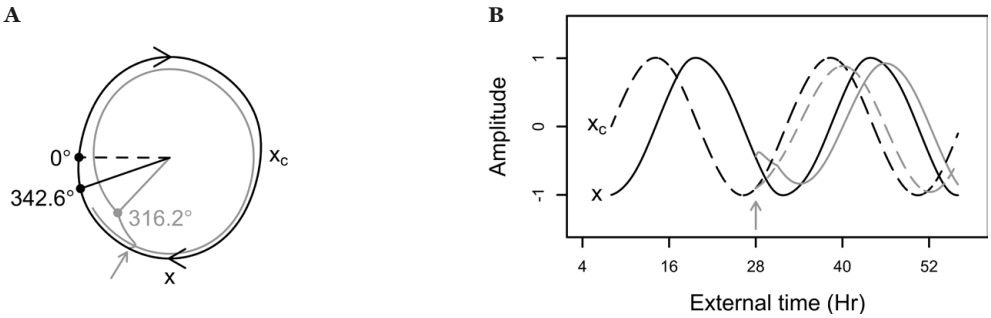

Figure 2. Example of a simulated phase-delay. The Kronauer model responds to a 3-hour 9500-lux light pulse (grey arrow) starting 5 hours before CBT_{min} (midnight in this example) **A)** At baseline, the pacemaker follows the limit-cycle oscillation (black curve). This oscillation is modeled by two coupled variables describing the state of the pacemaker, x and x_c. Variable x closely follows the core body temperature rhythm whereas x_c is a complementary variable that is mathematically required to achieve this oscillation. When the light stimulus is presented, the system is pushed away from the limit cycle (grey curve), leading to a deceleration of the pacemaker. At the end of the light-pulse (3 AM; filled circles connected to solid lines), the pacemaker is delayed as only 316.2° of one oscillation was traversed versus 342.6° in the absence of a light stimulus (0° and dashed line mark x_{min}, which corresponds to predicted CBT_{min} – 0.97h). **B)** Overview of the state variable responses (solid lines: x, dashed lines: x_c) to the same light pulse as in **A**. Compared to no light pulse (black lines), the rate of change in the two state variables (i.e. the speed of the pacemaker) is slowed down in response to light (grey curve), leading to a phase-delay.

Baseline model entrainment. With its phase-dependent sensitivity to light, Kronauer's oscillator has the property to entrain to a given 24-hour light-dark cycle. By letting the model entrain to the same light-dark cycle that each individual is entrained to, the phase of entrainment of Kronauer's oscillator can be directly compared to the measured phase marker (DLMO or CBT_{min}) of each individual. This comparison requires stable entrainment to the same light-dark cycle for both the model and the individual. As only one week of light data was available before the DLMO was measured, it was assumed that this week of light data was representative for the typical light-dark cycle to which each individual was stably entrained. Unlike what was assumed for the participants, the

model is not stably entrained to this one week of light data by default. In fact, the model requires time to stably entrain to any light-dark cycle it is presented with, analogous to recovering from a jetlag. Kronauer's model typically requires multiple baseline weeks to reach stable entrainment, which were here constructed from the light data that were obtained for each individual separately as follows: the first 7 days of the individual 8-days light profiles described earlier were repeated 4 times (i.e. 4 weeks of artificial baseline data), and used as an input for the model to entrain to. When constructing these artificial baseline weeks, day 8 was not included, as this was the semi-constant routine day at which DLMO was assessed and therefore not a representative day of light data. During the processing of each individual's artificial baseline weeks, the model's phase of entrainment gradually shifted towards an asymptote (a gradual day-to-day shift in predicted core-body temperature minimum) which, when reached, indicated that the requirement of stable entrainment was met. Although the time to reach stable entrainment varied between individual baseline profiles, the model was stably entrained after 4 weeks. The entire 8 days of individual light data were then added to the end of this 4-weeks baseline period. This procedure allowed for a direct comparison between the model-predicted DLMO on the last Saturday (day 8 of "week 5") evening (predicted CBT_{min} on the Sunday morning – 7 hours) to the actual DLMO measured on that Saturday evening.

It is important to note that for each individual baseline profile, the model will eventually always reach the same phase angle of (stable) entrainment, regardless of the initial state of the model at the start of the baseline weeks. This is analogous to an SCN that will recover from jetlag reaching stable entrainment to the new time zone, regardless of the initial time zone. Therefore, no a-priori knowledge on the state of the oscillator is required at the start of the baseline procedure. Nevertheless, a value needs to be assigned to each of the variables describing the initial state of the model to start processing the data. For completeness; the initial state variable values (x and x_c) were set to -1.04 and 0.09 respectively, whereas variable n was set to 0.014. This is the state of the model that would occur at predicted CBT_{min}, when simulating stable entrainment to days consisting of 16 hours of wakefulness under 150 lux and 8 hours of sleep under 0 lux (Jewett et al., 1999) at the beginning of the baseline weeks. At the start of week 5, the state of the model was unique for each individual, as it was uniquely entrained to each individual's baseline 4-weeks light profile.

Statistical analyses

Statistical analyses were performed in R (R Core Team, 2015; version: 3.2.3), using the most recent shell of Rstudio (version: 0.99.491). Linear regression models were fitted with the base *lm* function. To test whether individual terms significantly ($\alpha = 0.05$) contributed to the model when multiple explanatory variables were included, the *drop1* function from the *lme4* library (Bates et al., 2012) was implemented. Model selection was based on the Akaike-information criterion (AIC) using a backward step-wise multiple regression approach.

Results

Table 1. Participant demographics

Demographic	Mean ±SD [min. to max.]
Gender	9/11 (M/F)
Age	23.2 ± 1.7 [20.0 to 27.0]
MSF	4.6 ± 1.3 [2.8 to 7.8]
Average sleep onset	24.0 ± 1.2 [21.5 to 26.9]
Average sleep offset	8.0 ± 1.2 [6.3 to 12.5]
Average midpoint of sleep	4.0 ± 1.2 [1.9 to 7.7]
Activity acrophase	15.9 ± 1.5 [13.9 to 19.0]
Average CBT_{min}	3.6 ± 2.1 [1.2 to 9.9]
DLMO	20.5 ± 1.9 [17.0 to 26.3]
Average light intensity (log(lux); lux > 0)	1.3 ± 0.2 [0.7 to 1.6]

For each participant, the final dataset contained ~8 days of activity and light intensity data, at least (depending on metabolic rate) two days of CBT data (day 1 and day 5), one DLMO value (day 8), the cosine-fitted average activity acrophase and the average CBT_{min} clock times of at least 2 nights. As an example, Figure 3 provides the compiled dataset of one participant.

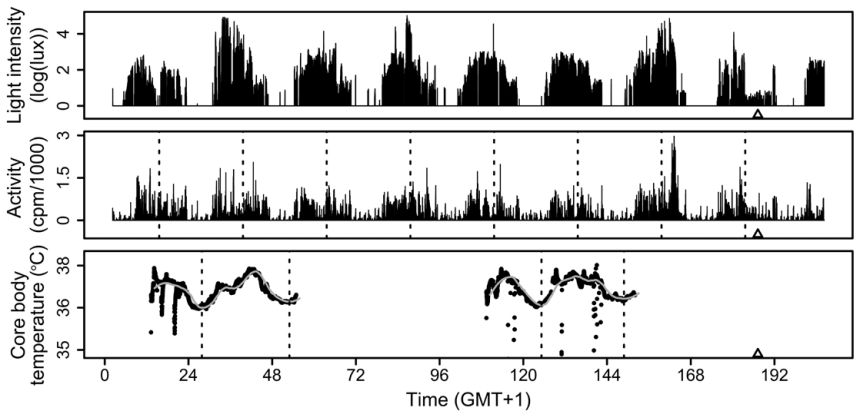

Figure 3. Compiled dataset of participant "BCM15". *Top panel:* 9 days of ambulatory light intensity data, plotted as log(lux; >1 lux), although the actual modeling was performed on the untransformed lux values. *Middle panel:* concomitant ambulatory activity data. Dashed lines mark the estimated time of maximum activity. *Bottom panel:* Core body temperature data collected by two separate CBT-pills. The dashed vertical lines mark CBT_{min} times for days 1, 2, 5 and 6. The grey curve follows the smoothed fit of CBT. denotes measured DLMO in all panels.

Relationship between DLMO and ambulatory CBT_{min}

First we assessed whether core-body temperature minimum (CBT_{min}) can be a reliable estimate of circadian phase in the field. Linear regression analysis revealed a significantly positive relationship between DLMO and CBT_{min} (Figure 4; $F(1,18) = 19.2$; $p < 0.001$). The average difference between DLMO and CBT_{min} was 7.1 ± 1.5 hrs (± SD). As the data points were non-equidistant due to the inclusion of one individual with a relatively late DLMO, the strength of the relationship between DLMO and CBT_{min} was tested by repeating the regression analysis without this individual ($F(1,17) = 3.59$; $p = 0.07$).

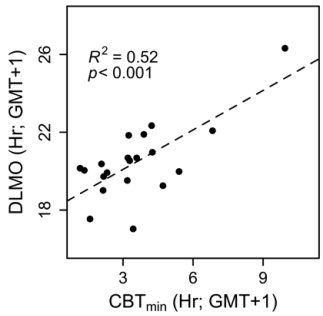

Figure 4. Relationship DLMO and time of core-body temperature minimum. Each data point represents the average of all CBT_{min} times available for each participant.

Predicting DLMO with ambulatory light and actigraphy data

Next, we tested whether modeling ambulatory light data could generate accurate predictions of clock phase. For each participant, the individual 8-days light profile was processed by Kronauer's model, resulting in 8 individual daily predictions of CBT_{min}. From these 8 predicted CBT_{min} values, only those days on which CBT_{min} data were available were used for further analysis, together with the predicted CBT_{min} following the day of DLMO assessment (Figure 5).

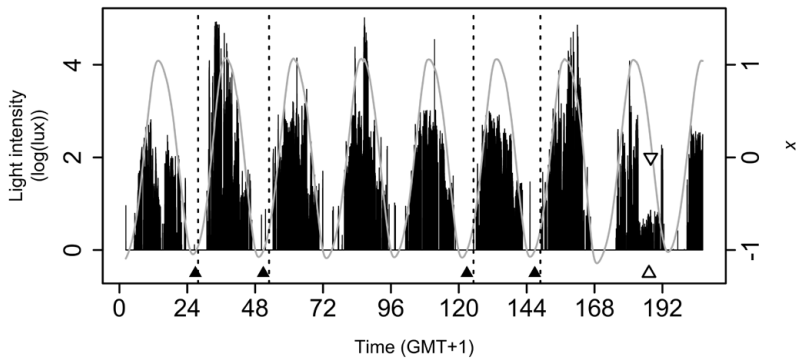

Figure 5. Model predictions for participant "BCM15". Model-predicted CBT_{min} and DLMO ($CBT_{min}{}^{p}$▲, DLMO^{p}▽), DLMO△ and Kronauer's model prediction (variable *x*; grey curve) are plotted together with the relevant light profile. For this individual, DLMO^{p} was at 19:49 whereas measured DLMO was at 19:15. Only intensities higher than 0 log(lux) were included for graphical purposes. The actual modeling involved the raw lux values. The vertical dashed lines mark the measured CBT_{min} times during nights 1, 2, 5 and 6.

Predicted DLMO ($DLMO^p$) was calculated from the predicted CBT_{min} following the DLMO assessment day. For this calculation, a phase difference of 7 hours was assumed between DLMO and CBT_{min}, which is in line with the phase difference of 7.1 hours reported here and the phase difference of ~7 hours reported previously (e.g. Brown et al., 1997; Benloucif et al., 2005). Accordingly, $DLMO^p$ was calculated as (predicted CBT_{min} on night 8) – 7. Finally, average predicted CBT_{min} ($CBT_{min}{}^p$) was calculated as the average of the predicted CBT_{min} values determined for the nights on which CBT data was available. For clarity: the model-predicted time of CBT_{min} should not be confused with the measured CBT_{min} values. Predicted CBT_{min} is a phase-marker of the limit-cycle oscillator (from which predicted DLMO was directly calculated by subtracting 7 hours), whereas measured CBT_{min} and DLMO can be considered measured phase markers of the individuals. As Kronauer's model returns the time of core body temperature minimum as a circadian phase marker, we first tested whether average CBT_{min} was related to $CBT_{min}{}^p$ and a significant positive relationship was found (Figure 6A; $F(1,18) = 19.58$; $p < 0.001$). Also in this analysis, the data points are non-equidistant, and when the regression was repeated without the late individual, a trend was observed ($F(1,17) = 3.612$; $p = 0.07$). Furthermore, $DLMO^p$ values were positively related to the measured DLMO values (Figure 6C; $F(1,18) = 19.44$; $p < 0.001$). This significant relationship disappeared when the late individual was omitted from the analysis ($F(1,17) = 2.876$; $p = 0.11$). Although $DLMO^p$ and $CBT_{min}{}^p$ both significantly explained 52% of the variance in the measured DLMO and average CBT_{min} values respectively, a considerable amount of residual variance was still observed (Figure 6A and C; $CBT_{min}{}^p$ and $DLMO^p$). As CBT measurements are especially sensitive to masking by activity, it was tested whether a combination of $CBT_{min}{}^p$ and time of activity acrophase would explain more variance in average CBT_{min}, than $CBT_{min}{}^p$ alone. A simple regression analysis revealed that $CBT_{min}{}^p$ together with activity acrophase (added as a covariate) explained 67% (an increase of 15%) of the variance in average CBT_{min} (Figure 6B; $F(2,17) = 17.5$, $p < 0.001$). Next, it was tested whether more variance in DLMO could be explained with a combination of $DLMO^p$ and time of activity acrophase (covariate), than with $DLMO^p$ alone. Together, $DLMO^p$ and activity acrophase explained 71% (an increase of 19%) of the total variance in DLMO (Figure 6D; $F(2,17) = 20.74$, $p < 0.001$). When the late individual was omitted from the latter two analyses, Kronauer's model prediction did not significantly contribute to either one of these regression models ($CBT_{min}{}^p$: $p = 0.15$; $DLMO^p$: $p = 0.1$). These results suggest that the relation between clock phase and Kronauer's model predictions is stronger when the range of DLMO values included in the analysis extends to DLMO values outside the normal range.

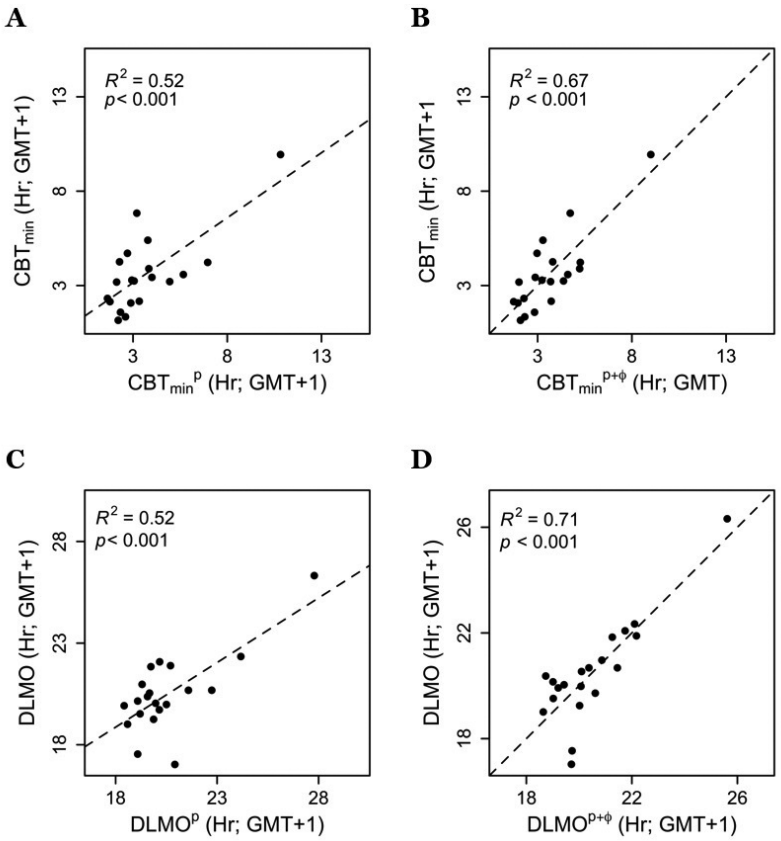

Figure 6. Model predictions for both CBT_{min} and DLMO. A and C) The model-predicted CBT_{min} and DLMO times ($CBT_{min}{}^{p}$ and $DLMO^{p}$**)** show a significant positive relationship with CBT_{min} and DLMO respectively. **B and D)** When correcting the model-predictions of CBT_{min} and DLMO for activity acrophase ($CBT_{min}{}^{p+\varphi}$ and $DLMO^{p+\varphi}$ respectively), 15% more variance in CBT_{min} and 19% more variance in DLMO was explained. The residual standard deviations corresponding to the regression analyses presented in panels A, B, C and D were 1.46, 1.24, 1.4 and 1.1h.

We finally tested how well the model would predict DLMO when the default light settings of the model were used, by assuming 150 lux during wake and 0 lux during sleep. The residual sum of squares between $DLMO^{p}$ and DLMO was reduced (by 51%) from 90.83h² when default light settings were used, to 46.18h² when individual light profiles were used. A consistent bias towards later DLMO predictions (+1.82 ± 1.14h (±SD)) was also observed using the default settings, but not when using the individualized light profiles (+0.07 ± 1.56h (±SD)). This suggests that assuming 150 lux during the wake period results in an overestimation of light exposure in the evening.

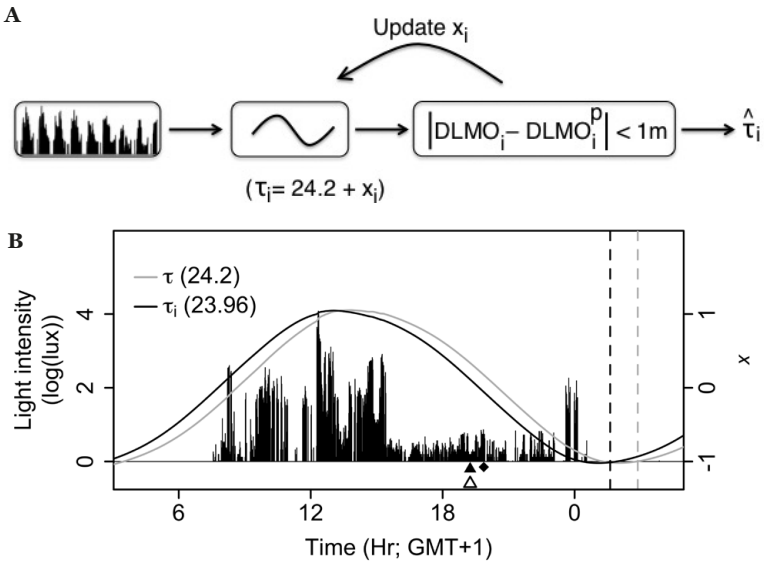

Figure 7. Intrinsic period estimation method. A) The intrinsic τ of the model was iterated step-wise (from the initial τ of 24.2h) for each participant until the time between $DLMO_i$ and $DLMO^p$ was < 1 minute. **B)** Light intensity data of day 8 of participant "BCM15" who showed a DLMO (△) earlier than predicted by the model with the default τ (◆). For this individual, a τ of 23.96 hours resulted in a $DLMO^p$ (▲) that was identical to the measured DLMO. Dashed lines show $CBT_{min}{}^p$ using the default (grey) and individual (black) τ. Solid lines show the value of state-variable x when the default (grey) or individual (black) τ was used.

Estimating intrinsic circadian period with ambulatory light data and measured DLMO

The results indicate that not all variance in circadian phase can be explained by modeling light data only, a finding that was assumed to originate mainly from individual variation in intrinsic circadian period. To obtain the set of estimated individual τ values $\hat{\tau}(\{i....n\})$ that could explain the remaining variance, the difference between $DLMO^p$ and DLMO was minimized (< 1 minute) for each individual separately by manipulating the value of the τ parameter according to the schematic in Figure 7A (an example is presented in Figure 7B).

Intrinsic period distribution

The intrinsic period estimates ranged from 23:50 to 24:34, with an average of 24:14 (± 00:12 (± SD)). We found our distribution to match previous literature well (Figure 8A), as average intrinsic periods from previous literature were 24:18 ± 00:22 (±SD; Hiddinga et al., 1997), 24:11 ± 00:08 (±SD; Czeisler et al., 1999), 24:04 ± 00:10 (±SD; Wright et al., 2005), 24:06 ± 00:20 (Gronfier et al., 2007), 24:12 ± 00:08 (±SD; Burgess & Eastman, 2008) and 24:09 ± 00:12 (Duffy et al., 2011). This similarity suggests that the discrepancy observed between DLMO and $DLMO^p$ may be attributable to a distribution of intrinsic periods in our sample that is comparable to distributions reported previously.

Acknowledging the possibility that there are other physiological parameters than τ that could explain the observed remaining variance in phase angle of entrainment (e.g. light sensitivity, differently shaped PRCs), we tested whether the individual variation around a laboratory-constructed PRC (Khalsa et al., 2003) followed the distribution that would be expected based on a known distribution of τ (Czeisler et al., 1999). This was found to be the case (Figure S1), suggesting that τ is indeed the dominant factor determining phase in human circadian entrainment. Next, we tested whether tuning other model variables (while leaving τ at the default value of 24.2h) could minimize the discrepancy between DLMO and $DLMO^p$. For six participants, adjusting the saturating level of light intensity did not result in an optimal solution (DLMO = $DLMO^p$), by manually tuning I_o, leaving an unexplained variance of $14.32h^2$ which was 69% of the total variance in DLMO. Parameter values leading to a solution were often unrealistic (e.g. more than half of the required saturating light levels were <200 or >30000 lux). Also tuning B and $\hat{B}$ variable values did not lead to an optimal solution in four participants, leaving an unexplained variance of $12.62h^2$ (72.7% of the total variance). These findings support our assumption that τ may be the dominant source of individual variation when using Kronauer's model to predict clock phase.

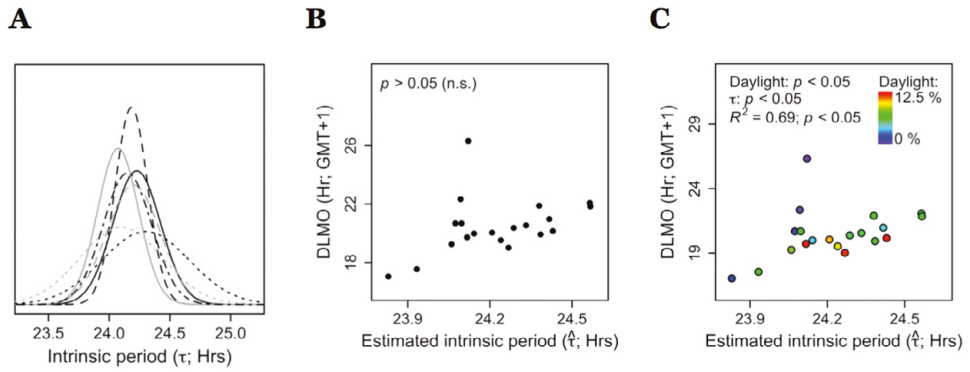

Figure 8. Distribution and relationships of $\hat{\tau}$ **A)** Distribution of estimated intrinsic period compared to a sample of intrinsic period distributions reported using forced desynchrony protocols. The separate intrinsic periods are distributed with means (±SD) of 24.23 (± 0.20; $\hat{\tau}_{\{i....n\}}$; field estimation; solid black line), 24.3 (± 0.36; Hiddinga et al., 1997; dotted black line), 24.18 (± 0.13; Czeisler et al., 1999; dashed black line), 24.07 (± 0.17; Wright et al., 2005; solid grey line), 24.10 (± 0.34; Gronfier et al., 2007; dotted grey line), 24.2 (± 0.13; Burgess & Eastman, 2008; dashed grey line) and 24.15 (±0.20; Duffy et al., 2011; black dotted dashed line). **B)** The relationship between DLMO and estimated intrinsic period was not significant. **C)** The same relationship as in **B**. The color-coding indicates the amount of daylight (% of minutes > 615 lux, see methods) each individual was exposed to. Later DLMO values were related to longer intrinsic periods, apart from the individuals with the lowest amount of daylight exposure (dark blue points at $\tau \sim 24.1$). DLMO was significantly ($p < 0.001$) explained by both estimated intrinsic period and the amount of daylight exposure, together contributing to a linear model that explained 69% of the variance in DLMO.

Relationship between estimated intrinsic period and measured clock phase

As intrinsic period was directly calculated from DLMO, we expected to find a correlation between these two measures. However, no relationship between estimated intrinsic period and clock phase was found (Figure 8B; $p = 0.1$). A significant relationship between the timing of CBT_{min} and intrinsic period has been reported by Duffy et al. (2001), which could not be replicated by Wright Jr et al. (2005) when DLMO was taken as the circadian phase marker. To explain these conflicting results, we considered the origin of light our subjects were exposed to. We hypothesized DLMO to be earlier in individuals when the majority of light exposure originated from daylight rather than artificial light for two reasons. First, the intensity of daylight is relatively high compared to artificial light, and higher light intensities have been related to an earlier sleep timing in humans (Roenneberg et al., 2003). Second, daylight typically precedes artificial light (which mostly occurs after sunset rather than before sunrise; Wright et al., 2013). A larger amount of daylight is therefore expected to be related to earlier DLMO values due to both its high intensity and relatively early timing. To test this hypothesis, the relationship between DLMO and estimated intrinsic period was controlled for the log-transformed estimated amount of daylight (minutes > 615 lux; see methods) each individual was exposed to. After adding the log-transformed amount of daylight as a covariate to the regression equation, 69% of the variance in DLMO was significantly explained ($F(2,17) = 18.53$; $p < 0.001$) by both intrinsic period and the amount of daylight exposure. A later DLMO was related to a longer estimated intrinsic period and more estimated daylight exposure was related to earlier DLMO values (Figure 8C). This improved fit was not only attributable to the late individual: both log-transformed daylight and τ remained significant contributors to the regression model when this individual was omitted from the regression analysis ($F(2,16) = 21.25$; $p < 0.001$). This shows that the amount of daylight indeed influences the relationship between DLMO and τ, in particular for individuals with very low amounts of daylight exposure (Figure 8C). These results suggest that individual differences in the amount of daylight exposure obscure the expected relationship between DLMO and intrinsic period. As a consequence, when by chance there is little variation between participants in the timing and intensity of the light schedule (indicated by the amount of daylight exposure), a relationship between DLMO and intrinsic period may be revealed, perhaps explaining conflicting results in literature.

Relationship between estimated intrinsic period and the phase difference between DLMO and sleep timing

To correct for the timing of the light schedule, phase of entrainment can be expressed as the phase angle between DLMO and the light-dark cycle. For this reason, the interval between DLMO and sleep onset (which can be considered as the onset of the dark phase) has been shown to be more strongly related with intrinsic period, and is conceptually a more reasonable measure of phase of entrainment (clock phase with respect to zeitgeber phase) than the clock time of DLMO without light timing information (Wright Jr et al., 2005; Gronfier et al., 2007; Burgess & Eastman, 2008; Hasan et al., 2012; Eastman et

al., 2015). Therefore, we tested whether a relationship between phase of entrainment and intrinsic period could be revealed in the current dataset. Phase of entrainment was calculated with respect to sleep onset (i.e. lights off; DLMO – sleep onset) and sleep offset (i.e. lights on; DLMO – sleep offset) separately. Estimated intrinsic period was significantly related to the phase difference between DLMO and sleep onset (Figure 9A; $F(1,18) = 4.67$; $p < 0.05$), and DLMO and sleep offset (Figure 9B; $F(1,18) = 12$; $p < 0.01$). The analysis revealed that individuals with longer estimated intrinsic periods showed a shorter time interval between DLMO and sleep onset/offset and vice versa for individuals with shorter estimated intrinsic periods.

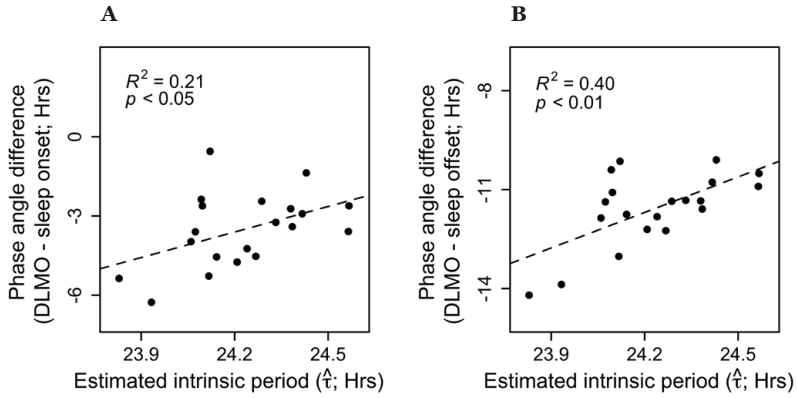

Figure 9. Relationships between sleep timing and estimated $\hat{\tau}$. The phase angles between **A)** sleep onset and DLMO and between **B)** sleep offset and DLMO were both significantly and positively related to estimated intrinsic period such that individuals with longer estimated intrinsic periods scheduled their sleep window at a relatively early circadian phase (shorter duration between DLMO and sleep onset).

Relationship between estimated intrinsic period and phase of entrainment, corrected for light intensity

As stated previously, phase of entrainment is not only influenced by intrinsic period, but also by light intensity. To test the assumption that higher light intensities are related to an earlier phase of entrainment (Roenneberg et al., 2003), we tested whether phase of entrainment could be significantly explained by both intrinsic period and average light intensity. Therefore, the average of the log-transformed lux values (only values > 0 lux included) were calculated for each individual separately as a measure of average light intensity. Regression analysis revealed that the phase angle between DLMO and sleep onset ($R^2 = 0.55$; $F(2,17) = 10.4$; $p < 0.01$) and sleep offset ($R^2 = 0.72$; $F(2,17) = 21.6$; $p < 0.001$) were significantly related to both estimated intrinsic period (as above) and the average light intensity (now added as a covariate). As expected, later intrinsic period was related to later phase of entrainment, whereas higher light intensities were related to earlier phase of entrainment. For (DLMO – sleep offset), an increase of 1 hour in intrinsic period was estimated to delay phase of entrainment by 4.6 ± 0.77 (±SE) hours, whereas an increase in average light intensity by 1 log(lux) was estimated to advance phase of entrainment by 2.84

± 0.65 (±SE) hours. For (DLMO – sleep onset), a delay of 4.54 ± 1.21 (±SE) and an advance of 3.71 ± 1.03 (±SE) hours were estimated for these parameters respectively.

Discussion

The results provide evidence that analyzing ambulatory light, activity and core-body temperature (CBT) data provides reliable estimations of human clock phase (DLMO). Although CBT_{min} by itself correlated with DLMO, analyzing the combination of light and activity data provided more accurate estimations. The finding that CBT_{min} only is a less accurate predictor of DLMO than a combination of light and activity data is likely attributable to known masking effects on CBT (Klerman et al., 1999). By modeling the circadian impact of ambulatory collected light data, we show that Kronauer's model predictions explain a significant amount of variance in DLMO. This shows that this model may be a useful tool for estimating clock phase in the field, especially when it is combined with activity measurements. The relationship between the $DLMO^P$ and $CBT_{min}{}^P$ values and Kronauer's model predictions of these circadian phase markers was not strong, which is likely attributable to large inter individual variation in intrinsic period. As a result, a relationship between DLMO and $DLMO^P$ may be more readily shown in a dataset of equidistant, broadly distributed DLMO values, effectively increasing the signal-to-noise ratio in the regression analyses. Inclusion of individuals with DLMO values deviating from the normal range (shift-workers, patients) will be interesting for future testing, as this may show that Kronauer's model can give a rough estimation of DLMO, even for individuals who are entrained outside the normal range. The fact that the model predicts a late DLMO for the late individual in our dataset is promising, but further testing is required. Furthermore, to the authors' knowledge, the current study is the first to highlight the possibility that intrinsic period may be estimated by modeling ambulatory light exposure data followed by one clock-phase assessment in the lab. Finally, the results presented here provide experimental and theoretical support for the notion that intrinsic period and zeitgeber strength of the light-dark cycle are the dominant factors in determining human phase of entrainment.

Both methods described rely on the integrity of ambulatory collected light data. It should be noted that light was measured at the level of the wrist, not the eye, which might have influenced the model predictions. Furthermore, the device returns light intensity in units of photopic illuminance (lux), which is not entirely representative for the human circadian system. Where Kronauer's model should ideally be modified to take melanopic lux (Lucas et al., 2014) as an input, the impact of light on the clock can likely be more accurately described when actigraph devices return melanopic lux or photon flux corrected for the spectral sensitivity of melanopsin. It might be that individual differences in light sensitivity may have induced additional variance as well. Nevertheless, tuning of the light-sensitivity parameter in Kronauer's model indicated that, unlike differences in intrinsic period, differences in light sensitivity are an unlikely factor in explaining the majority of the mismatch between DLMO and predicted DLMO. Finally, the methods

presented here will not be applicable to blind individuals and models incorporating non-photic entrainment (i.e. St. Hilaire et al., 2007) could perhaps offer a suitable alternative.

Modeling ambulatory light data explained 52% of the total variance in measured DLMO and timing of CBT_{min}. Accounting for activity acrophase (added as a covariate) generated more accurate predictions of these parameters (67% and 71% respectively). CBT_{min} is particularly sensitive to masking by activity (Klerman et al., 1999) and correcting for activity acrophase may have therefore resulted in the additional amount of explained variance (15%). As DLMO was assessed in a posture-controlled setting, it is unlikely that the additional amount of variance explained in DLMO (19%) originated by accounting for masking effects by activity. It is also unlikely that time of activity acrophase increased the accuracy of DLMO phase estimations through non-photic effects, since the non-photic circadian drive by activity is expected to be small in light-entrained individuals (St.Hilaire et al., 2007). The most parsimonious explanation is that activity acrophase in itself is a reliable phase marker of the central clock (Lim et al., 2012), therefore adding to the predictive power of the light data. This may allow for other indirect measures of clock phase to increase the estimation accuracy of human circadian clock phase.

When entrainment is considered as a mathematical system with three unknown variables (light exposure, intrinsic period and resulting clock phase), the value of one of these variables can be calculated when the remaining two are known. Our method to estimate intrinsic period builds on the assumption that these are the dominant factors determining human entrainment. This is likely a simplification of the human circadian system. Other factors such as measurement errors in DLMO and light intensity and individual differences in the shape of the PRC and sensitivity to light could have also contributed to the remaining variance, which we have herewith included in our intrinsic period estimations. Therefore, our method awaits validation using individual τ estimates in a laboratory study. However, we show that deviations from the PRC reported in Khalsa et al. (2003) could be explained by accounting only for individual differences in intrinsic period (see Figure S1), and that tuning the model parameter describing light sensitivity did not reliably result in a minimization of the discrepancy between DLMO and $DLMO^p$ in our dataset (see Supplementary Material). Together with the observed similarity between the distribution of estimated τ values and distributions of τ reported using forced-desynchrony protocols (e.g. Hiddinga et al., 1997; Czeisler et al., 1999; Wright Jr et al., 2005; Gronfier et al., 2007; Burgess & Eastman, 2008; Duffy et al., 2011), our results indicate the validity of our τ estimates.

The data suggests that DLMO is related to intrinsic period, as long as the average amount of daylight exposure is accounted for (Figure 8C). The weak relationship between DLMO and intrinsic period (Wright Jr et al., 2005) may be due to individual differences in the timing and intensity of light exposure, which are both expected to be related to the amount of daylight exposure (Roenneberg et al., 2003; Wright et al., 2013). Our analyses predict a relationship between DLMO and intrinsic period to be observable when there is little inter-individual variability in the timing and intensity of light exposure. Indeed, those individuals with the least amounts of daylight exposure showed DLMO values that were later than predicted by the corresponding τ estimations. Importantly, the

low amount of daylight exposure also explains the DLMO of the latest individual in our dataset, suggesting that this DLMO was the result of deviating daylight exposure, rather than being of clinical nature. By correcting for individual differences in the timing of light exposure (sleep-wake cycle), it has previously been shown that the phase difference between DLMO and sleep onset (DLMO – sleep onset) is positively related with intrinsic period (Wright et al., 2005; Burgess & Eastman, 2008; Gronfier et al., 2007; Hasan et al., 2012; Eastman et al., 2015). Our intrinsic period estimates show the same positive relationship, suggesting that our estimations were valid. It is unlikely that this finding is caused by a 'regression to the mean', because DLMO and estimated intrinsic period did not correlate (Figure 8B; $R2 = 0.144$; $p = 0.099$). As a result, the probability of finding a significant relationship between (DLMO – sleep onset/offset) and intrinsic period purely by chance was only 5% (see Supplementary Material).

The positive relationship between phase angle of entrainment (DLMO – sleep onset/offset) and estimated intrinsic period reported here is in line with the premise that humans obey the phase-period rule: individuals with long intrinsic periods show a late phase of entrainment with regard to the light-dark cycle such that the majority of the light hits the advance zone of a typical PRC (i.e. sleep is scheduled at an early phase such that darkness coincides with the delay zone of that PRC). Additionally, as expected (Roenneberg et al., 2003), light intensity exerts an additional influence on phase angle of entrainment over estimated intrinsic period, where higher light intensities are related to an earlier phase of entrainment. Although sleep onset and offset both contain information on the timing of light exposure in humans, our analysis revealed a relationship with intrinsic period that was weaker for (DLMO – sleep onset) than for (DLMO – sleep offset). This suggests that most humans are stronger entrained to lights-on (morning light) than to lights-off (evening light), as expected when $\tau > 24h$.

In summary, the distribution of estimated intrinsic periods and their relationship with phase of entrainment suggest that we developed an accurate method to estimate circadian period from field data. Our results show that low-cost estimations of circadian phase, intrinsic period and phase of entrainment may be possible by analyzing ambulatory collected light and activity data, while imposing no restrictions on the participants' daily routines. Such advances are not only useful from a scientific point of view, but may prove to be of crucial importance when optimizing individual light treatment for shift work and jetlag applications and designing individualized chronotherapy treatment schedules.

Acknowledgements

We would like to thank Dr. Andrew Philips (Modeling unit, Harvard Medical School) for his helpful comments on the manuscript. Original data, analyses, and R-codes can be accessed by contacting the corresponding author. The complete dataset (original and analysed) and R-codes will also be available at the data repository at the University of Groningen.

References

Bates, D., Mächler, M., & Bolker, B. (2012). Fitting linear mixed-effects models using lme4. *J. Stat. Softw.*, 51.

Beck, A.T., Steer, R.A., & Brown, G. K. (1996). *Manual for the Beck Depression Inventory-II*. San Antonio, TX: Psychological Corporation.

Benloucif, S., Guico, M. J., Reid, K. J., Wolfe, L. F., L'hermite-Balériaux, M., & Zee, P. C. (2005). Stability of melatonin and temperature as circadian phase markers and their relation to sleep times in humans. *J. Biol. Rhythm. Rhythm.*, *20*(2), 178–188.

Bonmati-Carrion, M. A., Arguelles-Prieto, R., Martinez-Madrid, M. J., Reiter, R., Hardeland, R., Rol, M. A., & Madrid, J. A. (2014). Protecting the melatonin rhythm through circadian healthy light exposure. *Int. J. Mol. Sci.*, *15*(12), 23448–23500.

Brown, E. N., Choe, Y., Shanahan, T. L., & Czeisler, C. A. (1997). A mathematical model of diurnal variations in human plasma melatonin levels. *Am. J. Physiol.*, *272*(3 Pt 1), E506-16.

Burgess, H. J., & Eastman, C. I. (2008). Human Tau in an Ultradian Light-Dark Cycle. *J. Biol. Rhythms*, *23*(4), 374–376.

Buysse, D. J., III, C. F. R., Monk, T. H., Berman, S. R., & Kupfer, D. J. (1989). The Pittsburgh Sleep Quality Index: a new instrument for psychiatric practice and research. *Psychiatry Res.*, *28*(2), 193–213. article.

Clark, J. H. (1924). The Ishihara test for color blindness. *Am. J. Physiol. Opt.*, *5*, 269–276.

Cleveland, W., Grosse, E., Shyu, W., Chambers, J., & Hastie, T. (1992). Local regression models. *Stat. Model. S.*

Czeisler, C. A., Duffy, J. F., Shanahan, T. L., Brown, E. N., Jude, F., Rimmer, D. W., Ronda, J. M., Silva, E. J., Allan, J. S., Jonathan, S., Dijk, D. J., Kronauer, R. E., Brown, E. N., Mitchell, J. F., Rimmer, D. W., Ronda, J. M., Silva, E. J., Allan, J. S., Emens, J. S., Dijk, D. J., & Kronauer, R. E. (1999). Stability, precision, and near-24-hour period of the human circadian pacemaker. *Science (80-.).*, *284*(5423), 2177–2181.

Duffy, J. F., Cain, S. W., Chang, A.-M., Phillips, A. J. K., Munch, M. Y., Gronfier, C., Wyatt, J. K., Dijk, D.-J., Wright, K. P., & Czeisler, C. A. (2011). Sex difference in the near-24-hour intrinsic period of the human circadian timing system. *Proc. Natl. Acad. Sci.*, *108*(Supplement_3), 15602–15608.

Duffy, J. F., Rimmer, D. W., & Czeisler, C. a. (2001). Association of intrinsic circadian period with morningness-eveningness, usual wake time, and circadian phase. *Behav. Neurosci.*, *115*(4), 895–899.

Duffy, J. F., & Wright Jr., K. P. (2005). Entrainment of the human circadian system by light. *J Biol Rhythm.*, *20*(4), 326–338.

Eastman, C. I., Suh, C., Tomaka, V. A., & Crowley, S. J. (2015). Circadian rhythm phase shifts and endogenous free-running circadian period differ between African-Americans and European-Americans. *Sci. Rep.*, *5*, 8381.

Gronfier, C., Wright, K. P., Kronauer, R. E., & Czeisler, C. A. (2007). Entrainment of the human circadian pacemaker to longer-than-24-h days. *Proc. Natl. Acad. Sci. U. S. A.*, *104*(21), 9081–6.

Hasan, S., Santhi, N., Lazar, A. S., Slak, A., Lo, J., von Schantz, M., Archer, S. N., Johnston, J. D., & Dijk, D.-J. (2012). Assessment of circadian rhythms in humans: comparison of real-time fibroblast reporter imaging with plasma melatonin. *FASEB J.*, *26*(6), 2414–2423.

Hiddinga, a E., Beersma, D. G., & Van den Hoofdakker, R. H. (1997). Endogenous and exogenous components in the circadian variation of core body temperature in humans. *J. Sleep Res.*, *6*(3), 156–63.

Jewett, M. E., Forger, D. B., & Kronauer, R. E. (1999). Revised limit cycle oscillator model of human circadian pacemaker. *J. Biol. Rhythms*, *14*(6), 493–499.

Jewett, M. E., Kronauer, R. E., & Czeisler, C. A. (1991). Light-induced suppression of endogenous circadian amplitude in humans. *Nature*, *350*(6313), 59–62.

Jewett, M. E., Kronauer, R. E., & Czeisler, C. A. (1994). Phase-amplitude resetting of the human circadian pacemaker via bright light: a further analysis. *J. Biol. Rhythms*, *9*(3–4), 295–314.

Khalsa, S.B.S., Jewett, M.E., Klerman, E.B., Duffy, J.F., Rimmer, D.W., Kronauer, R.E. and Czeisler, C. A. (1997). Type 0 resetting of the human circadian pacemaker to consecutive bright light pulses against a background of very dim light. *Sleep Res.*, *26*, 722.

Khalsa, S. B., Jewett, M. E., Cajochen, C., & Czeisler, C. A. (2003). A phase response curve to single bright light pulses in human subjects. *J. Physiol.*, *549*(3), 945–952. article.

Khalsa, S. B. S., Jewett, M. E., Cajochen, C., & Czeisler, C. a. (2003). A phase response curve to single bright light pulses in human subjects. *J. Physiol.*, *549*(3), 945–952. article.

Klerman, E. B., Lee, Y., Czeisler, C. A., & Kronauer, R. E. (1999). Linear demasking techniques are unreliable for estimating the circadian phase of ambulatory temperature data. *J. Biol. Rhythms*, *14*(4), 260–74.

Kronauer, R. E. (1990). A quantitative model for the effects of light on the amplitude and phase of the deep circadian pacemaker, based on human data. In J. Horne (Ed.), *Sleep `90, Proceedings of the Tenth European Congress on Sleep Research* (p. 306). Dusseldorf: Pontenagel Press.

Kronauer, R. E., Forger, D. B., & Jewett, M. E. (1999). Quantifying Human Circadian Pacemaker Response to Brief, Extended, and Repeated Light Stimuli over the Phototopic Range. *J. Biol. Rhythms*, *14*(6), 501–516.

Lim, A. S. P., Chang, A.-M., Shulman, J. M., Raj, T., Chibnik, L. B., Cain, S. W., Rothamel, K., Benoist, C., Myers, A. J., Czeisler, C. A., Buchman, A. S., Bennett, D. A., Duffy, J. F., Saper, C. B., & De Jager, P. L. (2012). A common polymorphism near PER1 and the timing of human behavioral rhythms. *Ann. Neurol.*, *72*(3), 324–334.

Lucas, R. J., Peirson, S. N., Berson, D. M., Brown, T. M., Cooper, H. M., Czeisler, C. a, Figueiro, M. G., Gamlin, P. D., Lockley, S. W., O'Hagan, J. B., Price, L. L. a, Provencio, I., Skene, D. J., & Brainard, G. C. (2014). Measuring and using light in the melanopsin age. *Trends Neurosci.*, *37*(1), 1–9.

May, C.D., Dean, D.A., Jewett, M. E. (2002). A revised definition of core body temperature phase that incorporates both state variables of a limit-cycle human circadian pacemaker model improves model stability at low circadian amplitudes. In *Soc. Res. Biol. Rhythm*.

Merrow, M., Boesl, C., Ricken, J., Messerschmitt, M., Goedel, M., & Roenneberg, T. (2006). Entrainment of the *Neurospora* Circadian Clock. *Chronobiol. Int.*, *23*(1–2), 71–80.

Pittendrigh, C. S., & Daan, S. (1976). A functional analysis of circadian pacemakers in nocturnal rodents. *J. Comp. Physiol. A*, *106*(3), 333–355.

Roenneberg, T., Wirz-Justice, A., & Merrow, M. (2003). Life between Clocks: Daily Temporal Patterns of Human Chronotypes. *J. Biol. Rhythms*, *18*(1), 80–90. article.

Schmidt, C., Collette, F., Cajochen, C., & Peigneux, P. (2007). A time to think: circadian rhythms in human cognition. *Cogn Neuropsychol*, *24*(7), 755–789.

St Hilaire, M. A., Gronfier, C., Zeitzer, J. M., & Klerman, E. B. (2007). A physiologically based mathematical model of melatonin including ocular light suppression and interactions with the circadian pacemaker. *J. Pineal Res.*, *43*(3), 294–304.

St. Hilaire, M. A. S., Klerman, E. B., Khalsa, S. B. S., Wright, K. P., Czeisler, C. A., & Kronauer, R. E. (2007). Addition of a non-photic component to a light-based mathematical model of the human circadian pacemaker. *J. Theor. Biol.*, *247*(4), 583–599.

Wright, K. P., McHill, A. W., Birks, B. R., Griffin, B. R., Rusterholz, T., & Chinoy, E. D. (2013). Entrainment of the Human Circadian Clock to the Natural Light-Dark Cycle. *Curr. Biol.*, *23*(16), 1554–1558.

Wright, K. P., Gronfier, C., Duffy, J.F., Czeisler, C. A. (2005). Intrinsic Period and Light Intensity Determine the Phase Relationship between Melatonin and Sleep in Humans. *J. Biol. Rhythms*, *20*(2), 168–177.

Zavada, A., Gordijn, M. C. M., Beersma, D. G. M., Daan, S., & Roenneberg, T. (2005). Comparison of the Munich Chronotype Questionnaire with the Horne-Ostberg's Morningness-Eveningness Score. *Chronobiol. Int.*, *22*(2), 267–78.

Zigmond, a S., & Snaith, R. P. (1983). The hospital anxiety and depression scale. *Acta Psychiatr. Scand.*, *67*(6), 361–370.

Supplementary Information

Correlation between DLMO and intrinsic period. As DLMO showed a weak but almost significant correlation with estimated intrinsic period (R^2 = 0.144; p = 0.099), we tested whether the significant relationships between (DLMO – sleep onset/offset) and intrinsic period could be solely explained by this weak relationship between DLMO and intrinsic period. To this end, we simulated 20 sets of intrinsic period values that correlated with DLMO with an R^2 of 0.144 and calculated the chance of finding a significant relationship between both (DLMO – sleep onset) and intrinsic period and (DLMO – sleep offset) and intrinsic period. This chance was only 5%, suggesting that there is a very slight chance that our findings were only due to DLMO being slightly related to intrinsic period.

Optimizing remaining model parameters. To confirm that intrinsic period was the dominant model parameter that could minimize the difference between measured and predicted DLMO with reasonable parameter values, we tested whether optimizing other model parameters (light sensitivity, strength of B and strength of $\hat{B}$) could minimize the difference between measured DLMO and $DLMO^p$ by applying the method we used to estimate intrinsic period, while substituting $\hat{\tau}$ with the parameter of interest. For six participants, adjusting light sensitivity and the strength of $\hat{B}$ did not result in a solution, whereas optimizing B lead to no solution in four participants. The parameter values that did lead to a solution required unreasonable parameter values in more than half of the participants (e.g. saturating light levels of < 200 or > 30000 lux and > 5-fold increases in B or $\hat{B}$ values). Although the entire landscape of combinations of model parameters was not explored, this strongly suggests that the dominant model parameter in Kronauer's model that leaves room for improvement in predicting DLMO is intrinsic circadian period.

Table S1. Equations and parameter valuess of the limit cycle oscillator model

1) $\alpha = \alpha_0 \left(\frac{I}{I_0} \right)^p \left(\frac{I}{I+100} \right)$

2) $\widehat{B} = G(1-n)\alpha$

3) $\dot{n} = 60[\alpha(1-n) - \beta n$

4) $\dot{x} = \left(\frac{\pi}{12} \right) \left[x_c + \mu \left(\frac{1}{3} \mathrm{x} + \frac{4}{3} x^3 - \frac{256}{105} x^7 \right) + B \right]$

5) $\dot{x}_c = \left(\frac{\pi}{12} \right) \left\{ qBx_c - x \left[\left(\frac{24}{0.97729\tau_x} \right)^2 + kB \right] \right\}$

6) $B = \hat{B}(1-0.4x)(1-0.4x_c)$

7) $\mathrm{CBT}_{\min} = \varphi_{\mathrm{XcX}} + \varphi_{\mathrm{ref}}$

$q = \frac{1}{3}$

$\mu =$ 0.13

$\tau_x = 24.2$

$k =$ 0.55

$\beta =$ 0.007 min^{-1}

$G =$ 37

$\alpha_0 =$ 0.1 min^{-1}

$p =$ 0.5

$I_0 =$ 9500

$\varphi_{ref} =$ 0.97

$\varphi_{XcX} =$ −2.98 rad

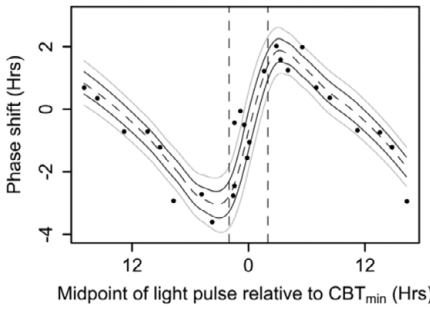

Figure S1. Kronauer's model prediction on PRC data from Khalsa et al. (2003). Kronauer's model showed an accurate fit to the data (dashed black curve), with a mean-square error (MSE) of 0.58h for the entire dataset, and an MSE of 0.2h when the light pulses timed close to CBT_{min} (4-hour window, marked by dashed vertical lines) were omitted. The MSE was calculated as the sum of squared deviations from the data points to the model fit divided by the number of data points. We allowed the model parameter for intrinsic period to deviate from 24.18 with one standard deviation (black solid lines; 68% confidence band) or two standard deviations (grey solid lines; 95% confidence band) based on the distribution reported by Czeisler et al. (1999). This approach showed that 13 out of 20 data points (65%; 58% when data within the critical region was omitted) fell within (or very close to) the 68% confidence band, whereas 3 out of 20 data points (15%; 8.3% when data within the critical region was omitted) fell outside the 95% confidence band. The fact that the data points are distributed around the default model prediction with a distribution similar to what would be expected based on differences in intrinsic period, suggest that the majority of error in predicting Khalsa's PRC data originates from these individual differences in circadian period length. As in uncontrolled conditions, the majority of light exposure occurs outside the critical region of the PRC, the model should be able to predict clock phase with a very high accuracy in our dataset.

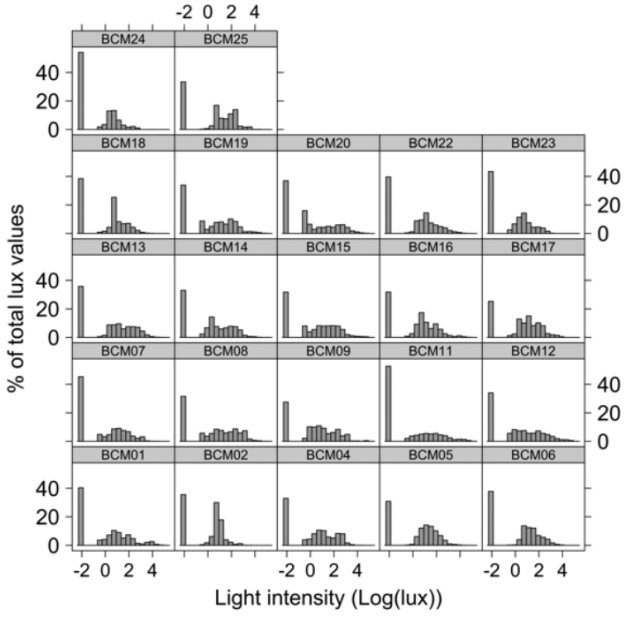

Figure S2. Distribution of light intensities measured during the total 9-days protocol. For each intensity bin (bin-size: 0.4 log(lux)), the number of lux values in that bin is plotted as a percentage of the total amount of lux values measured for each participant separately.

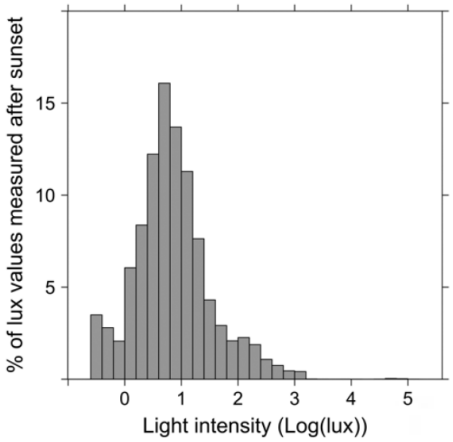

Figure S3. Distribution of light intensities measured during solar darkness. For this distribution, a subset of data was analyzed where only lux-values measured during solar darkness (solar angle relative to horizon: < -6°) were included. For each intensity bin (bin-size: 0.2 log(lux)), the number of lux values in that bin is plotted as a percentage of the total amount of lux values measured during solar darkness for all participants combined. During solar darkness, 99% of the data fell below 615 lux (2.79 log(lux)).

Chapter 3

Melanopsin and L-cone induced pupil constriction is inhibited by S- and M-cones in humans

Tom Woelders,
Thomas Leenheers,
Marijke C.M. Gordijn,
Roelof A. Hut,
Domien G.M. Beersma
and Emma J. Wams

Proceedings of the National Academy of Sciences 115 (4), 792-797

Abstract

The human retina contains five photoreceptor types: rods, S-, M- and L-cones and melanopsin-expressing ganglion cells. Recently, it has been shown that selective increments in M-cone activation are paradoxically perceived as brightness decrements, as opposed to L-cone increments. Here we show that similar effects are also observed in the pupillary light response, where M-cone or S-cone increments lead to pupil dilation, while L-cone or melanopic illuminance increments resulted in pupil constriction. Additionally, intermittent photoreceptor activation increased pupil constriction over a 30-minutes interval. Modulation of L-cone or melanopic illuminance within the 0.25-4 Hz frequency range resulted in more sustained pupillary constriction than constant intensity light. Opposite results were found for S-cone and M-cone modulations (2 Hz), mirroring the dichotomy observed in the transient responses. Both the transient and sustained pupillary light responses thus suggest that S- and M-cones provide inhibitory input to the pupillary control system when selectively activated, whereas L-cones and melanopsin response fulfil an excitatory role. These findings provide insight into functional networks in the human retina and the effect of color-coding in nonvisual responses to light, and imply that both nonvisual and visual brightness discrimination may share a common pathway that starts in the retina.

The primate retina contains rods and three types of cones defined by their short-, mid- and long-wavelength spectral sensitivity (S-, M- and L-cones). Light information travels from the photoreceptive layer down to the ganglion cell layer, which eventually relays light information to the brain (reviewed in (1)). The ganglion cells that are involved in visual perception project basic information on color and luminance provided by the photoreceptors that indirectly innervate them. There are three major classes of retinal ganglion cells involved in visual color and/or luminance coding: the parasol cells, the midget ganglion cells and the bistratified ganglion cells. Parasol cells are involved in luminance coding, with responses mainly mediated by a summation of M- and L-cone activation (L+M). Midget ganglion cells are involved in red-green color discrimination by comparing activation originating from L-cones and M-cones (L-M or M-L). Finally, the bistratified ganglion cell is thought to be involved in encoding color on the blue-yellow scale in an S – (L+M) manner. These cells thus receive excitatory input from the S-cones, while receiving inhibitory input from a mixture of M- and L-cones. Besides its image forming function, light also elicits nonvisual effects such as the pupillary light response. Light information is relayed to brain areas involved in nonvisual responses via a specialized subset of retinal ganglion cells (ipRGCs) that are intrinsically photosensitive by expressing melanopsin (2, 3). In the primate retina, ipRGCs have been shown to encode color on a blue-yellow scale, much like the bistratified retinal ganglion cells, but ipRGCs have been shown to receive input in an (L+M) – S opponent manner (4). The human pupillary light response seems to reflect this retinal wiring, since S-cone illuminance increments result in paradoxical pupil dilations (5).

To study the contribution of one photoreceptor type, the silent substitution method (6) can be employed. This method allows for selective modulation of the photoreceptor channel of interest. Any change in downstream neural processes is then a direct consequence of modulating the pathways that the selected photoreceptor is involved in. This is achieved by designing two spectra that are indistinguishable for all but one photoreceptor type. Temporally alternating these two spectra will then result in a selective modulation of the photoreceptor for which the transition is non-silent. For example, a selective increment of M-cone activation will change the ratio between L- and M-cone stimulation, which will then alter the output of the associated midget ganglion cells, shifting the perceived stimulus color along the red-green scale. This method has recently been used to show that selective decrements in M-cone illuminance are paradoxically perceived as brightness increments (7). M-cone square-wave modulations furthermore produce electroretinogram (ERG) traces that are in opposite phase with traces resulting from L-cone (or L+M-cone) modulations (8, 9), which has also been shown in visually evoked potentials (VEP) recorded at occipital scalp locations (10). Thus, at different levels of visual processing, M-cone increments are perceived as brightness decrements, whereas L-cone increments and (L+M) increments are perceived as brightness increments.

Although red-green color-opponent ipRGCs have not been described in the primate retina, it is interesting to test whether M-cone decrements result in paradoxical pupil constrictions, congruent with the aforementioned psychophysical, ERG and VEP results. We therefore measured pupillary light responses in a silent substitution protocol. Contrary

to the previously mentioned studies, we did not only account for the 3 cone types in the human retina (i.e. triple silent substitution), but also for the spectral sensitivity of melanopsin. With a peak absorbance at 480 nm (3), the spectral sensitivity of melanopsin overlaps substantially with that of S- and M-cones, such that under triple silent substitution, the effects resulting from isolated S- or M-cone modulations may be confounded by concomitant melanopsin modulations. This approach thus allows for a selective square-wave modulation of isolated S-, M-, L-cone or melanopsin responses, while maintaining a constant response for the remaining three receptor channels. The first purpose of this study was therefore to test how the human pupil responds to transient changes in photoreceptor-specific illuminance to provide insight into the retinal pathways involved in nonvisual brightness coding mediated by ipRGCs.

Another interesting phenomenon regarding brightness-coding is that flickering light may appear brighter than light of constant intensity, also known as the Brucke-Bartley effect (11). Similar effects have recently been described for the pupillary light response (12). During prolonged exposure to light of constant intensity (~30 minutes), the pupil gradually dilates towards the dark-adapted diameter (pupillary escape) after an initial constriction at lights on, suggesting that encoded brightness gradually decays due to light-adaptation in cones. This pupillary escape is countered by presenting the light in a flickering (0.1 – 8 Hz) manner (12, 13), suggesting that a high level of encoded brightness is sustained in response to flickering light. These effects may be explained by considering retinal adaptation: by repeatedly allowing the cone-signalling pathway to dark-adapt, the response to each subsequent light pulse is increased, resulting in an increased overall contribution of these pathways to the sustained pupillary light response (effectively countering the effects of light-adaptation that result in pupillary escape under constant light). Using whole-cell recordings of mouse ipRGCs, it has been shown that ipRGC spiking rate increases during exposure to flickering on-off light in comparison with light of constant intensity (13), suggesting that increased nonvisual light responses to flickering light emerge at the retinal level. Although square-wave temporal modulation of one photoreceptor type may not cause complete dark-adaptation at each cycle, it will increase its response to each photoreceptor-specific illuminance increment. The silent substitution method thus allows for testing the effect of intermittent stimulation for each photoreceptor type separately, which may yield different results than those obtained under on-off flickering light exposure where all photoreceptors are modulated in concert. Given the inhibitory input of S-cones to ipRGCs in primates and the inhibitory nature of M-cones in subjective brightness perception in humans, it may be expected that enhanced S- and M-cone activation might paradoxically stimulate pupil dilation as measured by increased pupillary escape. The second question we address in this study is whether an increased time-averaged activity of photoreceptor channels (by effectively countering light-adaptation) decreases or increases encoded brightness over the time course of 30 minutes, for which pupillary escape is taken as a proxy. We expect that pupillary escape will decrease (more sustained constriction), as compared to constant light, when increased activity of the modulated receptor results in increased encoded brightness, and vice versa.

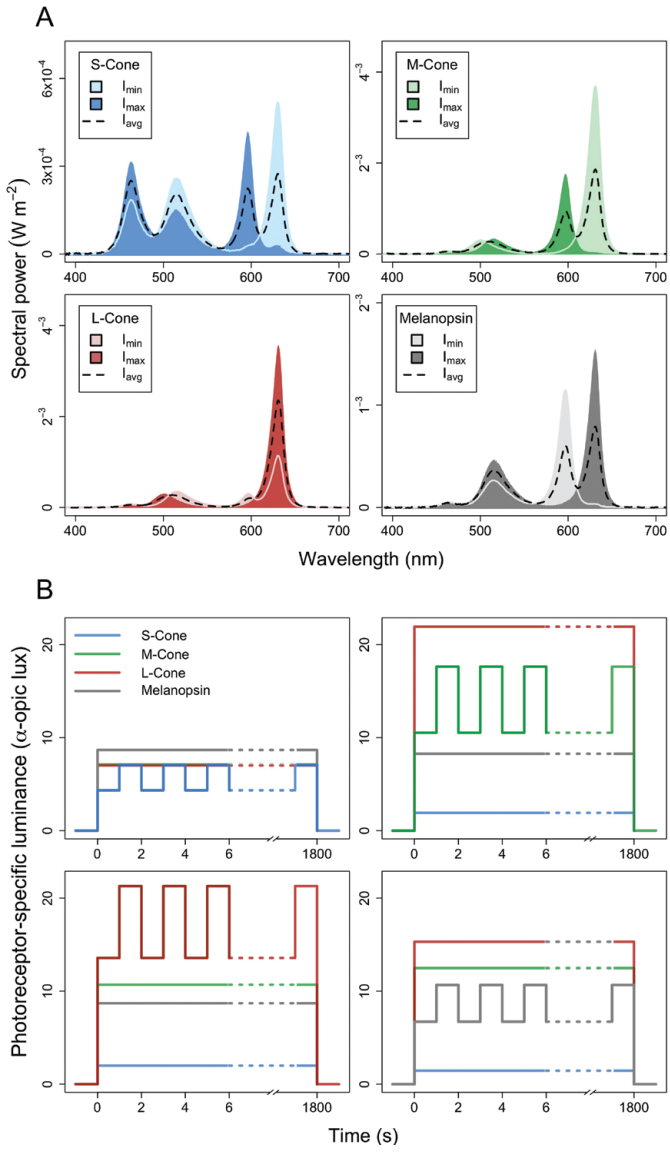

Figure 1. (A) Silent substitution spectra per non-silent photoreptor. In each panel, the light and dark shaded areas correspond to the minimal (I_{min}) and maximal (I_{max}) photoreceptor-specific illuminance respectively. Where the two spectra overlap, the solid line corresponds to the I_{min} spectrum. The dashed black line follows the average of I_{min} and I_{max}, which was used in the constant condition. (B) A schematic overview of photoreceptor-specific illuminance values for the 0.25 Hz condition. Separate panels show the spectra and protocols for the S- (top, left), M- (top, right), L-cones (bottom, left) and melanopsin (bottom, right) modulations.

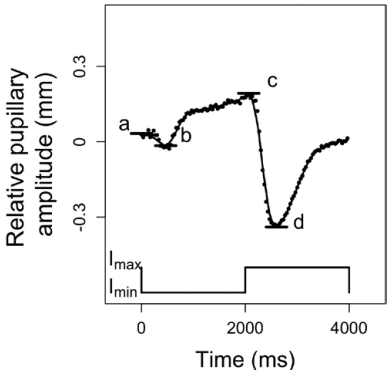

Figure 2. Example event-related pupil response (ERPR) for a representative participant that was exposed to the 0.25 Hz L-cone isolating flicker. The solid line follows the smoothed trend line that was used to calculate constriction amplitudes for statistical analyses. Horizontal line segments denote the local minima and maxima from which constriction amplitudes were calculated (see Methods and Materials). Constriction to I_{min} and I_{max} were calculated as |b – a| and |d – c| respectively. Square-wave traces illustrate the photoreceptor-specific illuminance modulations.

Results

With an infrared camera, pupil diameter was continuously measured for 30 minutes, while participants viewed two temporally alternating silent substitution spectra (Fig. 1A). The spectra were designed so that one photoreceptor type (S-, M-, L-cones or ipRGCs) was repeatedly exposed to illuminance increments and decrements, while illuminance values remained constant for all other receptors (Fig. 1B). The spectra were alternated at a frequency of 0.25, 0.5, 1, 2 and 4 Hz on separate occasions for each individual, with one modulated receptor per participant (4 participants per modulated receptor). To study the effect of photoreceptor-selective increments and decrements on pupil dilation, we calculated the event-related pupil response (ERPR). The ERPR represents the average pupil response to a photoreceptor-specific square-wave modulation. One ERPR was constructed per frequency condition per participant (Fig. 2). From these individual ERPRs, an average ERPR was created for each modulated photoreceptor, which are presented in Figure 3 for the 0.25 Hz condition. For the L-cone and melanopsin modulating conditions, large-amplitude constrictions (0.64 mm ± 0.10 and 0.29 mm ± 0.04 respectively) were measured in response to an illuminance increment ($p < 0.001$), whereas the pupil constriction in response to a decrement (0.07 mm ± 0.10 and 0.03 mm ± 0.04 (± SEM) respectively) did not reach significance. For the S-cone ($p < 0.01$) and M-cone ($p < 0.01$) modulating conditions, the largest constrictions were observed in response to decrements (0.25 mm ± 0.05 and 0.29 mm ± 0.05 (± SEM) respectively), whereas the constriction induced by increments (0.07 mm ± 0.05 and 0.11 mm ± 0.05 (± SEM) respectively) did not reach significance. ERPR amplitudes and test-statistics are summarized in Table S1 for the 0.25 Hz condition. The ERPR results demonstrate that L-cone and melanopsin increments result in enhanced pupil constriction, whereas

the opposite is observed for S-cone and M-cone increments. This phase-reversal was observed for all frequency modulations (up to 2 Hz; Fig. 4), where maximal constriction was reached ~500 ms after stimulus onset (L-cones and melanopsin) or offset (S- and M-cones).

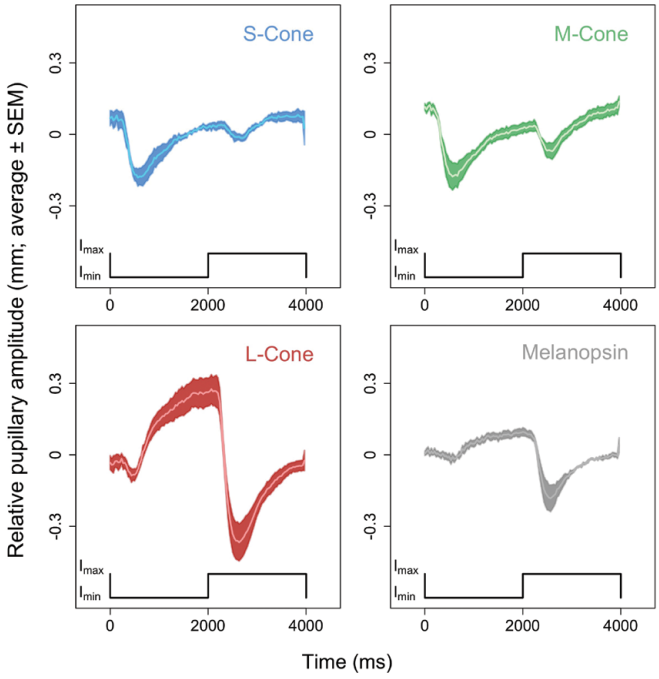

Figure 3. Averaged event-related pupil responses (ERPRs) ± SEM. Each panel contains data from 4 participants. Separate panels show S-cone (blue), M-cone (green), L-cone (red) and melanopsin (grey) ERPRs. Square-wave traces illustrate the photoreceptor-specific illuminance modulations.

By repeatedly incrementing and decrementing the illuminance for one photoreceptor over the course of 30 minutes, we expect that the net-output of that photoreceptor remained at a high level due to adaptation processes. As a control, participants also viewed a non-modulating stimulus that was the average of the incremental and decremental stimulus (Fig. 1A). Pupillary escape was thus expected to decrease as compared to constant light (i.e. more sustained constriction) when an 'excitatory' channel receives additional stimulation (Fig. 5A). The opposite was expected for an 'inhibitory' channel, such that the pupil shows more dilation during the 30-minute light exposure protocol. For each non-silent photoreceptor, a linear regression model was constructed to explain pupil diameter by elapsed time (0-30 minutes) and modulation frequency. The interaction coefficients were then extracted as a quantification of pupillary escape for each modulation frequency (Fig. 5B). For the S-cone and M-cone conditions, all frequency modulations were associated with enhanced pupillary escape as compared to the constant condition, although this effect was only significant for the 2 Hz condition for

both the S-cone ($p < 0.05$) and the M-cone ($p < 0.05$) modulations. For the L-cone and melanopsin conditions, all modulation frequencies resulted in a smaller pupillary escape as compared to the constant condition, which was significant for all conditions ($p < 0.001$ and $p < 0.05$ respectively) except for the 0.05 Hz melanopsin condition. This implies that stimuli are encoded as being less bright when S- or M-cones receive additional activation. The opposite was found for L-cones or ipRGCs, such that the stimulus is encoded as being brighter by the pupillary control system when these receptors receive additional activation. Pupillary escape test-statistics are summarized in Table S2.

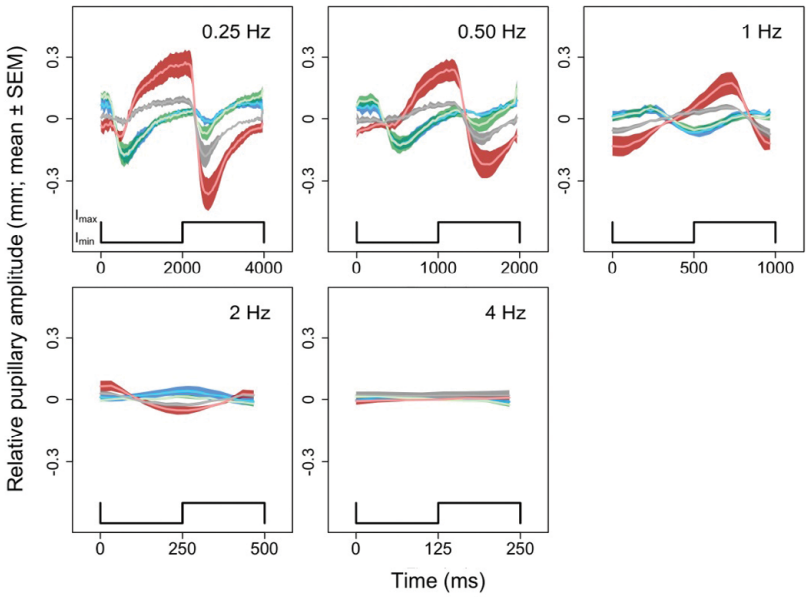

Figure 4. ERPRs for the 0.25 (top, left), 0.5 (top, middle), 1 (top, right), 2 (bottom, left) and 4 (bottom, right) Hz conditions. Square-wave traces illustrate the photoreceptor-specific illuminance modulations. Each panel contains data from all 16 participants (4 participants per trace), except for the 1 Hz S-cone modulation, which contains data from 3 individuals (see Materials and Methods).

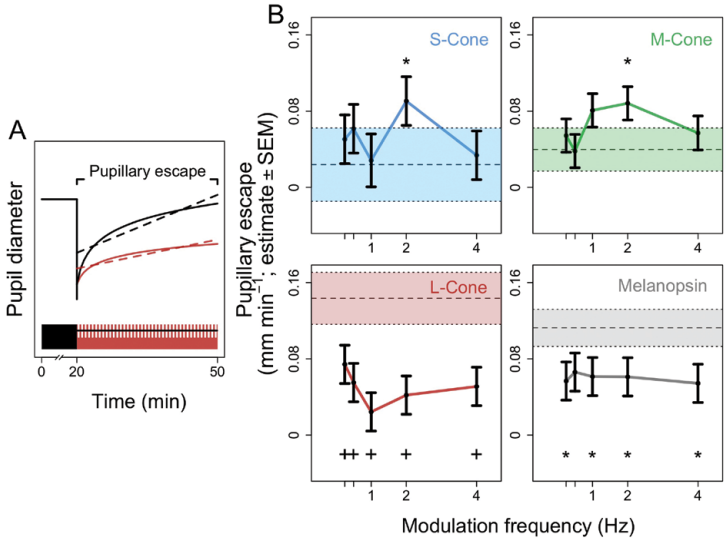

Figure 5. (A) Schematic of pupillary escape calculation under constant (black line, bottom) and L-cone modulating (red trace, bottom) light. There is more pupillary escape in the constant condition, as the fitted slope for the constant condition is steeper than for the modulating condition. (B) Estimated (see Materials and Methods) pupillary escape (mean ± SEM) over the 30-minutes light exposure window. Each panel contains data from 4 participants. Separate panels correspond to the S- (top, left), M- (top, right), L-cone (bottom, left) and melanopsin (bottom, right) modulations. The symbols indicate the significance level at which the estimated pupillary escape at each frequency modulation differs from the constant condition for each photoreceptor-modulation separately (* $p < 0.05$; + $p < 0.001$). The colored shaded areas indicate the level of pupillary escape for the constant conditions (dashed line: estimated pupillary escape, dotted boundaries: ± SEM).

Discussion

Recently, L- and M-cone opponent processing has been demonstrated to affect perceived brightness (7), the flicker electroretinogram (8, 9) and visually evoked potentials at occipital scalp locations (10). In all these parameters, selective increments of L-cone illuminance are encoded as brightness increments, whereas M-Cone increments are encoded as brightness decrements. S-cones have previously been reported to contribute negatively to visual luminance perception (14, 15). The ERPR results presented here extend this body of evidence to the domain of nonvisual photoreception, by showing that the human pupillary control system encodes both M-cone decrements and L-cone increments as brightness increments. We furthermore confirm the recently reported paradoxical pupillary constriction in response to S-cone increments (5). L-cone and melanopsin responses were of an excitatory nature, such that increments in photoreceptor-specific illuminance were followed by pupil constrictions. Importantly, ipRGCs have been shown to be involved in visual brightness discrimination in both mice

and humans (16). This places our results in context with psychophysiological findings, with strong indications that both nonvisual and visual brightness discrimination share a common pathway that starts in the retina. The large-amplitude ERPRs to L-cone modulations suggests a relatively large role for L-cones in the pupil response, which may be explained by the fact that the human retina expresses a relatively high number of L-cones in comparison to other receptors (17). Modulation of identical contrast for each receptor is therefore expected to result in relatively large-amplitude responses for L-cone isolating modulations. The finding that with higher frequency modulations the ERPR amplitude is dampened for all receptors, likely reflects that with increasing modulation frequencies, the pupil constriction dynamics become too sluggish to track the intensity modulations, resulting in dampened response amplitudes.

Interestingly, the dichotomy (S- and M-cones versus L-cones and melanopsin) observed in the ERPR results was mirrored by the effects of photoreceptor-specific flicker on pupillary escape: S-cone and M-cone flicker increased pupillary escape (more dilation) whereas L-cone and melanopsin flicker resulted in a reduced pupillary escape (less dilation) as compared to the constant light conditions. As the magnitude of pupillary escape is negatively correlated with light intensity (12) our findings raise the possibility that a flickering S-cone and M-cone modulating light source is encoded as being less bright by the pupillary control system than constant light. The opposite appears to be true for the L-cone and melanopsin modulations under the employed intensities and frequency modulations. For cones, the frequencies resulting in the largest pupillary escape effects occur around frequencies of 1-2 Hz. Such frequency tuning was expected. Photoreceptors require enough time to 'dark-adapt' to increase their sensitivity while at the same time enough time in the 'light' phase is required to evoke an increased overall response as compared to light of constant intensity. The optimal trade-off between light and 'dark' duration appears to lie in the 1-2 Hz range for pupillary escape, which has been reported previously (13). Our finding that effects on pupillary escape (Fig. 5) are only significant at a 2 Hz modulation for S- and M-cones is interesting, and suggests that long-term inhibitory S- and M-cone mediated effects are more frequency dependent than excitatory L-cone and melanopsin effects. Whether this is because recruitment of different retinal circuits, or because pupillary escape effects for S- and M-cones are generally smaller (where relatively small effects only transcend baseline noise for the optimal frequency) remains to be validated using electrophysiological experiments.

Although spectra were designed according to the method of silent substitution, photoreceptor-specific modulations should be interpreted as stimuli that are biased in favour of one photoreceptor type, as substitutions may not have been perfectly silent for the other types. This nuance is important as differences in photoreceptor spectral sensitivity are expected, as well as differences in effective photoreceptor spectral sensitivity across the retina due to the appearance of macular pigment in the fovea, mainly affecting short wavelength light (<500 nm). To explore how these factors may have affected our results, we performed 100 simulations, assuming peripheral (variation in peak spectral sensitivity of photoreceptors) or foveal retinal organization (assuming

both variation in photoreceptor sensitivity, individual variation in macular pigmentation and different foveal photopigment optical densities). As melanopsin and rods are known to be practically absent in the fovea and are thus not affected by macular pigmentation, only S-, M- and L-cone specific illuminance values were simulated for the fovea. These simulations revealed that a difference in cone contrast may indeed be expected between the fovea and the peripheral retina. More importantly, however, both in the fovea and in the periphery, stimuli were expected to be heavily biased towards the targeted photoreceptor (see Table S3 and S4), with minimal residual contrast for other receptor types (typically ~1-2% contrast with ~1-2% standard deviation). It is therefore likely that all constrictions measured (including the unexpected insignificant but visually observable constriction in response to I_{min} for the melanopsin condition) partially reflect the presence of residual cone contrast or apparent color changes, but that the large-amplitude constrictions mainly reflect the intended photoreceptor-modulations.

Our findings suggest that, in addition to the (L+M) – S color opponent ipRGCs (4), a subset of ipRGCs may receive color-opponent input on the red – green scale, with inhibitory and excitatory inputs from M-cone and L-cone dominated pathways respectively (+L-M). A similar statement can be made for a stimulus that shifts along the blue-cyan 'axis', where a blue to cyan shift results in a constriction and an opposite shift results in a dilation (+Mel –S). As there are +L-M but also -M+L midget ganglion cells, an explanation for our findings is that there are also +L-M and -L+M ipRGCs. Thus, although ipRGCs may be quite distinct from conventional RGCs (for example in the expression of melanopsin, dendritic arborization patterns and S-OFF (L+M)-ON responses), red-green colour discrimination may be a shared property of at least a subset of ipRGCs and midget ganglion cells. Our results are then likely explained by a higher number of +L-M ipRGCs (7). When these cells are the dominant response mediators when the stimulus shifts along the red-green scale, constrictions are expected for both L-cone increments and M-cone decrements. An alternative is that the M-cone inhibitory responses do not occur in the retina but may in fact be mediated by cortical processes. Although this possibility should not be neglected, the fact that inhibitory M-cone responses are recorded at the level of the retina (8, 9) suggests that the results reported here reflect properties of retinal processing.

It is worth noting that under a sine-wave modulation of M-cone illuminance, pupil diameter was previously not found to be out of phase with the M-cone illuminance modulation as we report here (18). This may be due to methodological differences, as in that study the central 10.5°of a circular 30° visual field was blocked. Based on our simulations (Fig. S3 and S4), it is not expected that the opposite phase M-cone responses are an artefact of incomplete silencing of foveal cones. A more parsimonious explanation is that variations along the red–green scale are most efficiently encoded at the fovea, with a decline towards the periphery (19). This decline in red-green sensitivity (+L-M or –L+M mediated) is steeper than for luminance (mediated by +L+M channels). It is therefore possible that M-cone modulating stimuli applied to the periphery predominantly feed into the achromatic luminance pathway (L+M) instead of the red-green chromatic pathway.

Hence, an M-cone increment delivered at the periphery will induce a larger response in the (L+M) – S ipRGCs than in the putative (+L-M) ipRGCs, resulting in pupil constriction.

It is important to consider that the rods were not silenced in any of the silent substitution pairs, which may have influenced our results, as in mice it has been shown that rods persist signaling at higher intensity levels than was previously thought (20). However, recent reports showed that in humans, rod-inducible pupil constrictions were measurable only at low light levels that are consistent with the human rod-saturation threshold determined previously (21). The lowest scotopic intensity used in the current study was 7.75 lux (I_{max} spectrum), which translates to 2.15 log scotopic trolands (sc td) at a pupil diameter of 3.13 mm (i.e. the average pupil diameter recorded over all testing sessions). At this background illumination level, increments in illuminance are not perceived via the scotopic system, which has been shown to saturate at ~1.0 - 1.5 log sc td under similar conditions (22). Thus, as rods are expected to be saturated at the light intensities employed here, it is also expected that rods are incapable of responding to illuminance modulations under these conditions in humans. Similarly, it is unlikely that rod-specific illuminance modulations have resulted in repeated dark- and light-adaptation, and that the pupillary escape effects are due to adaptation processes in rods. Therefore, with the light intensities used in the current study, it is unlikely that rod-intrusions have contaminated the results presented here.

Our results provide important insights into the functional retinal organization that affects brightness-coding in nonvisual light responses. Such advances may prove to be important in understanding brightness-coding in other nonvisual responses mediated by ipRGCs, such as modulation of alertness, melatonin suppression and timing of the sleep wake cycle.

Materials and Methods

Participants. For this study, 16 healthy young participants (10 female, 6 male), aged 22.13 ± 2.09 (average ± SD; range 19-25) were recruited. Participants were screened for color blindness by performing an Ishihara color blindness test. Failure to complete this test without errors was a direct exclusion criterion.

Pupillometer. Pupil diameter was measured simultaneously from both eyes at a sampling frequency of 30 Hz, using an Eyetribe® eye tracker (The Eye Tribe ApS, Copenhagen, Denmark) consisting of high-frequency infrared LED illumination and a camera allowing for quantification of pupil diameter (in camera pixels). To convert camera pixels into pupil diameter in millimetres, a calibration procedure was performed in which pupil diameter was simultaneously measured with the eye tracker (in pixels) and a separate pupilometer that expresses pupil diameter in millimetres (PLR-2000TM Pupillometer). At a distance of 40 cm between the eye tracker and the center between both eyes (i.e. the distance that was also maintained in the experiment by a chinrest), one pixel corresponded to 0.13 mm.

Light Box. The light source used was an in-house developed light box. Light-emitting diodes (LED) of five different colors (blue, cyan, green, yellow and red; Fig. S1) were controlled separately via an Arduino Uno (https://www.arduino.cc) microcontroller. For each light channel the intensity was controlled digitally (range: 0-255) via pulse-width modulation. The LED panel was placed in a non-transparent plastic box with a flat spectrum diffuser, required to obtain a uniform distribution of color and intensity over the light-emitting surface of the light box.

Silent Substitution. The method of silent substitution (6) is based on the principle of univariance, which states that two different light spectra will both affect a given photoreceptor cell identically, as long as the number of photons absorbed by its opsins is also identical between the two. This principle makes it possible to extract photoreceptor-specific illuminance values from any light spectrum, by correcting the spectrum for pre-receptoral filtering, the known absorption curves for each opsin, and finally the peak axial optical density of individual photoreceptors. A recently developed method that accounts for all of these factors was used to calculate photoreceptor-specific illuminance, expressed in lux (23). Whenever in the current study illuminance values were calculated, this method was used. When a light spectrum with a given set of photoreceptor-specific illuminance values is substituted for a different spectrum with the same set of illuminance values, none of the photoreceptors will be affected differently (i.e. substituting one spectrum for the other is silent for all photoreceptors). Similarly, it is possible to design a pair of spectra that can be silently substituted for all but one photoreceptor, granting independent control over the photoreceptor for which the substitution is non-silent. The previously described light box was designed to produce such pairs of silent substitution spectra. The typical strong linear relationship between LED intensity and each photoreceptor-specific illuminance value allows for predicting the photoreceptor-specific illuminance values that the light-box will produce, given a certain configuration of intensity settings. Importantly, the reverse is also true: given a desired set of photoreceptor-specific illuminance values, it is possible to calculate the required intensity level for each LED color that would produce a spectrum with these illuminance values. With the use of a mixed integer linear programming (MILP) solver ('lpSolveAPI' package in R (version 3.2.3)), the light intensity configuration settings required to obtain 4 pairs of silent substitution spectra were calculated, where each pair was either non-silent for one of the S-, M-, L-cone or the melanopsin photopigments. The solver was run with the constraint that the Michelson contrast for the non-silent photoreceptor was always 23% (Michelson contrast was calculated as $(I_{max} - I_{min})/ (I_{max} + I_{min})$ where 'I' denotes the photoreceptor-specific illuminance). Michelson contrast describes the contrast of a periodic signal, relative to its average value, and is a universally accepted metric of luminance contrast (24). In addition, the amount of melanopic lux for the 3 pairs of cone-specific silent substitution spectra was always set to ~8.5 melanopic lux, to control for the substantial melanopsin-mediated contribution to the sustained pupillary light response (12). The average amount of melanopic lux over the two melanopsin-specific silent substitution spectra was also set to this level, while maintaining the 23% contrast between minimal and maximal melanopic illuminance. Finally, the rods were not silenced

as these were expected to be saturated at intensities employed here (see Discussion). All spectra were validated with a spectroradiometer (SpecBos 1211 LAN UV, JETI Technische Instrumente GmbH). The spectra for each of the silent substitution pairs are presented in Figure 1A. An overview of the measured photometric properties of the silent substitution spectra can be found in Table S3.

Experimental Protocol. The study took place in the human research facility of the GELIFES institute at the University of Groningen, the Netherlands. Time of measurement was at daytime, limited to five time slots: 9-11, 10:30-11:30, 12-13, 13:30-14:30 and 15-16, where only one time slot was allowed per participant to minimize time of day effects. Participants (10 female, 6 male) were seated in isolated rooms in which light, sound and temperature conditions were regulated. Participants were asked to perform 6 testing sessions (1 session per condition, see Study Design) with a minimum of 2 days in between two testing sessions. At the start of each session, participants were seated in front of a desk, facing both the light-emitting surface of the light box and the eye tracker. Movement artefacts were minimized with the use of a chin rest. The height of the chin rest was adjusted to achieve horizontal alignment between the center of the eyes and the center of the light box. The distance between the eyes and the light box was 40 cm for all individuals. At this distance, the angular size of the light-emitting surface (17.5 x 8.5 cm) was 24.68° horizontally and 12.13° vertically. Participants were asked to remain seated as still as possible for the rest of the testing session while fixating on the center of the light box, which was marked with a 5 x 5 mm crosshair. When the participant was ready, the eye tracker was set to record the pupil diameter and the experimental protocol started with a 20-minutes dark adaptation period. After 20 minutes, the 30-min light schedule (corresponding to the condition the participant was assigned to for each particular testing session) started. After the light schedule was finished, the pupil recording was stopped and the data, consisting of one file containing timing of intensity configurations sent to the light box and one file containing pupil diameter measurements at a frequency of 30 Hz, were collected.

Study Design. The study followed a between-within subject design with non-silent photoreceptor as between and frequency modulation as within subject factors. The 16 participants were divided in groups of four, where a different photoreceptor was targeted for each group. In five of the six testing sessions, individuals were exposed to a pair of silent substitution spectra that alternated in a square-wave fashion at a frequency of either 0.25, 0.5, 1, 2 or 4 Hz. In the remaining session, individuals were exposed to light of constant intensity and spectral composition. In the constant light condition, the illuminance for the silenced photoreceptors was identical to the illuminance levels in both silent substitution spectra, whereas the illuminance for the 'non-silent' photoreceptor was now fixed at the average illuminance level of I_{max} and I_{min}. Within each group of four participants, the order of conditions was constant, 0.25, 0.5, 1, 2 and 4 Hz for two individuals and for the other two individuals the order was reversed. Figure 1B provides an example for the 0.25 Hz condition for all photoreceptor conditions.

Artefact Removal. All data-preprocessing was performed in R (version 3.2.3; Rstudio version 1.0.136). For the pupil diameter data, samples containing unreliable data were excluded from the dataset (for each individual testing session separately). These unreliable samples were primarily recognized by an absolute difference > 5 pixels between the pupil diameters of both eyes. This threshold was chosen as 95% of the data contained samples where the absolute difference in pupil size was < 5 pixels, and in case of a steady signal the pupil diameters of both eyes were visually consistently observed to be < 5 pixels apart for all individuals. Samples where at least one of the two pupil diameter values were missing were also considered unreliable samples and were removed accordingly. These instances occurred when the pupil was partially covered by the eye lid, during eye blinks and during movement. Next, additional artefacts that were not recognized by the procedures described above were identified and removed via a local polynomial regression fitting procedure ('loess' function in R (25)). With this procedure, a smoothed trend line was fitted through the data points, after which the residuals were extracted. Residuals > 1.5 inter-quartile-range (IQR) above or below the upper and lower quartiles of the residual distribution respectively were identified as outliers and removed from the dataset. For each sample, pupil diameter was calculated as the average pupil diameter of both eyes. Next, the pupil data were synchronized with the light-stimulus event log files. For one individual (S-cone modulation, 1 Hz condition), no usable data remained after artefact-removal. This subset of the data was therefore removed from further analysis procedures.

Event-related Pupil Responses (ERPRs). To construct ERPRs, the timing of each sample was first expressed relative to the latest onset of I_{min} for each sample. The average pupil diameter was then calculated for each of these relative time points, revealing the typical (average) pupil diameter trace for an I_{min} – I_{max} cycle. Relative pupillary amplitude was then calculated by subtracting the average of each individual trace from each constituent (averaged) data point, which yielded an ERPR with a mean of 0 for each individual separately. The amplitude of constriction in response to I_{min} and I_{max} was calculated for each individual separately. To do this, a loess trend line was fitted through the individual ERPRs (see Fig. 2). From the smoothed trend line, maxima and minima were determined for I_{min} and I_{max}. Constriction amplitudes were then calculated as the absolute difference between the maximum and the minimum pupil size, for I_{min} and I_{max} separately.

Pupillary Escape. For the analysis of pupillary escape, the data from each individual testing session were smoothed by averaging pupil diameter over bins of 30 seconds. Only the data obtained during the light intervention period were included.

Statistical Procedures. All statistics were performed in R (version 3.2.3; Rstudio version 1.0.136). A critical significance level (α) of 0.05 was maintained for all analyses. For the ERPR results, only the slowest frequency employed (0.25 Hz) was statistically analysed, as in the other conditions we observed intrusion of pupil responses (which

are relatively slow) to I_{max} into the I_{min} window and *vice versa*. For the other conditions, the ERPR traces are provided in Figure 4 as a reference. For the analysis of constriction amplitudes, four (one for each non-silent photoreceptor) simple regression models (base function 'lm' in R) were constructed. In these models, the independent variable was illuminance level (I_{min} versus I_{max}) and the dependent variable was pupil constriction amplitude. For these regression models, two-tailed p-values were calculated. Pupillary escape was estimated for each combination of photoreceptor/frequency modulation separately via a mixed linear regression approach using the 'lme4' package in R (26). Models were created for each non-silent photoreceptor separately with time, frequency modulation and the interaction term as fixed effects. To account for individual random variation in pupil diameter and pupillary escape, a random intercept and random slope was included in the model at the level of participant ID. For each model, the interaction contrasts were subjected to a multiple comparison procedure ('multcomp' package in R). This procedure effectively tests whether the change in pupil diameter over time for each of the flickering conditions is significantly different from the change over time in the constant light condition.

Data Availability. Original data, analyses, and R-codes can be accessed by contacting one of the corresponding author. The complete data-set (original and analyzed) and R-codes are also available at the data repository at the University of Groningen.

Ethics Statement. The study procedures were approved by the Medical Ethical Research Committee of the University Medical Centre Groningen (NL53779.042.15), Netherlands, and are in accordance with the Declaration of Helsinki (2013). All participants gave written informed consent.

Acknowledgements

We thank all subjects for participating in the experiment, and Gerard Overkamp for his help in developing the LED box. Financial support was obtained from an NWO-STW (Nederlandse Organisatie voor Wetenschappelijk onderzoek/Stichting voor de Technische Wetenschappen 10.13039/501100003958) OnTime Program Grant (project 12187).

References

1. Lee BB (2011) Visual pathways and psychophysical channels in the primate. *J Physiol* 589(Pt 1):41–7.
2. Güler AD, et al. (2008) Melanopsin cells are the principal conduits for rod-cone input to non-image-forming vision. *Nature* 453(7191):102–105.
3. Berson DM, Dunn FA, Takao M (2002) Phototransduction by retinal ganglion cells that set the circadian clock. *Science* 295(5557):1070–3.
4. Dacey DM, et al. (2005) Melanopsin-expressing ganglion cells in primate retina signal colour and irradiance and project to the LGN. *Nature* 433(7027):749–754.
5. Spitschan M, Jain S, Brainard DH, Aguirre GK (2014) Opponent melanopsin and S-cone signals in the human pupillary light response. 2014(7):2–7.
6. Estévez O, Spekreijse H (1982) The "silent substitution" method in visual research. *Vision Res* 22(6):681–91.
7. Parry NRA, McKeefry DJ, Kremers J, Murray IJ (2016) A dim view of M-cone onsets. *J Opt Soc Am A* 33(3):207–213.
8. McKeefry D, et al. (2014) Incremental and decremental L- and M-cone-driven ERG responses: I Square-wave pulse stimulation. *J Opt Soc Am A* 31(4):A159.
9. Kremers J, et al. (2014) Incremental and decremental L- and M-cone driven ERG responses: II. Sawtooth stimulation. *J Opt Soc Am A* 31(4):A170–A178.
10. Barboni MTS, et al. (2017) L-/M-cone opponency in visual evoked potentials of human cortex. *J Vis* 17(9):20.
11. Bartley SH (1939) Some effects of intermittent photic stimulation. *J Exp Psychol* 25(5):462–480.
12. Gooley JJ, et al. (2012) Melanopsin and rod-cone photoreceptors play different roles in mediating pupillary light responses during exposure to continuous light in humans. *J Neurosci* 32(41):14242–14253.
13. Vartanian G V., Zhao X, Wong KY (2015) Using flickering light to enhance nonimage-forming visual stimulation in humans. *Investig Ophthalmol Vis Sci* 56(8):4680–4688.
14. Lee J, Stromeyer CF (1989) Contribution of human short-wave cones to luminance and motion detection. *J Physiol* 413:563–93.
15. Stockman A, MacLeod DI, DePriest DD (1991) The temporal properties of the human short-wave photoreceptors and their associated pathways. *Vision Res* 31(2):189–208.
16. Brown TM, et al. (2012) Melanopsin-based brightness discrimination in mice and humans. *Curr Biol* 22(12):1134–1141.
17. Hofer H, Carroll J, Neitz J, Neitz M, Williams DR (2005) Organization of the Human Trichromatic Cone Mosaic. 25(42):9669–9679.
18. Cao D, Barrionuevo PA (2015) A five-primary photostimulator suitable for studying intrinsically photosensitive retinal ganglion cell functions in humans. *J Vis* 15:1–13.
19. Hansen T, Pracejus L, Gegenfurtner KR (2009) Color perception in the intermediate periphery of the visual field. *J Vis* 9(4):26.1-12.
20. Altimus CM, et al. (2010) Rod photoreceptors drive circadian photoentrainment across a wide range of light intensities. *Nat Neurosci* 13(9):1107–12.
21. Barrionuevo PA, Cao D (2016) Luminance and chromatic signals interact differently with melanopsin activation to control the pupil light response. *J Vis* 16(11):29.
22. Adelson EH (1982) Saturation and adaptation in the rod system. *Vision Res* 22(10):1299–1312.
23. Lucas RJ, et al. (2014) Measuring and using light in the melanopsin age. *Trends Neurosci* 37(1):1–9.
24. Switkes E, Crognale MA (1999) Comparison of color and luminance contrast: Apples versus oranges? *Vision Res* 39(10):1823–1831.
25. Cleveland, W.S., Grosse, E. and Shyu WM (1992) Local regression models. *Statistical Models in S*, pp 309–376.

26. Bates D, Mächler M, Bolker B, Walker S (2014) Fitting Linear Mixed-Effects Models using lme4. *eprint arXiv:14065823* 67(1):51.
27. Stockman A, Sharpe LT (2000) The spectral sensitivities of the middle- and long-wavelength-sensitive cones derived from measurements in observers of known genotype. *Vision Res* 40(13):1711–1737.
28. Beatty S, Koh HH, Carden D, Murray IJ (2000) Macular pigment optical density measurement: a novel compact instrument. *Ophthalmic Physiol Opt* 20(2):105–11.
29. Bone RA, Landrum JT, Cains A (1992) Optical density spectra of the macular pigment in vivo and in vitro. *Vision Res* 32(1):105–110.

Supplementary information

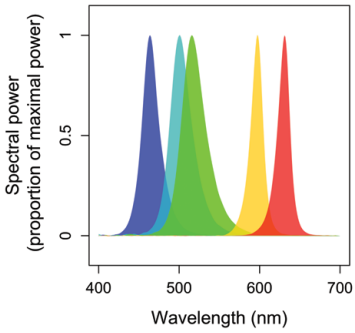

Figure S1. Spectral power distributions of the LEDs used in this experiment. The light box contained blue, cyan, green, yellow and red LEDs, with maximal spectral power at 465, 500, 515, 595 and 635 nm respectively.

Table S1. Regression coefficients and test statistics for the pupil constriction amplitudes (0.25 Hz condition).

	I_{min} constriction (mm; mean ± SEM)	I_{min} t-value (df)	I_{max} constriction (mm; mean ± SEM)	I_{max} t-value (df)
S-Cone	0.25 + 0.05	4.93 (6) **	0.07 ± 0.05	1.29 (6)
M-Cone	0.29 ± 0.05	5.46 (6) **	0.11 ± 0.05	2.02 (6)
L-Cone	0.07± 0.10	0.73 (6)	0.64 ± 0.10	6.57 (6) ***
Melanopsin	0.03 ± 0.04	0.61 (6)	0.29 ± 0.04	6.48 (6) ***

(** $p < 0.01$; *** $p < 0.001$).

Table S2. Test statistics for pupillary escape. Pupillary escape is expressed relative to the constant condition

	Frequency modulation (Hz)	Pupillary escape (mm min^{-1}) (mean ± SEM)	z-value (df)	p-value
S-cones	0.25	0.026653 ± 0.025538	1.044 (5)	0.7498
	0.5	0.037691 ± 0.025538	1.476 (5)	0.4410
	1	0.004438 ± 0.027770	0.160 (5)	0.9999
	2	0.066688 ± 0.025538	2.611 (5)	0.0383*
	4	0.009780 ± 0.025538	0.383 (5)	0.9952
M-cones	0.25	0.014579 ± 0.017508	0.833 (5)	0.8753
	0.5	-0.001708 ± 0.017508	-0.098 (5)	1.0000
	1	0.041067 ± 0.017527	2.343 (5)	0.0772
	2	0.048456 ± 0.017508	2.768 (5)	0.0247*
	4	0.017300 ± 0.017861	0.969 (5)	0.7960
L-cones	0.25	-0.06932 ± 0.02013	-3.444 (5)	0.00266**
	0.5	-0.08842 ± 0.02013	-4.393 (5)	< 0.001***
	1	-0.11918 ± 0.02013	-5.922 (5)	< 0.001***
	2	-0.10159 ± 0.02013	-5.048 (5)	< 0.001***
	4	-0.09248 ± 0.02013	-4.595 (5)	< 0.001***
ipRGCs(Melanopsin)	0.25	-0.05584 ± 0.02005	-2.785 (5)	0.0234*
	0.5	-0.04644 ± 0.02005	-2.316 (5)	0.0823
	1	-0.05117 ± 0.02005	-2.552 (5)	0.0447*
	2	-0.05144± 0.02007	-2.563 (5)	0.0436*
	4	-0.05822 ± 0.02005	-2.904 (5)	0.0162*

(* $p < 0.05$; ** $p < 0.01$; *** $p < 0.001$).

Table S3. Photometric properties of the different silent substitution spectra, assuming peripheral retinal organization (23). For each non-silent photoreceptor, measured photoreceptor-specific illuminance values (in lux) are provided for the I_{min} and I_{max} spectra separately. In the far-left column, S, M and L correspond to S-, M- and L-cone specific lux. R and I correspond to rhodopic and melanopic lux levels respectively. The Michelson contrast between I_{min} and I_{max} is provided for each non-silent photoreceptor condition (C_m). Bold and underlined values indicate the Michelson contrasts for the receptors that were selectively modulated. Standard deviations describe the variation in lux-values and resulting contrasts expected from inter-individual variation in peak spectral sensitivity of photoreceptor types. Standard deviations are obtained via 100 simulations assuming varying peak spectral sensitivities about mean values of 419, 530.8, 558.4 and 480 nm and standard deviations of 0.8, 0.9, 1.5 and 1.5 nm for S-, M-, L-cones and melanopsin respectively (5).

	S-Cones			M-Cones			L-Cones			ipRGCs (Melanopsin)		
Lux	I_{min}	I_{max}	C_m	I_{min}	I_{max}	C_m	I_{min}	I_{max}	C_m	I_{min}	I_{max}	C_m
S	4.18	6.82	**23.95**	1.81	1.87	1.61	1.91	1.87	-1.09	1.37	1.38	0.09
(± SD)	0.09	0.13	**0.10**	0.07	0.05	0.65	0.05	0.07	0.60	0.03	0.04	0.40
M	7.24	7.40	1.11	10.03	16.74	**25.07**	10.49	9.83	-3.25	11.90	11.92	0.11
(± SD)	0.03	0.00	0.19	0.19	0.21	**0.32**	0.06	0.18	0.67	0.12	0.03	0.39
L	7.03	7.29	1.80	20.19	21.58	3.35	13.11	19.65	**19.93**	14.81	14.36	-1.53
(± SD)	0.01	0.03	0.27	0.70	0.13	1.42	0.13	0.54	**0.83**	0.07	0.17	0.38
I	8.65	8.73	0.44	8.28	8.68	2.38	8.74	8.30	-2.57	6.73	10.7	**19.47**
(± SD)	0.09	0.03	0.69	0.09	0.20	0.59	0.19	0.09	0.53	0.16	0.27	**0.04**
R	8.43	7.92	-3.10	7.80	10.21	13.42	9.36	7.75	-9.40	7.81	11.58	22.77

Table S4. Photometric properties of the different silent substitution spectra, assuming foveal retinal organization. In the far-left column, S, M and L correspond to S-, M- and L-cone specific lux. Standard deviations are obtained via 100 simulations assuming varying peak spectral sensitivities about mean values of 419, 530.8, 558.4 and standard deviations of 0.8, 0.9, 1.5 nm for S-, M- and L-cones. Furthermore, optical densities were assumed to be 0.4, 0.5 and 0.5 for S-, M- and L-cones respectively (27). Macular pigment optical density was additionally varied about a mean value of 0.496 (at 460 nm) and standard deviation of 0.257 (28), based on the macular pigment density spectrum reported by (29).

	S-Cones			M-Cones			L-Cones			ipRGCs (Melanopsin)		
Lux	I_{min}	I_{max}	C_m	I_{min}	I_{max}	C_m	I_{min}	I_{max}	C_m	I_{min}	I_{max}	C_m
S	3.69	5.86	**22.63**	1.80	1.77	-0.80	1.78	1.82	1.15	1.30	1.41	3.84
(± SD)	0.35	0.66	**0.84**	0.10	0.09	0.92	0.07	0.09	0.56	0.08	0.07	2.14
M	6.75	6.99	1.81	10.42	19.35	**29.96**	11.11	10.12	-4.69	13.52	12.23	-4.93
(± SD)	0.26	0.24	0.38	0.26	0.86	**1.75**	0.08	0.28	1.07	0.79	0.20	2.29
L	6.84	7.08	1.71	22.48	23.37	1.98	13.94	21.89	**22.16**	15.86	15.04	-2.64
(± SD)	0.16	0.11	0.55	0.91	0.61	1.47	0.18	0.80	**1.11**	0.60	0.31	1.31
I	8.65	8.73	0.44	8.28	8.68	2.38	8.74	8.30	-2.57	6.73	10.7	**19.47**
(± SD)	0.09	0.03	0.69	0.09	0.20	0.59	0.19	0.09	0.53	0.16	0.27	**0.04**

Chapter 4

Circadian photoreception as a sundial responding to intensity and spectral composition

Tom Woelders,
Emma J. Wams,
Marijke C.M. Gordijn,
Domien G.M. Beersma
and Roelof A. Hut

Revision published in Scientific Reports (8, 15214)

Abstract

The mammalian circadian system encodes both absolute levels of light intensity and color to phase-lock (entrain) its rhythm to the 24-h solar cycle. The evolutionary benefits of circadian color-coding over intensity-coding per se is yet far from understood. A detailed characterization of daylight is crucial in understanding how and why circadian photoreception integrates color and intensity information. To this end, we continuously measured 100 days of sunlight spectra over the course of a year. Our analyses suggest that circadian color-coding may have evolved to cope with cloud-induced variation in light intensity. We proceed to show how an integration of intensity and spectral composition reduces day-to-day variability in the synchronizing signal (*Zeitgeber*). As a consequence, entrained phase angle of the circadian clock will be more stable, which will be beneficial for the organism. The presented characterization of daylight dynamics may become important in designing lighting solutions aimed at minimizing the detrimental effects of light-at-night in modern societies.

Mammals possess a circadian oscillator, located in the suprachiasmatic nucleus (SCN) of the hypothalamus. On their own, circadian clocks rarely cycle with a period of exactly 24 hours[1]. For the circadian oscillator to serve as a reliable internal representation of the light-dark cycle, a stable phase relationship is required between the solar cycle and the circadian rhythm. This is realized via entrainment; as first described by Christiaan Huygens illustrating how two interacting oscillators assume a common period and stable phase relationship[2]. The circadian oscillator system interacts with the solar cycle via its sensitivity to light; the most potent time-cue (i.e *'Zeitgeber'*, german for time-giver) for circadian timekeeping. Light accelerates or decelerates the cycling rate of the circadian oscillator, with direction and magnitude depending on the timing of light reception. Light in the early morning typically accelerates the clock, whereas light in the late evening slows it down[3]. This response is positively related to light intensity[4,5]. Entrainment occurs when the phase-relationship between the circadian oscillator and the solar cycle is stable, such that the daily integrated effect of light on the cycling-rate of the clock makes up for the difference that exists between the periods of the daily solar cycle (T) and the circadian oscillator (τ). The phase-angle difference between the solar cycle and the circadian oscillator satisfying this condition is known as the phase angle of entrainment. In the average human, the phase angle of entrainment would ensure a daily acceleration of 0.2 hours[6,7].

Thus, circadian clocks have evolved to represent solar time by entraining to a signal that closely corresponds to solar time (i.e. light intensity), implying that circadian clocks have evolved to obtain maximal stability from day to day. However, considering the circadian system as an oscillator driven solely by light intensity poses a potential problem in fulfilling this purpose. For example, during an overcast evening following clear-sky days, the delaying effect of light will be smaller than usual, which would cause an unwanted advance. It has therefore been proposed that circadian systems have evolved color-vision to obtain a more accurate indication of solar time[8–12]. This is plausible, as wavelength-dependent photon scattering in the atmosphere depends on solar angle, such that distinct changes in the color of the sky may be observed during twilight transitions[13]. However, whether color indeed provides additional information on solar time over intensity *per se* remains unclear. Additionally, how color and intensity information can be integrated to maximize *Zeitgeber* stability has not been systematically described. Therefore, we collected 100 days of omnidirectional daylight spectra over the year under varying weather conditions to provide the first data-driven evidence that the color of the sky, in addition to its intensity, provides more information on solar time than intensity alone.

Methods and Materials

Data collection

Measurements were performed on the roof of the Bernoulliborg, a 27 meters high building located on the Zernike campus of the University of Groningen, the Netherlands (latitude: 53.24°, longitude: 6.54°), providing clear measurements of the horizon. As our parameter of interest was the perceived daylight spectrum irrespective of the direction of gaze, we decided to measure spherical (or scalar) irradiance, which is defined as the irradiance on a point where all directions are weighted equally[14]. To this end, a special designed spherical milk glass diffusor was used (4pi diffusor), which was designed to project incident light from any direction onto an inserted cosine corrected diffusor mounted on a 5m long fiber optics cable. Importantly, this sensor efficiently captures light from angles close to the horizon, which is required given our interest in twilight color changes[13]. The fiber optics cable was used to guide incoming light onto the light-sensitive element of a SpecBos 1211 LAN UV spectroradiometer (JETI Technische Instrumente GmbH, Germany). The setup, which was fully calibrated by the manufacturer, thus allowed for the measurement of irradiance from all directions simultaneously, except for the part of the sphere blocked by the diffusor part and fiber optics cable. For semi-continuous sampling, measurements were programmed to start automatically each full minute. The integration time of the device was set to automatic mode, meaning that the duration of each measurement was inversely related to the intensity of the captured light to avoid under- or overexposure of the light-receiving element. Consequently, the sampling frequency of once per minute was reduced during darkness. A total of 88960 samples were acquired over the time course of 100 days throughout the year (11, 30, 22 and 37 spring, summer, autumn and winter days respectively). Each sample contained one irradiance value (W/m^2) for each wavelength within the 380-780 nm range at a resolution of 1 nm. All light intensity data were expressed in photons cm^{-2} s^{-1} and further processed in *R* (version: 3.2.3), using the 'RStudio' shell (version: 1.0.136).

Setup validation

Human color discrimination occurs via a well-described comparison between the activation of short-, mid- and long-wavelength cones (S-, M- and L-cones respectively) in the human retina[15]. For any stimulus, its perceived color can be numerically described, typically by calculating the two CIE 1931 *xy* chromaticity coordinates from the associated irradiance spectrum. For validation purposes, we calculated the CIE 1931 *xy* chromaticity coordinates of all samples, together with the total irradiance measured per solar angle integrated over the 380-780 nm wavelength range (see Supplementary Fig. S1). These values corresponded closely to previously reported values using daylight measurements in an urban setting [13]. As expected from these published data, light pollution was apparent in the dataset until solar elevations exceeded -6° over the horizon as measurements were performed on the edge of an urban environment. Therefore, solar angles below -6° were discarded from the data, leaving a range of -6° to 60° for analysis.

Human circadian photometrics

In the mammalian retina, light information is conveyed to the SCN via a specialized subset of retinal ganglion cells that encode irradiance via expression of the melanopsin photopigment. Both, in primates (macaques) and rodents, these intrinsically photosensitive retinal ganglion cells (ipRGCs) have additionally been shown to receive indirect synaptic input from cones, such that spectral changes modulate the ipRGC response in addition to changes in absolute intensity[10,16,17]. In the macaque retina, S-cones exert an inhibiting effect on the ipRGC response and M- and L-cones together fulfill an excitatory role[10]. For human circadian photoreception, evidence regarding the role of cones in circadian entrainment is not conclusive, posing a potential problem for calculating the circadian equivalent of visual chromaticity coordinates. However, given the remarkable similarity of color-coding in human and macaque retinae[18], together with recent findings that the human pupillary control system encodes color information in a manner very similar to what was reported for macaques[19,20], we decided to formulate a human circadian color index as the difference between L+M and S-cone activation, calculated as (log L-photons + log M-photons)/2 – log S-photons. This human color index describes the color of daylight on a blue-yellow axis, where the bluest and yellowest light respectively result in the smallest and largest color-indices. In order to extract these values from the irradiance spectra, it is necessary to calculate the estimated number of photons absorbed per second for each photoreceptor separately. First, each measured spectrum was corrected for pre-receptoral lens filtering of mainly the shortest visible wavelengths according to a reported human lens-transmittance function for a 30 y/o standard observer[21]. The estimated number of photons transmitted through the lens and projected onto a 30 y/o human retina (i.e. lens-corrected photons) was calculated from the lens-corrected irradiance values for each wavelength separately. The estimated number of absorbed photons per second per cm^2 was then calculated for S-, M- and L-cones and the intrinsic ipRGC (melanopic) absorption, hereafter referred to as lens-corrected S-, M-, L-, and melanopic photons. These estimations were based on full photopigment absorption curves[22] and published λ_{max} values (wavelength of maximal sensitivity) of human photopigments[23]. The widths of the absorption curves were corrected to accommodate for the broadening effect of peak optical axial density, with density values set to 0.3, 0.38, 0.38 respectively for the S-, M- and L-cones, and to a value of 1 for melanopsin[21].

Data preparation for solar angle estimations

The integration time of the spectrometer increases at lower light levels (lower solar angles) to ensure reliable spectral intensity measurements. This resulted in non-uniform data distribution over each solar angle, which may induce modelling artifacts due to an underrepresentation of samples at low solar angles. Therefore, a resampling procedure was performed to obtain a uniform distribution of solar angles over the complete dataset. The dataset was first divided into 1-degree solar angle bins. The target sample size of each bin was then set to the size of the largest bin (2382 spectral measurements per solar angle bin) and resampling was performed until each bin reached the target sample size,

resulting in a uniform sampling distribution over each solar angle. Thus, the uniform dataset contained 159594 samples, divided over 67 solar angle bins, with 2382 samples per bin. Additionally, color index and log melanopic photons were normalized by z-transformation, yielding an average of 0 and a standard deviation of 1 for these metrics.

Predictive modelling of solar angle by color and intensity

To model the nonlinear relationship between solar angle, color and intensity, a *k*-nearest neighbors (KNN) machine learning approach was employed. KNN models are non-parametric; no a-priori assumptions are made on the relationship between the explanatory and dependent variables. This minimizes the possibility of incorrectly modelling the underlying data distribution, and is therefore well-suited to reveal nonlinear patterns in the data. Before constructing a KNN-model, the dataset is usually partitioned into a training set and a validation set. The algorithm underlying KNN modelling identifies the *k* nearest neighbors for each sample in the training set, based on Euclidean distance on the color vs. intensity plane. Each sample in the training set is then assigned the average solar angle of its *k* nearest neighbors. Samples that are similar in both color index and intensity are thus likely to be assigned similar solar angle estimates. When such patterns have been learned using the training data, the *k* nearest neighbors from the training set are identified for each sample in the validation dataset. The average estimated solar angle of these *k* nearest neighbors from the training set is then calculated for each sample in the validation set, effectively providing an estimated solar angle for each sample in the validation set. The root mean square error (RMSE) between estimated and measured solar angles in the validation set serves as a performance measure for the constructed model. A low RMSE value indicates that the model that was constructed based on the training data provides accurate estimations on the independent dataset that was left out of the training procedure, and can thus be regarded as a reliable description of nonlinear patterns in the entire dataset.

The optimal number of nearest neighbors was determined via *K*-fold repeated cross-validation. In this process, the data is partitioned into *K* (*K* = 10, not to be confused with *k*) equally sized randomly chosen subsets for each value of *k* (1 to 40 in steps of 1), where *K*-1 subsets are combined and used as training data and the remaining subset is used as validation data. This step is then performed *K* times, each time using a different part of the data (10%) as the validation set, resulting in 10 models for each value of *k*. This procedure was additionally performed 3 times to maximize reliability of the model, each time randomly assigning different samples to the 10 subsets, such that for each value of *k*, 3 x 10 models were fit. The average RMSE was then calculated for each value of *k*, where the 30 models constructed for *k* = 21 described predictable patterns in the dataset most accurately. This model was then used to assign an estimated solar angle to each sample in the uniform dataset. This procedure is effectively a spatial smoothing process, and reveals spatial patterns in the color vs. intensity plane that are mostly associated with particular solar angles. KNN models were trained using the 'caret' library in *R*.

Weather conditions

Cloud cover information for the measurement days was obtained from the Dutch national meteorological institute (KNMI). A KNMI weather station is located at Groningen Airport Eelde, the Netherlands (latitude: 53.13°, longitude: 6.59°), at a distance of 14km from our spectral measurement location, which keeps records on the average cloud cover amount per day. This station is equipped with a cloud-sensor that works according to the light detection and ranging (LIDAR) principle. Once every 15 seconds, the sensor sends an infrared signal vertically into the atmosphere and determines the presence of a cloud depending on the recurrent signal. The total cloud cover amount over a 24-hour day is then calculated from the percentage of cloud-cover detections over a day. Cloud cover (i.e. KNMI index) is expressed on a linear 0-8 scale (i.e. 'oktas'), where a value of 8 means that at every sample over the 24-hour day the sky was not detectable, whereas a value of 0 indicates that at none of the samples a cloud was detected.

Statistical procedures

Linear regression models (for the data presented in Figure 3A, B and C) were constructed in *R*, using the native '*lm*' function, where a significant contribution of individual terms was determined using the '*drop1'* function. Student's t-tests were performed using the native *'t.test'* function. A critical p-value of 0.05 was maintained for these analyses. Two-dimensional density distributions (for the data presented in Figures 2A, B and C and 4C) were calculated for data visualization using the Two-Dimensional Kernel Density Estimation function ('*kde2d')* from the '*MASS*' library in *R*. These 2D-density distributions were calculated from the uniform dataset. For data visualization of the combined model (for data presented in Figure 3C), a smoothed relationship between color and estimated solar angle was obtained per intensity bin (steps of 0.25 log melanopic photons), by local polynomial regression fitting (native R *'loess'* function)[24]. The *loess* procedure was also used to assign cloud-corrected melanopic photon values to individual samples based on the associated estimated solar angles (for data presented in Figure 5B). First, a *loess* model was created to predict melanopic photons from solar angle for clear-sky data only. Then, the estimated solar angle of each sample (obtained using the KNN model) was plugged into this *loess* model, yielding a predicted number of cloud-corrected melanopic photons for each sample.

Results

Solar-angle dependent effects of cloud cover on the daylight spectrum

Retinal irradiance (i.e. lens-corrected photons) increases with increasing solar angles (Fig. 1A), but the decrease of lens-corrected photons by cloud cover, depends on wavelength and solar angle (Fig. 1B). Typically, incident photons of shorter wavelengths are less affected by cloud cover than photons of longer wavelengths, especially during lower solar angles (-6° to 12°).

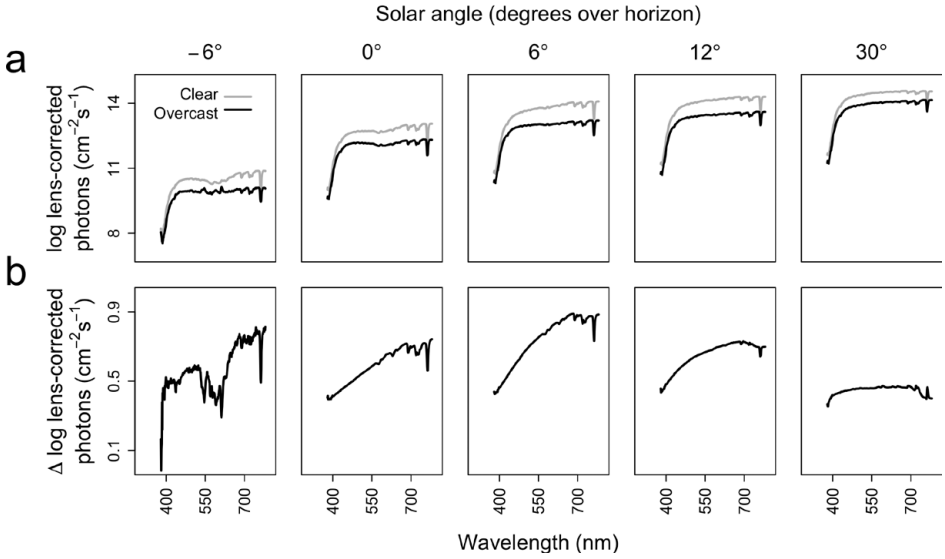

Figure 1. Progression of daylight power spectra. *A:* progression of daylight power spectra for 5 representative solar angles, for 11 clear (KNMI index < 3) and 43 overcast (KNMI index > 6) days. *B:* Difference between power spectra at clear and overcast skies for 5 representative solar angles.

Effects of cloud cover on encoded intensity and color

To quantify how these dynamics in daylight spectra are processed by the human retina, the effect of solar angle and weather conditions on circadian light intensity (i.e. log melanopic photons) and color-index were determined. The log-transformed integration (380-780) of human lens-corrected photons was included as a reference. As expected, the total number of lens-corrected (melanopic) photons increased with increasing solar angles, and at each solar angle, cloud cover decreased the amount of (melanopic) photons (Fig. 2A and B). On average, color index increased with increasing solar angles, indicating a transition from 'blue' to 'yellow' (Fig. 2C). Clear skies are typically relatively yellow compared to overcast skies, especially within the 0-30° solar angle range.

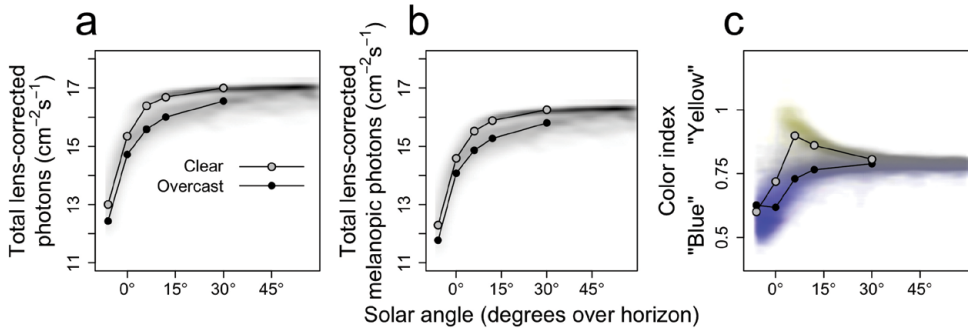

Figure 2. Density profiles of intensity and color index against solar angle. 2D density profiles of the total dataset for solar angle against *A:* total lens-corrected photons, *B:* total lens-corrected melanopic photons and *C:* color index. Higher transparency indicates a lower density of samples. Samples with a color index lower or higher than average are displayed in blue or yellow respectively, with the purest hues at the extremes. Overlays are drawn for the average clear (n=11; KNMI index <3) and overcast (n=43; KNMI index >6) days.

We then determined the effects of various amounts of cloud cover on the lens-corrected (melanopic) photons (Fig. 3A and B) and color index (Fig. 3C). Linear regression analyses revealed a significant main effect of cloud cover amount on lens-corrected photons ($F(1,39) = 272.83$, $p < 0.001$) and lens-corrected melanopic photons ($F(1,39) = 269.09$, $p < 0.001$). Each additional increase of cloud cover (on KNMI scale 0 (clear sky) to 8 (sky not visible)), decreased the number of lens-corrected and melanopic photons by 0.09 ± 0.006 and 0.08 ± 0.005 (±SEM) log photons respectively. An interaction effect was observed when explaining color index by both the amount of cloud cover and solar angle ($F_{4,35} = 16.31$, $p < 0.001$). Typically, more cloud cover was related to more 'blue' skies, an effect that was especially pronounced at solar angles between 0° and 30° (Fig. 3). These analyses reveal that there is a solar-angle dependent effect of cloud cover on sunlight color, where clouds cause a blue-shift of the sunlight spectrum especially at lower solar angles. This could potentially provide the circadian system with the information necessary to obtain a solar-angle dependent *Zeitgeber* signal regardless of cloud conditions.

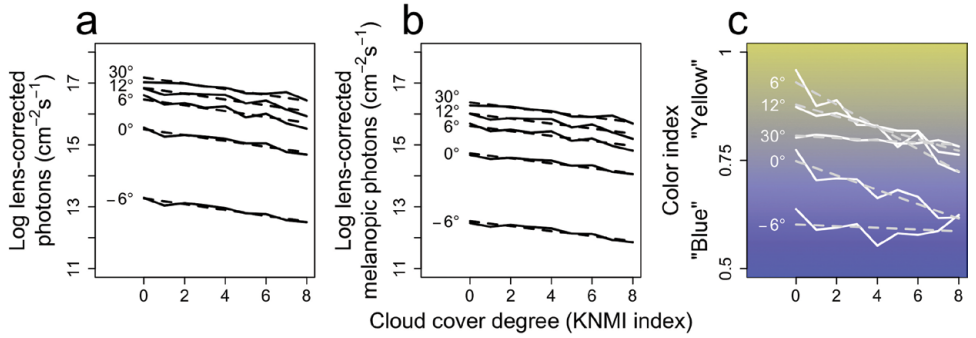

Figure 3. Effects of cloud cover on intensity and color. Effect cloud cover on *A:* total lens-corrected photons, *B:* total lens-corrected melanopic photons and *C:* color index. Dashed lines represent linear regression6 model fits.

Predictable patterns in the color vs. intensity plane

To reveal spatial patterns in the color vs. intensity plane that may be used by the circadian photoreceptive system to obtain accurate solar angle estimations, a *k*-nearest neighbors model was constructed (see methods). This model provides solar angle estimations for all samples ($R^2 = 0.87$), based on intensity and color index (Fig. 4A). Solar angle was found to be related with intensity and color index in a nonlinear manner, according to predictable weather and solar angle-driven patterns (Fig. 4B and C). For example, at a solar angle of 6°, 'yellow' skies, intermediate color indices and 'blue' skies are associated with high, low and intermediate intensities respectively (Fig. 4B). These different clusters reflect samples obtained under clear skies, completely overcast skies and partially overcast skies where direct sunlight is blocked. The circadian system may thus use these predictable cloud-induced patterns observable in the data to obtain a more accurate estimation of solar time, irrespective of overcast conditions.

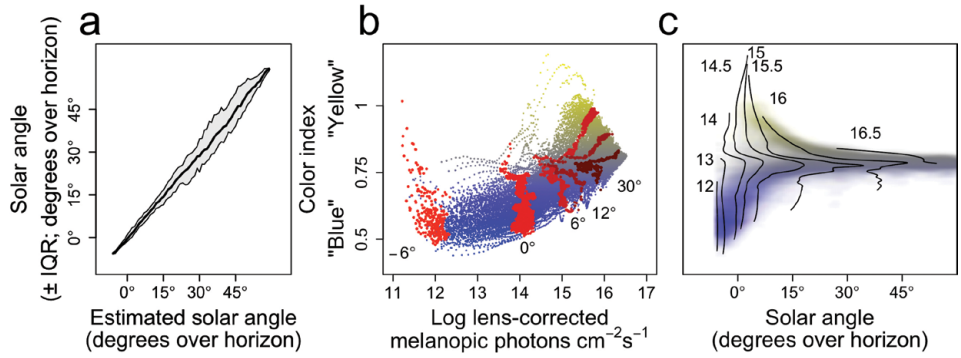

Figure 4. Solar angle estimations by circadian photoreception. *A:* median solar angle plotted against the estimated solar angle. The grey shaded area illustrates the interquartile range around the median solar angles. *B:* all possible intensity and color index combinations (on a blue-yellow scale). The red points indicate the intensity and color combinations that resulted in 1 of 5 representative solar angle estimates (where the brightest and darkest shades correspond to the lowest and highest solar angle estimates respectively). *C:* 2D density profile for color index against solar angle. The overlays provide smoothed (see methods) solar angle estimations for eight representative intensities (log melanopic photons). Lower solar angles are associated with a relatively large color range compared to the intensity range, and *vice versa* for higher solar angles.

Increasing *Zeitgeber* stability by estimating solar time

We next turned to the question as to how such estimations of solar angle may be translated into a *Zeitgeber* signal that is more stable and provides more information on solar time than a signal depending solely on light intensity. One possibility is that the circadian system 'corrects' the effect of perceived light intensity when the associated color index indicates overcast skies. Such a process may be used to alter the strength of the entraining signal to mimic a clear-sky response associated with the estimated solar angle. We obtained the clear-sky progression of intensity by calculating the 95-percentile boundary of the distribution of melanopic photons for each solar angle (1-degree bins) separately (Fig. 5A). For each solar angle estimation, we next calculated the number of melanopic photons that would occur at that solar angle under clear skies (i.e. cloud-corrected melanopic photons). The number of cloud-corrected melanopic photons is thus an approximation of the number of melanopic photons under a clear sky, by making use of the known relationship between solar angle and cloud-corrected melanopic photons. Per solar angle, the distribution in lens-corrected melanopic photons was broader than for cloud-corrected melanopic photons, indicating that the latter is more resilient to weather-induced noise and is subject to relatively little day-to-day variability (Fig. 5B). A comparison of the inter-quartile ranges for melanopic and cloud-corrected melanopic photons revealed that for solar angles above 0 degrees over the horizon, cloud-corrected melanopic photons provide the most reliable *Zeitgeber* signal for the human circadian system (Fig. 5C). On average, the IQR for cloud-corrected melanopic photons was 0.13 ± 0.14 (±SD) and 0.51 ± 0.14 (±SD) for the uncorrected number of melanopic photons (t_{132} = 15.85, $p < 0.001$).

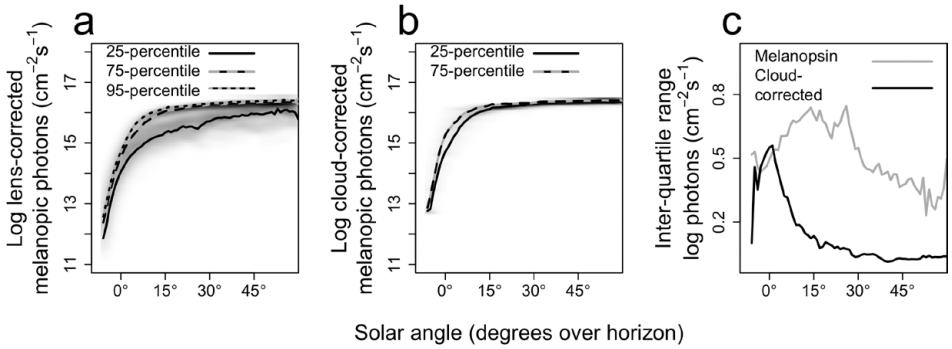

Figure 5. Spectrum corrected solar angle estimations minimize *zeitgeber* day-to-day variability. *A:* 2D density profile for the melanopic photons progression, including 25-, 75- and 95-percentile boundaries per solar angle (1-degree bins). *B:* 2D density plot of cloud-corrected melanopic photons, including 25- and 75-percentile boundaries. *C:* Comparison of the inter-quartile range in melanopic and cloud-corrected melanopic photons per solar angle (1-degree bins).

Discussion

Thus far, it has been difficult to formulate clear hypotheses regarding the evolutionary benefits of circadian color-coding, as a detailed evaluation of daylight from a circadian perspective was lacking. Our analyses show that predictable weather- and solar angle-induced effects on both the color and intensity of daylight are prime candidates to be used by circadian clocks to acquire maximal information on solar time. We show that being able to accurately estimate solar angle from both daylight intensity and color may be an important feature for circadian systems to correct for the effects of cloud cover on the encoded intensity of daylight. Although the theoretical notion that color may be a more precise *Zeitgeber* than light intensity at twilight transitions has been around for some time[8–12], this assumption has never been thoroughly tested. In fact, this assumption does not seem to be in line with our findings that the color of the sky at lower solar angles is very much influenced by cloud-cover, arguably more so than light intensity (Fig. 3B and 3C). We therefore conclude that, also at twilight transitions, an integration of color and intensity provides the most accurate *Zeitgeber* that the human eye can extract from daylight.

Such circadian color coding may be beneficial by allowing circadian systems to discriminate between solar angle- and weather-induced effects on the intensity of daylight. Light-intensity decrease under an overcast sky in the evening, would reduce its circadian phase delaying effect at that time of day, thus generating an unwanted advance in circadian phase angle of entrainment. When the *Zeitgeber* strength in the evening however corresponds to the encoded solar angle based on both color and intensity, the *Zeitgeber* may be buffered against such weather-induced noise, preventing such an advance, and therefore maximizing day-to-day stability in phase of entrainment. Circadian color-coding may be even more crucial for a strictly diurnal species that does

not witness dusk or dawn transitions, such as the European ground squirrel that retreats and leaves its burrow at a solar elevation of approximately 15°[25,26]. This animal therefore perceives almost no intensity modulations over the course of the day that transcend the intensity modulations that may occur due to variation in weather conditions (see Fig. 5A), which is theoretically difficult to entrain to: a small delay in its circadian phase does not shift part of its delaying circadian phase into darkness, hence no advancing correction may occur the following day. In fact, at the presence of both weather-induced noise on daylight intensity, the *Zeitgeber* signal that is perceived the following day may be exactly the same as the day before. Because reliable solar angle estimations are possible by integrating intensity and color information (see Fig. 5B), a possible strategy for this species to entrain would be to encode solar angles below 15° as 'solar darkness', such that slight deviations in phase of entrainment alter the *Zeitgeber* signal that is perceived the following day. This mechanism can work in synergy with the previously proposed parametric entrainment mechanism for diurnal animals, where the intrinsic circadian period is tuned to 24h (effectively increasing the Zeitgeber signal-to-noise ratio by low pass filtering)[27]. Forms of parametric entrainment in diurnal mammals will gain stability when the *Zeitgeber* signal contains as much information as possible on solar time on a daily basis. In addition, the all-cone retina of ground squirrels will further maximize the possibility for cone driven color coding in the ipRCG pathway projecting to their SCN[28].

Evolution has likely gone a great way in minimizing the effects of noise in the *Zeitgeber* signal driving our circadian clocks. IpRGC cells projecting to the SCN are capable of maintaining steady levels of firing until several minutes after lights-off[17], presumably such that short instances of behavior-induced darkness (e.g. burrowing) are still accompanied by a *Zeitgeber* signal that corresponds to the solar light phase. Entraining to an averaged *Zeitgeber* signal over multiple days (e.g. what was proposed for the European ground squirrel) may be beneficial for a diurnal burrower that is typically exposed to a noisy *Zeitgeber* signal on a daily basis[26]. We suggest that this list of noise-filtering properties by circadian systems might be extended by considering circadian color- and intensity-coding as a mechanism that ensures a *Zeitgeber* signal that corresponds to the actual solar angle, which is therefore maximally stable from day to day regardless of weather conditions.

Integration of color and intensity need not be functional for circadian entrainment only, but may in addition be used by functions displaying circannual rhythmicity. Indeed, in addition to circadian timekeeping, accurate estimation of solar time may be crucial for photoperiodic time measurement (i.e. to obtain an accurate indication of day length), which is of major importance in the timing of reproductive behavior for many species[29]. Photoperiodic time measurement in mammals relies on the same photoreceptor pathway as circadian photoreception[30,31], which seasonal breeders employ to keep track of day length over the course of the year, allowing for breeding to occur at a time of year of abundant food-availability. Encoding sunrise and sunset with maximal accuracy may provide a means of timing reproductive behavior as accurately as possible to maximize offspring survival.

Recent research shows that indeed the effect of color may contribute substantially to entrainment of the mammalian (mouse) SCN[11]. Phase of entrainment in mice is altered when housed under an artificial light-dark cycle that incorporates both color and intensity changes during twilight transitions, as compared to intensity modulations alone. One interpretation of these findings, which is in agreement with our postulated hypothesis, is that the strength of the *Zeitgeber* signal is modulated depending on both its color and intensity. Such studies raise the question as to whether also human phase of entrainment can be altered when indoor lighting schedules incorporate the intensity and color dynamics that are present in naturally occurring daylight. We and others have found that human phase of entrainment is advanced with more daylight exposure during the day[32,33]. Mimicking natural daylight in indoor environments may thus be beneficial in countering the delayed phase of entrainment that is so typical of humans living in modern societies[34,35]. As we expect that phase of entrainment in humans will be similar between overcast and sunny days, mimicking overcast days during day time (but not in the evening!) may provide the most cost- and energy-efficient means of doing so.

Given that many different species, displaying different types of behavior, may all benefit from circadian color coding (to be used for both circadian and circannual timekeeping), this topic may prove to be important to fully understand the mechanisms underlying natural circadian entrainment, especially in humans and other diurnal mammals.

References

1. Daan, S. & Pittendrigh, C. S. A Functional analysis of circadian pacemakers in nocturnal rodents II. The variability of phase response curves. *J. Comp. Physiol.* **106,** 253–266 (1976).
2. Floessner, T. & Hut, R. A. in *Biological Timekeeping: Clocks, Rhythms and Behaviour* (ed. Kumar, V.) 47–58 (Springer India, 2017). doi:10.1007/978-81-322-3688-7_3
3. Khalsa, S. B. S., Jewett, M. E., Cajochen, C. & Czeisler, C. A. A phase response curve to single bright light pulses in human subjects. *J. Physiol.* **549,** 945–952 (2003).
4. Cajochen, C., Zeitzer, J. M., Czeisler, C. A. & Dijk, D.-J. J. Dose-response relationship for light intensity and ocular and electroencephalographic correlates of human alertness. *Behav. Brain Res.* **115,** 75–83 (2000).
5. Hut, R. A., Oklejewicz, M., Rieux, C. & Cooper, H. M. Photic Sensitivity Ranges of Hamster Pupillary and Circadian Phase Responses Do Not Overlap. *J. Biol. Rhythms* **23,** 37–48 (2008).
6. Czeisler, C. A. *et al.* Stability, precision, and near-24-hour period of the human circadian pacemaker. *Science (80-.).* **284,** 2177–2181 (1999).
7. Roenneberg, T., Hut, R., Daan, S. & Merrow, M. Entrainment Concepts Revisited. *J. Biol. Rhythms* **25,** 329–339 (2010).
8. Krüll, F., Demmelmeyer, H. & Remmert, H. On the circadian rhythm of animals in high polar latitudes. *Naturwissenschaften* **72,** 197–203 (1985).
9. Roenneberg, T. & Foster, R. G. Invited Review Twilight Times: Light and the Circadian System. *Photochem. Photobiol.* **66,** 549–561 (1997).
10. Dacey, D. M. *et al.* Melanopsin-expressing ganglion cells in primate retina signal colour and irradiance and project to the LGN. *Nature* **433,** 749–754 (2005).
11. Walmsley, L. *et al.* Colour As a Signal for Entraining the Mammalian Circadian Clock. *PLOS Biol.* **13,** e1002127 (2015).
12. Brown, T. M. Using light to tell the time of day: sensory coding in the mammalian circadian visual network. *J. Exp. Biol.* **219,** 1779–1792 (2016).
13. Spitschan, M., Aguirre, G. K., Brainard, D. H. & Sweeney, A. M. Variation of outdoor illumination as a function of solar elevation and light pollution. *Sci. Rep.* **6,** 26756 (2016).
14. Smith, R. C. & Wilson, W. H. Photon scalar irradiance. *Appl. Opt.* **11,** 934–8 (1972).
15. Solomon, S. G. & Lennie, P. The machinery of colour vision. *Nat. Rev. Neurosci.* **8,** 276–286 (2007).
16. Belenky, M. A., Smeraski, C. A., Provencio, I., Sollars, P. J. & Pickard, G. E. Melanopsin retinal ganglion cells receive bipolar and amacrine cell synapses. *J. Comp. Neurol.* **460,** 380–393 (2003).
17. Wong, K. Y., Dunn, F. A., Graham, D. M. & Berson, D. M. Synaptic influences on rat ganglion-cell photoreceptors. *J. Physiol.* **582,** 279–296 (2007).
18. Horwitz, G. D. What studies of macaque monkeys have told us about human color vision. *Neuroscience* **296,** 110–115 (2015).
19. Spitschan, M., Jain, S., Brainard, D. H. & Aguirre, G. K. Opponent melanopsin and S-cone signals in the human pupillary light response. *Proc. Natl. Acad. Sci.* **2014,** 15568–15572 (2014).
20. Cao, D. & Barrionuevo, P. A. A five-primary photostimulator suitable for studying intrinsically photosensitive retinal ganglion cell functions in humans. *J. Vis.* **15,** 1–13 (2015).
21. Lucas, R. J. *et al.* Measuring and using light in the melanopsin age. *Trends Neurosci.* **37,** 1–9 (2014).
22. Govardovskii, V. I., Fyhrquist, N., Reuter, T., Kuzmin, D. G. & Donner, K. In search of the visual pigment template. *Vis. Neurosci.* **17,** 509–28 (2000).
23. Dartnall, H. J., Bowmaker, J. K. & Mollon, J. D. Human visual pigments: microspectrophotometric results from the eyes of seven persons. *Proc. R. Soc. London. Ser. B, Biol. Sci.* **220,** 115–30 (1983).
24. Jacoby, W. G. Loess: A nonparametric, graphical tool for depicting relationships between variables. *Elect. Stud.* **19,** 577–613 (2000).
25. Hut, R. A., Oort, B. E. H. van & Daan, S. Natural Entrainment without Dawn and Dusk: The Case of the European Ground Squirrel (Spermophilus citellus). *J. Biol. Rhythms* **14,** 290–299 (1999).

26. Daan, S. Colin Pittendrigh, Jürgen Aschoff, and the Natural Entrainment of Circadian Systems. *J. Biol. Rhythms* **15,** 195–207 (2000).
27. Beersma, D. G., Daan, S. & Hut, R. A. Accuracy of circadian entrainment under fluctuating light conditions: contributions of phase and period responses. *J. Biol. Rhythms* **14,** 320–329 (1999).
28. Hut, R. A., Scheper, A. & Daan, S. Can the circadian system of a diurnal and a nocturnal rodent entrain to ultraviolet light? *J. Comp. Physiol. - A Sensory, Neural, Behav. Physiol.* **186,** 707–715 (2000).
29. Ikegami, K. & Yoshimura, T. Seasonal time measurement during reproduction. *J. Reprod. Dev.* **59,** 327–33 (2013).
30. Hut, R. A., Dardente, H. & Riede, S. J. Seasonal Timing: How Does a Hibernator Know When to Stop Hibernating? *Curr. Biol.* **24,** R602–R605 (2014).
31. Hau, M. *et al.* Timing as a sexually selected trait: the right mate at the right moment. *Philos. Trans. R. Soc. B Biol. Sci.* **372,** 20160249 (2017).
32. Roenneberg, T., Wirz-Justice, A. & Merrow, M. Life between Clocks: Daily Temporal Patterns of Human Chronotypes. *J. Biol. Rhythms* **18,** 80–90 (2003).
33. Woelders, T., Beersma, D. G. M., Gordijn, M. C. M., Hut, R. A. & Wams, E. J. Daily Light Exposure Patterns Reveal Phase and Period of the Human Circadian Clock. *J. Biol. Rhythms* **32,** 274–286 (2017).
34. Yetish, G. *et al.* Natural Sleep and Its Seasonal Variations in Three Pre-industrial Societies. *Curr. Biol.* **25,** 2862–2868 (2015).
35. Wright, K. P. *et al.* Entrainment of the Human Circadian Clock to the Natural Light-Dark Cycle. *Curr. Biol.* **23,** 1554–1558 (2013).

Supplementary information

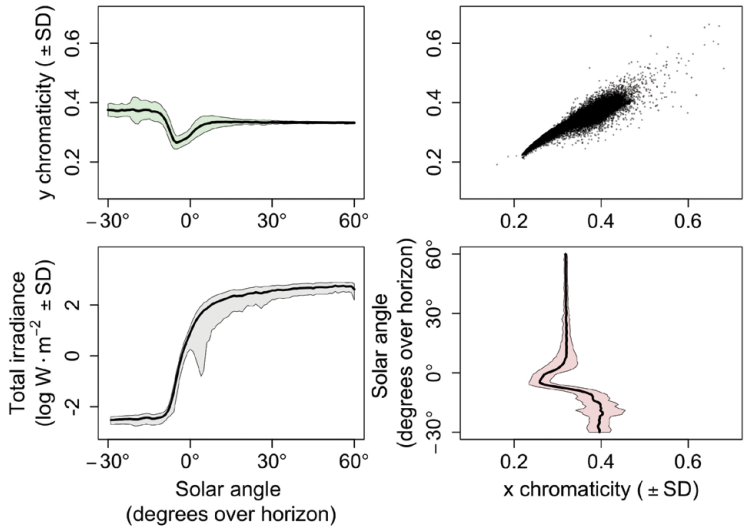

Figure S1. Progression of CIE chromaticity indices and irradiance with increasing solar angles.

4

Chapter 5:

Chapter 5

Linking light exposure and subsequent sleep: a field polysomnography study in humans

Emma J. Wams,
Tom Woelders,
Irene Marring,
Laura van Rosmalen,
Domien G.M. Beersma,
Marijke C.M. Gordijn
and Roelof A. Hut

Sleep 40 (12), zsx165

Abstract

The aim of this study was to determine the effect of light exposure on subsequent sleep characteristics under ambulatory field conditions. Twenty healthy participants were fitted with ambulatory PSG and wrist-actigraphs to assess light exposure, rest-activity, sleep quality, timing and architecture. Laboratory salivary dim-light melatonin onset (DLMO) was analyzed to determine endogenous circadian phase. Later circadian clock phase was associated with lower intensity ($R2=0.34$, $\chi2(1)=7.19$, $p<0.01$), later light exposure (quadratic, controlling for daylength, $R2=0.47$, $\chi2(3)=32.38$, $p<0.0001$), and to later sleep timing ($R2=0.71$, $\chi2(1)=20.39$, $p<0.0001$). Those with later first exposure to more than 10 lux of light had more awakenings during subsequent sleep (controlled for daylength, $R2=0.36$, $\chi2(2)=8.66$, $p<0.05$). Those with later light exposure subsequently had a shorter latency to first REM sleep episode ($R2=0.21$, $\chi2(1)=5.77$, $p<0.05$). Those with less light exposure subsequently had a higher percentage of REM sleep ($R2=0.43$, $\chi2(2)=13.90$, $p<0.001$) in a clock phase modulated manner. Slow wave sleep accumulation was observed to be larger after preceding exposure to high maximal intensity and early first light exposure ($p<0.05$). The quality and architecture of sleep is associated with preceding light exposure. We propose that light exposure timing and intensity does not only modulate circadian-driven aspects of sleep but also homeostatic sleep pressure. These novel ambulatory PSG findings are the first to highlight the direct relationship between light and subsequent sleep, combining knowledge of homeostatic and circadian regulation of sleep by light. Upon confirmation by interventional studies, this hypothesis could change current understanding of sleep regulation and its relationship to prior light exposure.

Light is the primary Zeitgeber (entraining cue) for the vertebrate circadian system. In mammals, light information is projected to the circadian pacemaker or synchronizer (located in the hypothalamic suprachiasmatic nucleus, SCN[1]) via intrinsically photosensitive retinal ganglion cells (ipRGCs)[2]. Light entrainment is modulated, not only by the duration of light exposure, but also by its intensity and spectral composition[3,4]. Additionally, light can influence sleep timing, duration, structure and quality[5]. These sleep characteristics[6–8]and the intensity of sleep[9] are controlled by the circadian drive for wakefulness and the accumulation of homeostatic sleep pressure during preceding wakefulness. We hypothesize that light has an influence on subsequent sleep by either altering the rate of sleep pressure build up or by altering the timing of the circadian-modulated wake drive.

Timing of light exposure has been observed to be linked to clock phase, estimated by the time of dim-light melatonin onset (DLMO), both in the laboratory[3,10,11] and in real life situations[12–16]. However, behavioral timing during some highly-controlled laboratory studies in animals do not match observations in the field, such as in the cases of House mice[17], Spiny mice[18], Golden hamsters[19] and Tuco tucos[20] (e.g. hamsters are nocturnal in the laboratory but diurnal in the wild). These contradictions might be explained by the multiple factors that could affect sleep timing, duration and structure, which are excluded under controlled laboratory conditions. For humans, social restrictions, environmental influences, eating patterns, artificial light, disturbances by family or pets, and work schedules are just a few examples that could alter circadian entrainment.

In laboratory settings, sleep timing, duration and structure have been linked to both evening[21–26] and morning single-day bright light exposure[8,10,25] with morning light advancing sleep timing and leading to a reduction of sleep duration at the expense of rapid-eye movement (REM) sleep[25]. Some field studies have gone further in assessing how light exposure influences sleep when individuals have the freedom to habitually sleep and conduct their usual daily routines. Objective actigraph and subjective field measurements have shown that earlier sleep timing is related to more daytime light exposure, either with[27]or without imposed sleep schedules[28–30]. Earlier light timing also resulted in earlier sleep phase[15] and repeated bright daytime light exposure has been observed to lead to earlier sleep phase in Alzheimer's disease patients in real-life settings[31]. Consistent with this, later and lower intensity light exposure has also been linked to later sleep phases in subjective field studies[32,33]. The relationship between light exposure and sleep duration remains less clear. In an intervention-field study, a reduction in daytime light intensity was linked to a decrease in sleep duration[34] whereas, without intervention, the presence of electrical lighting in addition to normal sunlight led to a decrease in sleep duration[35]. This paradox might be explained by the timing of light. In the evening, additional light seems to decrease sleep duration, whereas during the day it increases sleep duration. There is a lack of real-life modern society observational studies assessing the association of everyday light exposure with subsequent sleep timing and duration.

In subjective reports of sleep in non-intervention field studies it was observed that sleep quality was considerably reduced when individuals had low exposure to light during the day[36–38]. Laboratory electroencephalography (EEG) studies have shown that light directly before[24,39,40] or during sleep[41] increases sleep disturbance. Increased daytime light exposure through additional lighting in Alzheimer care homes have confirmed laboratory study findings that bright light during the day results in a reduction of sleep disturbances[42] and an increase in sleep consolidation[43]. These sleep parameters are key experimental targets for improving health[44], and therefore require more detailed description under ambulatory conditions.

With the current field study, we sought to simultaneously assess the link between light exposure and subsequent sleep timing, duration, sleep structure and objective quality without experimental intervention. Although observational field studies have gone far in corroborating laboratory findings, the influence of light exposure on sleep structure and objective quality have not been assessed in the field. Through a multiple-day, comparative analysis of both rest-activity data and polysomnography (PSG)-based sleep data, with preceding light exposure, we can determine if laboratory findings are transferable to real-life settings for the first time. Furthermore, we seek to assess whether sleep timing, quality or architecture depends on prior light intensity and timing, and whether these relationships are mediated by the individual's clock phase. We intend to assess whether current laboratory finding-based sleep regulation models remain valid under ambulatory conditions in the field.

Methods

Participants

For this study, 23 participants were recruited of which 20 healthy male (n=8) and female (n=12) subjects, aged 20-29 (average 23.4 ±2.2 (±SD) were used for analysis. Chronotype was assessed via the Munich Chronotype Questionnaire[30] (MCTQ) as mid-sleep on free days (MSF) regardless of alarm-clock use. To ensure large variation in chronotypes, the dataset contained eight very early (MSF range 2.75 to 3.79, 3.50 ±0.33 (Mean ±SD)), nine intermediate (MSF range 4.63 to 4.83, 4.72 ±0.09 (Mean ±SD)) and three very late (MSF range 7.04 to 7.75, 7.33 ±0.37 (Mean ±SD)) chronotypes. These cut-offs were aimed at obtaining 10% of the Dutch chronotype distribution in each category, as determined by the updated Dutch MCTQ database[45] consisting of 4132 people from the Netherlands aged 20-30. Participants were excluded when they had moderate or severe sleep disturbances (Pittsburgh Sleep Quality Index[46]; PSQI; ≥10), tendencies for anxiety and/or depression (Hospital Anxiety and Depression Scale[47]; HADS; ≥8; and Beck Depression Inventory[48]; BDI; ≥8), existing chronic medical conditions, the need for medication use, previous head injury, epilepsy, smoking, excessive use of alcohol or caffeine (>3 and >8 glasses per day respectively), any use of recreational drugs in the last year, having a BMI of <18 or >27 or a body weight of less than 36 kg, having travelled across more than one time-zone in the last month or had a history of shift work (in-house general health questionnaire), or color-blindness (Ishihara color blindness test[49]).

In total, 23 participants were recruited into the study after meeting all inclusion criteria. Of these, three were excluded from both analyses: one dropped out; one was excluded based on inaccurate completion of inclusion questionnaires; and one was excluded due to unreliable light data for both assessment periods. A further six participants were only excluded from PSG analyses either due to malfunction of the actigraph (5) or due to unreliable light data (1; Table S1).

The study procedures were approved by the Medical Ethical Research Committee of the University Medical Centre Groningen (NL48468.042.14), the Netherlands and are in accordance with the Declaration of Helsinki (2013). All participants gave written informed consent.

Study design

The data presented here are a subset of measures from a larger ambulatory assessment of biological rhythms in the field. Here, only rest-activity, light exposure and PSG measures are described. The study took place between November 2014 and January 2016 in Groningen, The Netherlands.

The study duration totaled three weeks, the first 6 days being an ambulatory field assessment of rest-activity (MotionWatch 8™, MW8™, CamNTech. Ltd.), light intensity monitoring from the same actigraph, followed by a weekend laboratory assessment of salivary melatonin to calculate clock phase under standardized dim light conditions of <10 lux (dim-light melatonin onset; DLMO; see Fig. 1). Eight samples were obtained, one per hour, ending at habitual sleep onset (weighted average of sleep onset for workdays and freedays). To avoid the dim light conditions affecting subsequent measurements, there were no observations for a minimum of one week after saliva sampling. After this break, participants undertook two nights of home polysomnography (PSG) recordings (Actiwave™, CamNTech Ltd.) to measure sleep architecture. The recordings took place on a Wednesday and Saturday night, in randomized order. Electrode placement and removal was conducted at the facility (a visit of max. 1hour, at least 3 hours before sleep onset). Concomitant actigraph light intensity monitoring continued throughout this period. There were no interventions throughout the study, however on two instances of <1hr participants were required to attend our facilities briefly during the first week of the study to have batteries replaced and to return other devices.

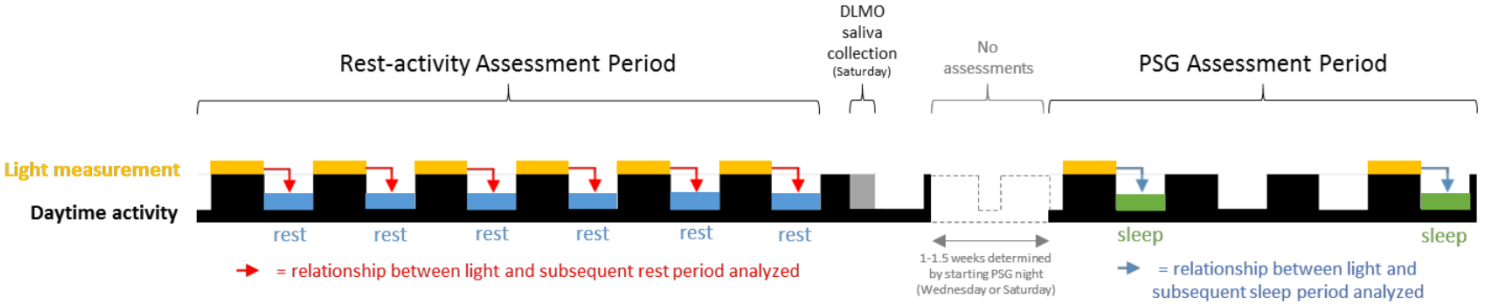

Figure 1. Study design representation. Timeline shows the two assessment periods (rest-activity; and PSG). Light measurements are shown in yellow with subsequent rest periods (blue); and sleep periods (green). The first half of the timeline indicates a week of rest-activity measurements with light and subsequent sleep comparisons indicated by the red arrows. All daily comparisons of light and subsequent sleep were included in the analyses controlling for subject. After this rest-activity measurement period a salivary melatonin collection was conducted to determine subject's DLMO (grey). Following this there was a period of no assessments lasting at least one week dependent on the subject's randomization of a Wednesday or Saturday first PSG assessment night (dotted lines). The two PSG recordings are shown in green and each was compared to the preceding light exposure (indicated by blue arrows).

Measurements

All time codes were converted to Greenwich mean time (GMT)+1h. All daylight savings time adjustments were removed.

Rest-activity. Activity counts were collected in one minute epochs using a MotionWatch 8™ (MW8™, CamNTech. Ltd.), worn on the non-dominant wrist. Activity timing and rest duration were calculated using Sleep analysis software (version 7, CamNTech Ltd.). Activity offsets were determined as the time when activity and light reduced and activity was observed to be less consolidated (assisted by software algorithm from Sleep Analysis 7, CamNTech Ltd., Cambridge, UK) and maintained at a reduced level for at least 10 min. Activity onsets were determined using the reverse algorithm of activity offset. Sleep onset and offset were assessed by PSG (see methods below).

DLMO assessment. Salivary melatonin was collected using Salivette®, Sarstedt™ Ltd., Germany. Samples were centrifuged and stored overnight at ~4 ˚C and then stored at -80 ˚C. On completion of the study, a double-antibody radioimmunoassay (RIA) was performed to assess melatonin concentration levels (Bühlmann Direct Saliva Melatonin kit, Bühlmann Laboratories AG, Switzerland; intra-assay variation: 13.97% and 9.11%; inter-assay variation: 13.99% and 14.64% for low and high concentration controls respectively). DLMO was marked as the first time where melatonin concentrations exceeded the 4 pg/ml threshold upon linear interpolation of subsequent melatonin values.

PSG details. PSG was measured using 5 scalp electrodes (Fpz, Cz, C3, C4 and Oz), a reference electrode on the left mastoid, 2 electro-oculogram (EOG) electrodes and 1 electromyogram (EMG) electrode either under the chin or on eyebrow muscle (when a beard obstructed chin electrode attachment). PSG signals were sampled at 128 Hz, 8 bits and scored in 30 s epochs according to AASM scoring criteria [50] with a 50 Hz notch filter, 0.3 Hz high-pass filter and a 32 Hz low-pass filter (Vitascore software, TEMEC, the Netherlands). Sleep onset was determined as the time of at least 5 consolidated minutes of sleep (stage N1, N2, N3 or REM). First slow-wave sleep (SWS) episode was defined as the first occurrence of an epoch of stage N3 sleep. First rapid-eye movement (REM) sleep episode was defined as the first REM epoch occurrence. The number of awakenings, i.e. transitions from sleep to wake epochs was utilized as a sleep disturbance proxy. Although electrodes were fitted at the Human study facility, University of Groningen, all participants slept at home at a self-chosen time. Sleep stage accumulation data were calculated based on hypnogram cumulative percentage of total sleep time. Division of sleep stage accumulation data by high or low maximum fitted light intensity was defined as individuals with a maximum light intensity on the day of subsequent sleep of either higher or lower than the median 3.01 $\log_{10}$(lux) (two groups of n=7). Splitting the group by time of first exposure to more than 10 lux (two groups of n=7) was at the median 8.90h. Once the groups were split by high or low light intensity, or early or late first exposure to more than 10 lux, the groups were further split by DLMO. This split was conducted on

the group as a whole at the median DLMO of 20.07h. This resulted in different sample sizes of 'early' and 'late' clock types, sample sizes are stated in the relevant figure legends. Detailed description of obtained light values and intra-individual distributions of light measurements in this study were described by Woelders and colleagues[51]. All DLMO split accumulation results are presented in the text.

Light data. Light data from the MotionWatch were cut to end at sleep onset of the sleep/rest period of interest (e.g. beginning of sleep according to PSG recording). The light data was cut to begin at the sleep onset preceding the night of interest. Therefore light data included light exposure throughout the night and day (approximately 24 hours) preceding the sleep of interest. Because circadian responses to light follow a log-linear relationship[52,53], all light data (measured in lux) were $\log_{10}$ transformed after values below device sensitivity threshold were set to 1 lux. To estimate the time of maximal light exposure, a linear harmonic regression analysis with a single sine wave, fitted per 24h due to the entrained nature of the participants' rhythms (CircWave[54], version 1.4, University of Groningen, The Netherlands), was fitted through the log-transformed lux values for each day separately. We smoothed the data by a local polynomial regression procedure (LOESS[55]; span of 72 minutes). We then calculated the first and last times at which the smoothed (LOESS) data crossed the 1 $\log_{10}$(lux) threshold on each day, to determine the times of first and last exposure to more than 10 lux. The threshold of 10 lux was chosen based on previous evidence of sleep alterations[56] and/or phase shifts[57] with lux values above this threshold. Maximal light intensity was calculated per day from the smoothed (LOESS) $\log_{10}$-transformed data. Raw average light intensity was calculated from the non-smoothed log-transformed data.

Statistical analysis

Light and sleep comparisons always were confined to a period of light exposure and the directly subsequent rest or sleep period (in rest-activity and PSG measurement periods, respectively). All reliable daily light-rest or light-sleep comparisons were included in statistical analyses, whilst controlling for subject. Linear model fitting was performed in R (R Core Team, 2015; version: 3.2.3), using the most recent shell of Rstudio (version: 0.99.491) and the 'lme4' R-package for mixed-effects modelling[58]. In all models, participant ID was included as a random effect. A critical p-value of 0.05 was maintained for all analyses. As a goodness-of-fit parameter for these mixed models, the marginal R^2 was reported, using the 'MuMIn' R-package. This parameter represents the variance explained by the fixed factors in the model[59]. Sleep parameters were included in the model as dependent variables, whereas light parameters were included as fixed effects (see Suppl. Tables 1 & 2). Daylength and DLMO (covariates) were included as additional fixed effects. Daylength was included as the timing and intensity of light exposure might be season-modulated. Daylength was calculated as dusk clock time – dawn clock time on the day of observation. DLMO was included in the analysis to observe the contribution of clock phase to these relationships. When fitting the models, Akaike

Information Criteria (AIC) ('drop1' function, 'lme4' package) were compared to perform backward selection on the most complex model, dropping the least significant term at each iteration. Insignificant covariates were considered before independent variables of primary interest were dropped from the model. Only in the models where maximal light intensity was significant, timing of maximal light intensity was tested for significance to investigate whether light intensity, independent of timing, could affect sleep. Timing of maximum light intensity was discarded when the model did not improve significantly. For all analyses a quadratic term of the independent variable was added to the model and discarded when not significant. All sleep and light parameters were regressed against DLMO and its quadratic term to assess the influence of clock phase on these parameters. For the analysis of the sleep stage accumulation over the sleep period, mixed-effects linear models were fitted using the 'lme4' library in R[60]. The dependent variable was either REM-sleep, slow-wave sleep, or wake accumulation since sleep onset (as a percentage of total sleep duration). Participant ID was included in these models as random factor. The first fixed factor was either the light intensity group, light timing group or the DLMO group, depending on how the data was split. Time since sleep onset (as a percentage of total sleep duration, rounded to the nearest integer) was included as the second fixed factor. To allow for testing of the difference between two groups (first fixed factor) for each time value since sleep onset (second fixed factor) separately, the latter factor was converted from a numerical factor into a categorical factor (101 categories, range: 0% - 100%) before fitting the models. The interaction term was included as the third and final fixed factor. After fitting these models to the data, each model contained 101 interaction coefficients (i.e. the difference between the two groups for each time after sleep onset). For each model, post-hoc analysis was then performed on these 101 interaction coefficients (H0: coefficient ≠ 0), via a general linear hypothesis testing procedure (the 'glht' function in the 'multcomp' R-library). The resulting p-values were corrected for multiplicity using the single-step method[61].

Throughout the results section all results are written as: *+quadratic term* if the quadratic of the independent variable (either light parameter or DLMO) significantly contributed to the model; *+daylength* if daylength significantly contributed to the model; *+DLMO* if DLMO timing significantly contributed to the model, in these cases details of the sign of the coefficient are provided to explain its interaction with the dependent variable (sleep parameter). If, on testing, only the linear term of the independent variable significantly contributed to explain the variance of the dependent variable *no covariate* is stated. Additionally, the R^2, chi-square statistic (χ^2), associated *degrees of freedom* and *p-value* for the final model are provided. Any models where the linear term of the independent variable did not significantly explain dependent variable variance, were deemed insignificant regardless of covariate significance. For results of models containing only the linear term or the linear terms and the quadratic term of the independent variable graphs are shown as raw data with model fit indicated (for PSG graphs average datapoints ±SE are provided).

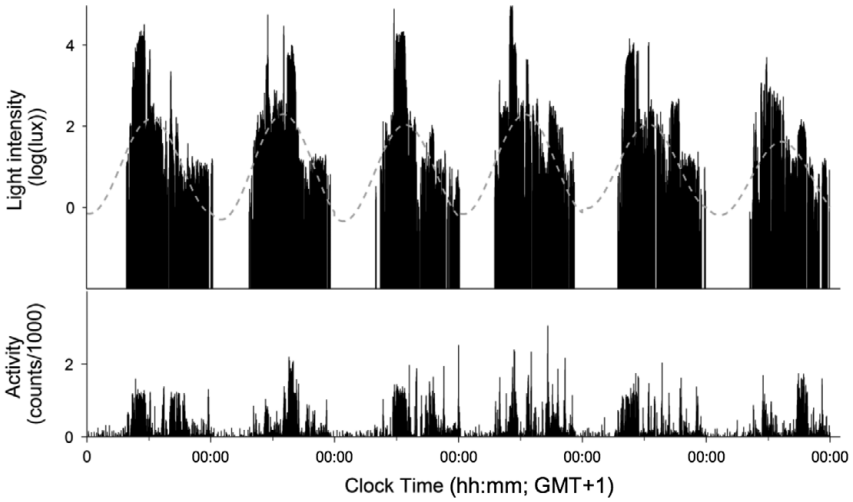

Figure 2. Example of original activity and light data trace. Data were obtained from an intermediate chronotype participant with a dim-light melatonin onset (DLMO) of 19.5h. *Top panel*: Log transformed light intensity data (black lines indicate intensity per min bin) with harmonic regression sine function (dashed line) plotted for the first week. *Bottom panel*: black lines indicate activity counts per minute, divided by 1000.

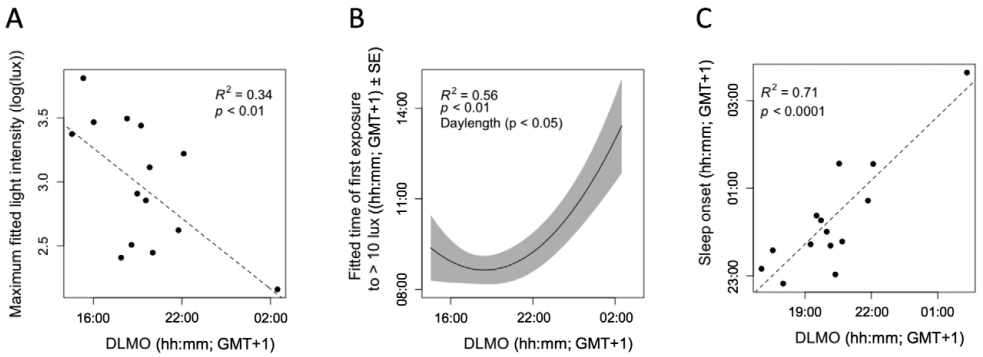

Figure 3. Relationships between dim-light melatonin onset, light exposure and sleep timing. A: Higher maximal fitted light intensity exposure was related to earlier DLMO timing. **B:** In a curvi-linear fashion later DLMO was generally related to later time of first exposure to > 10 lux when accounting for differences in daylength (model prediction: black line, standard error of mixed model: grey range). **C:** Later DLMO timing was related to later sleep onset.

For results of models containing any additional covariates (i.e. DLMO timing and/or daylength), data are shown as the model prediction ±model SE and raw data are omitted, to facilitate graphical representation.

Results

Light exposure

The large range of DLMO timing in this dataset (see Table 1) enabled an assessment of the relationship between DLMO timing (considered to represent clock phase) and light exposure. An example of the original data is provided (Fig. 2). In general, earlier light exposure was observed to be coupled to exposure to higher intensity light (Table 1). Later DLMO was related to lower maximal light exposure for both the rest-activity (+quadratic term, R^2=0.23, $\chi^2(2)$=10.01, p <0.01), and the PSG assessment periods (no covariate, R^2=0.34, $\chi^2(1)$=7.19, p <0.01; Fig. 3A; see Suppl. Table S2 for coefficient information). As well as a lower intensity of light exposure, later DLMO timing was also related to later light exposure. A later DLMO was observed to be associated with later first light exposure (+quadratic term, R^2=0.14, $\chi^2(2)$=9.82, p <0.01; Fig. 3B), and a later last light exposure to more than 10 lux during both the rest-activity assessment (no covariate, R^2=0.07, $\chi^2(1)$=4.24, p <0.05) and the PSG period (+quadratic term +daylength, R^2=0.56, $\chi^2(3)$=13.03, p <0.005, and +quadratic term, R^2=0.32, $\chi^2(2)$=6.23, p <0.05, respectively). Later DLMO was also associated with later time of maximal light exposure (+quadratic term, +daylength, R^2=0.47, $\chi^2(3)$=32.38, p <0.0001) for rest-activity assessment days (see Fig. 2 for an example) and PSG days (+quadratic, R^2=0.58, $\chi^2(2)$=19.39,p <0.0001).

Rest-activity and Sleep timing

As expected, clock phase (DLMO) correlated positively with behavioral measures of activity and PSG based measures of sleep. Later DLMO timing was related to a later activity offset (no covariate, R^2=0.27, $\chi^2(1)$=12.76, p<0.001; see Supp. Table S1 for coefficient information), and in agreement, a later sleep onset (no covariate, R^2=0.71, $\chi^2(1)$=20.39, p<0.0001; Fig. 3C). Later DLMO timing was related to a later activity onset (+quadratic term, R^2=0.50, $\chi^2(2)$=37.02, p<0.0001) and likewise to a later sleep offset (no covariate, R^2=0.53, $\chi^2(1)$=12.37, p<0.001). A later DLMO timing was observed to be associated with a longer rest duration (+quadratic term, R^2=0.08, $\chi^2(2)$=8.19, p<0.05), in contradiction to the lack of relationship observed for sleep duration (p>0.05). Although it might be expected that a similar relationship for rest and sleep would appear from the data, the rest duration actually consists of a consolidated period of inactivity, whereas sleep duration is the period between sleep onset and offset possibly accounting for this mismatch. In line with these findings, when splitting the study sample by DLMO timing, DLMO group was observed to be related to sleep onset timing and the phase angle between DLMO and sleep onset (see Table 1). This completes an overall picture of a later clock phase (DLMO timing) being related to later sleep timing and a shorter interval between DLMO and sleep onset. Interestingly, individuals classified as having low light exposure also a shorter phase angle between their DLMO and sleep onsets (Table 1).

Table 1. Demographic and average light exposure for all participant groups.

Demographic	Assessment period comparison (Mean ±SD)		DLMO (hh:mm) group comparison (Mean ±SD; PSG)		
	Rest-activity Assessment	PSG Sleep Assessment	Early (<19:00)	Intermediate (19:00-21:00)	Late (>21:00)
Gender (m/f)	8/12	8/6	1/2	4/4	3/0
Age (yrs.)	23.4 ±2.2	22.7 ±1.7	23.0 ±1.7	22.6 ±2.1	22.7 ±0.6
Dim-light Melatonin Onset (DLMO; hh:mm)	20:18 ±02:00	20:12 ±02:18	17:32 ±00:29	20:02 ±00:30	23:25 ±02:31
Average light intensity (log(lux))	0.9 ±0.3	0.9 ± 0.2	1.0 ±0.2	0.8 ±0.2	0.8 ±0.2
Maximal intensity of light exposure from fit (log(lux))	3.0 ±0.8	2.9 ± 0.5	3.5 ±0.3	2.9 ±0.5	2.6 ±0.5
Time of maximal light exposure from fit (hh:mm)	14:30 ±01:42	15:12 ±01:54	15:19 ±01:21	15:11 ±01:13	17:19 ±02:27
Time of first exposure to >10lux (hh:mm)	08:00 ±02:54	09:06 ±02:06	08:26 ±02:02	08:40 ±01:30	10:59 ±03:01
Time of last exposure to >10lux (hh:mm)	21:54 ±02:00	22:24 ±02:00	21:57 ±00:39	22:18 ±01:35	23:11 ±03:30
Sleep onset (hh:mm)	23:57 ±01:33	00:24 ±01:20	23:11 ±00:27	00:09 ±00:50	02:03 ±01:30
Sleep offset (hh:mm)	07:58 ±01:37	07:59 ±01:15	07:04 ±00:16	07:49 ±00:47	09:12 ±01:57
Sleep duration (hrs)	8.0 ±1.3	7.6 ±0.7	7.9 ±0.6	7.7 ±0.8	7.1 ±0.5
Time from last >10lux to sleep onset (hrs)	2.0 ±2.0	2.0 ±1.7	1.2 ±0.7	1.9 ±1.5	2.9 ±2.5
Time from sleep offset to first >10 lux (hrs)	-0.1 ±3.2	1.4 ±1.7	1.4 ±2.1	0.9 ±1.7	1.8 ±1.2
Phase angle of Sleep onset-DLMO (hrs)	3.7 ±1.7	4.1 ±1.4	5.8 ±0.7	4.2 ±0.9	2.4 ±1.0
PSQI score	3.5 ±1.6	3.8 ±1.9	3.0 ±1.7	4.0 ±1.9	4.0 ±2.7
BDI score	1.8 ±1.9	1.7 ±1.4	1.0 ±1.0	1.9 ±1.7	2.0 ±1.0

PSQI: Pittsburgh sleep quality index; BDI: Beck's depression inventory.

	F-test (Sig.)	First exposure to >10 lux group comparison (Mean ±SD; PSG)		t-test (Sig.)	Maximal light intensity group comparison (Mean ±SD; PSG)		t-test (Sig.)
		Earlier (<08:58)	Later (>08:58)		Low intensity exposure (<2.9 log lux)	High intensity exposure (>2.9 log lux)	
	n.s.	4/3	4/3	n.s.	4/3	4/3	n.s.
	n.s.	22.0 ±1.5	23.4 ±1.6	n.s.	22.1 ±1.2	23.3 ±2.0	n.s.
	23.6 (0.0001)	19:33 ±00:37	20:53 ±02:46	n.s.	21:27 ±02:23	20:07 ±01:50	n.s.
	n.s.	1.0 ±0.1	0.6 ±0.1	6.2 (0.0001)	0.8 ±0.2	0.9 ±0.3	n.s.
	n.s.	3.0 ±0.4	2.8 ±0.6	n.s.	2.5 ±0.3	3.4 ±0.3	-6.6 (0.0001)
	n.s.	15:10 ±00:47	16:14 ±02:12	n.s.	16:02 ±01:55	15:13 ±01:26	n.s.
	n.s.	07:41 ±00:54	10:43 ±01:58	-4.2 (0.0014)	09:47 ±02:19	08:17 ±01:37	n.s.
	n.s.	22:28 ±00:51	22:22 ±02:48	n.s.	22:39 ±02:20	22:08 ±01:28	n.s.
	8.0 (0.0071)	00:04 ±00:59	00:45 ±01:36	n.s.	00:34 ±01:30	00:11 ±01:07	n.s.
	n.s.	07:33 ±00:39	08:28 ±01:35	n.s.	08:13 ±01:32	07:41 ±00:43	n.s.
	n.s.	7.5 ±0.8	7.7 ±0.6	n.s.	7.7 ±0.8	7.5 ±0.7	n.s.
	n.s.	1.6 ±1.0	2.4 ±2.3	n.s.	1.9 ±1.6	2.1 ±1.9	n.s.
	n.s.	0.1 ±1.1	2.2 ±1.5	-3.3 (0.0069)	1.6 ±1.7	0.6 ±1.6	n.s.
	9.2 (0.0045)	4.7 ±1.2	3.6 ±1.7	n.s.	3.3 ±1.2	5.0 ±1.0	-2.6 (0.02)
	n.s.	2.7 ±1.1	4.9 ±2.0	-2.5 (0.0267)	4.4 ±2.4	3.1 ±1.1	n.s.
	n.s.	1.6 ±1.9	1.9 ±0.9	n.s.	2.0 ±1.2	1.4 ±1.7	n.s.

As DLMO timing was observed to be related to both light exposure and sleep timing, regression analysis was utilized to assess the relationship between light exposure, and activity and sleep timing on the same day. Activity timing was observed to have a quadratic relationship to the time of last exposure to more than 10 lux. A later activity offset was related to both very early and very late last exposure to more than 10 lux, when accounting for the positive relationship DLMO has with activity timing (+quadratic term, +DLMO, R^2=0.45, $\chi^2(3)$=44.75, p<0.0001). This same relationship was observed for activity onset (+quadratic and +DLMO, R^2=0.44, $\chi^2(3)$=30.93, p<0.0001). A similar relationship was observed for sleep onset and offset with last exposure to more than 10 lux, although DLMO timing was not observed to significantly be involved in the relationship (Sleep onset: +quadratic term, R^2=0.68, $\chi^2(2)$=22.09, p<0.0001; Sleep offset: +quadratic term, R^2=0.68, $\chi^2(2)$=20.39, p<0.0001). Activity onset was also positively associated with first exposure to more than 10 lux and time of maximal light exposure, when controlling for the positive relationship between DLMO timing and activity onset (First exposure: +DLMO, R^2=0.43, $\chi^2(2)$=28.32, p<0.0001), and time of maximal light exposure: +DLMO, R^2=0.49, $\chi^2(2)$=37.92, p<0.0001). Interestingly, longer rest duration was associated with lower maximal light intensity on the preceding day (no covariate, R^2=0.05, $\chi^2(1)$=4.83, p<0.05), and a later timing of maximal light exposure (no covariate, R^2=0.05, $\chi^2(1)$=4.82, p<0.05). In general, individuals who had more time between waking and being exposed to 10 lux for the first time were likely to have that first exposure later in the day (Table 1).

Phase angle between sleep onset and DLMO

The phase angle between sleep onset and DLMO was also assessed as covariate, but did not contribute significantly to any of the models tested (p>0.05).

Light exposure and subsequent sleep disturbance

Subjects with a late DLMO also showed less sleep stage transitions, except for one included subject, who had a very late DLMO while experiencing more sleep transitions than those with moderate late DLMO timing (+quadratic term, R^2=0.32, $\chi^2(2)$=6.81, p<0.05, Table S2). In general, individuals who were first exposed to 10 lux later had significantly more subjectively reported sleep disturbances (Table 1). Objectively recorded sleep disturbances were found to depend on previous light exposure, but time of maximal light exposure did not significantly contribute to this effect. Later time of first exposure to 10 lux was also related to more awakenings, when controlling for daylength (+daylength, R^2=0.36, $\chi^2(2)$=8.66, p<0.05, Fig. 4A). Lower maximal light exposure resulted in fewer awakenings, when accounting for variance explained by DLMO timing (+DLMO, R^2=0.26, $\chi^2(2)$=6.98, p<0.05, Fig. 4B). Timing of DLMO was found to additively contribute (coefficient: 1.01, p<0.05) such that that later DLMO timing was related to an increased number of awakenings (Figure 4B & Table 2). Additionally, later time of first exposure to more than 10 lux seemed related to more wake after sleep onset (trend: p=0.053). This seems in line with the finding that later first light exposure correlate with more awakenings (Figure 4A), but contrasts with the correlation showing less sleep stage

transitions in people with late DLMO (Table S2). Sleep characteristics are summarized in Table 2. No differences were found between the two PSG nights (weekday and weekend recordings) in terms of sleep disturbances, architecture, timing or stage accumulation; or their relationships with preceding light exposure (p>0.05; data not shown). No effect of randomization order of starting PSG night was observed (p>0.05; data not shown).

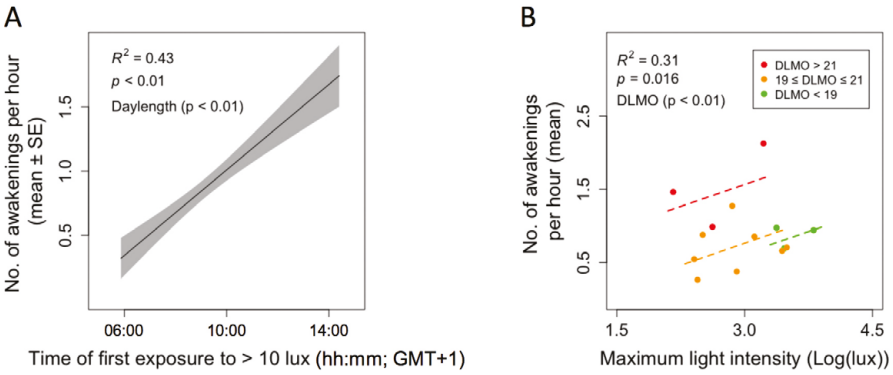

Figure 4. Light exposure and its relationship to subsequent sleep disturbances. A: Later first exposure to more than 10lux was related to increased sleep disturbance (number of awakenings per hour), when controlling for daylength (model prediction: black line, standard error of mixed model: grey range). **B:** Higher maximal light intensities during the day were followed by more sleep disturbances (number of awakenings per hour TST) within DLMO timing groups (DLMO) timing (red: DLMO >21h, orange: 19h ≤ DLMO ≤21h, green: DLMO <19h).

Table 2. Sleep characteristics for PSG assessment

Demographic	Group average (Mean ±SD)	DLMO (hh:mm) group comparison (Mean ±SD; PSG)			F-test (Sig.)
		Early (<19:00)	Inter (19:00-21:00)	Late (>21:00)	
Sleep duration (hrs)	7.6 ±0.7	7.9 ±0.6	7.7 ±0.6	7.2 ±0.5	n.s.
Time in bed (hrs)	8.0 ±1.1	7.4 ±1.5	7.9 ±0.6	8.7 ±1.2	n.s.
Sleep onset latency (mins)	24.2 ±35.5	12.0 ±2.3	25.9 ±25.4	26.0 ±14.8	n.s.
WASO (mins)	27.1 ±16.7	24.3 ±6.5	21.6 ±13.7	44.7 ±22.8	n.s.
% N1 sleep	4.1 ±1.7	2.7 ±1.7	4.1 ±1.1	4.8 ±0.7	n.s.
% N2 sleep	43.6 ±5.5	45.6 ±11.1	44.6 ±2.0	41.1 ±4.9	n.s.
% N3 sleep	25.0 ±4.9	25.5 ±9.2	24.6 ±3.7	25.0 ±2.9	n.s.
% REM sleep	23.0 ±3.8	22.0 ±3.4	23.0 ±3.4	22.0 ±2.0	n.s.
REM latency (hrs)	1.6 ±0.5	1.5 ±0.6	1.8 ±0.5	1.2 ±0.2	n.s.
N3 latency (mins)	13.1 ±5.7	11.2 ±4.3	14.1 ±6.9	12.7 ±4.0	n.s.
Mean awakenings per hour	0.9 ±0.5	0.9 ±0.2	0.7 ±0.3	1.5 ±0.6	5.91 (0.018)
No. of transitions	142.2 ±32.3	158.7 ±43.5	135.3 ±30.5	144.2 ±31.9	n.s.

WASO: Wake after sleep onset; REM: Rapid-eye movement sleep

First exposure to >10 lux group comparison (Mean ±SD; PSG)		t-test (Sig.)	Maximal light intensity group comparison (Mean ±SD; PSG)		t-test (Sig.)
Early (<08:58)	Late (>08:58)		Low intensity exposure (<2.9 log lux)	High intensity exposure (>2.9 log lux)	
7.6 ±0.8	7.7 ±0.4	n.s.	7.7 ±0.7	7.6 ±0.6	n.s.
7.8 ±0.6	8.1 ±1.3	n.s.	8.1 ±0.4	7.8 ±1.4	n.s.
15.0 ±7.4	30.9 ±26.4	n.s.	30.9 ±26.9	15.0 ±5.3	n.s.
22.1 ±8.0	32.1 ±22.0	n.s.	25.1 ±15.3	29.2 ±19.0	n.s.
3.8 ±1.4	4.2 ±1.3	n.s.	4.7 ±0.3	3.3 ±1.5	2.41 (0.033)
44.4 ±5.7	43.7 ±5.2	n.s.	43.9 ±3.2	44.2 ±7.0	n.s.
25.6 ±6.3	24.1 ±2.4	n.s.	23.5 ±2.9	26.2 ±5.9	n.s.
22.3 ±2.6	22.8 ±3.4	n.s.	23.9 ±2.9	21.2 ±2.5	n.s.
1.9 ±0.3	1.4 ±0.6	n.s.	1.5 ±0.4	1.7 ±0.6	n.s.
11.8 ±4.2	14.5 ±7.0	n.s.	15.2 ±6.0	11.1 ±5.0	n.s.
0.7 ±0.3	1.1 ±0.6	n.s.	0.8 ±0.5	1.0 ±0.5	n.s.
144.4 ±34.4	140.1 ±32.7	n.s.	140.2 ±31.9	144.2 ±35.1	n.s.

Sleep architecture

The timing of the DLMO was not related, on its own, to any aspect of subsequent sleep architecture ($p>0.05$). Light exposure variables on their own or combined with DLMO did explain variation in sleep architecture. A later time of first exposure to >10lux (no covariate, $R^2=0.21$, $\chi^2(1)=5.77$, $p<0.05$, Fig. 5A) and a later timing of maximal light exposure (+quadratic, +DLMO, $R^2=0.36$, $\chi^2(2)=11.17$, $p<0.01$, Fig. 5B) were associated with a subsequent shorter latency to first rapid-eye movement (REM) episode. The findings might seem paradoxical since REM sleep propensity is thought to be directly influenced by the circadian clock. Hence, at first sight, later DLMO was expected to correlate with the later occurrence of REM sleep. However, the first (or even second) REM sleep bout can be suppressed if non-REM propensity is high. Therefore, we investigated the effects of light intensity on subsequent non-REM and REM sleep. Higher maximal intensity of light on the day before sleeping with PSG was followed by lower percentages of REM sleep, when accounting for variance explained by DLMO timing (+DLMO, $R^2=0.43$, $\chi^2(2)=13.90$, $p<0.001$, Fig. 5C). The negative coefficient for DLMO timing as a covariate, indicate that later DLMO timing was related to a subsequent lower percentage of REM sleep (see Supp. Table S2 for coefficient information). Which may indicate that higher sleep deficit in late sleepers may reduce or eliminate the first REM sleep bout. In the same lines, the percentage of stage 1 sleep was observed to be lower in those individuals who were classified as being exposed to higher light intensity light (Table 2). This could indicate that shorter latencies to non-REM sleep occurring when individuals are exposed to higher maximal light a pressure for slow wave sleep (SWS) overrides the balance of other sleep stages. This can also be observed with the dominating increase in percentage of subsequent SWS at higher average light intensities over the day (+quadratic, no covariate, $R^2=0.25$, $\chi^2(2)=8.86$, $p<0.05$).

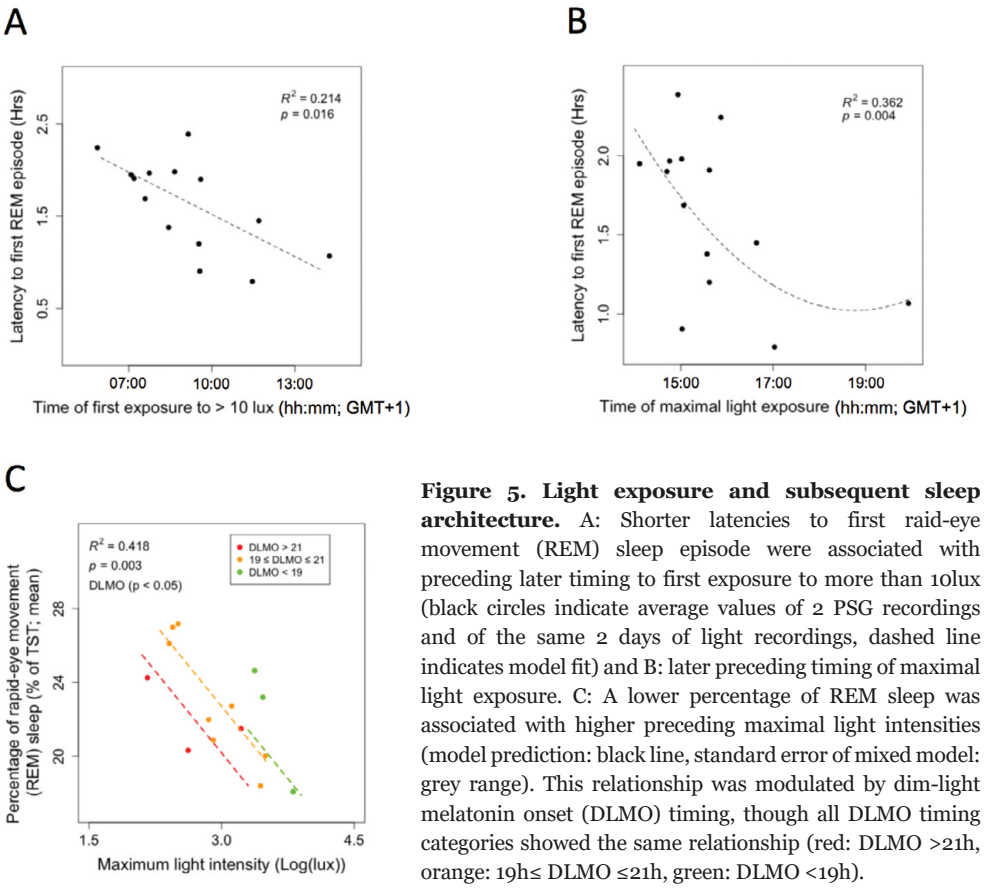

Figure 5. Light exposure and subsequent sleep architecture. A: Shorter latencies to first raid-eye movement (REM) sleep episode were associated with preceding later timing to first exposure to more than 10lux (black circles indicate average values of 2 PSG recordings and of the same 2 days of light recordings, dashed line indicates model fit) and B: later preceding timing of maximal light exposure. C: A lower percentage of REM sleep was associated with higher preceding maximal light intensities (model prediction: black line, standard error of mixed model: grey range). This relationship was modulated by dim-light melatonin onset (DLMO) timing, though all DLMO timing categories showed the same relationship (red: DLMO >21h, orange: 19h≤ DLMO ≤21h, green: DLMO <19h).

Sleep stage accumulation

In order to see how light timing and the intensity of light exposure interact with the subsequent accumulation rate of SWS, REM sleep and Wake, the sample was split into low and high maximal intensity exposure, and into early and late first exposure to > 10 lux. Those individuals exposed to higher maximal light intensities experienced larger subsequent SWS accumulation ($p<0.05$; Fig. 6A), lower subsequent REM sleep accumulation throughout the night ($p<0.05$; Fig. 6B), and lower subsequent wake accumulation at the beginning of the night ($p<0.05$; Fig. 6C). Those individuals who had their first exposure to > 10 lux earlier had significantly higher subsequent SWS accumulation (Fig. 7A) seemingly at the expense of the accumulation of REM sleep in the middle of the sleep period (Fig. 7B), and wake throughout the night (Fig. 7C; $p<0.05$).

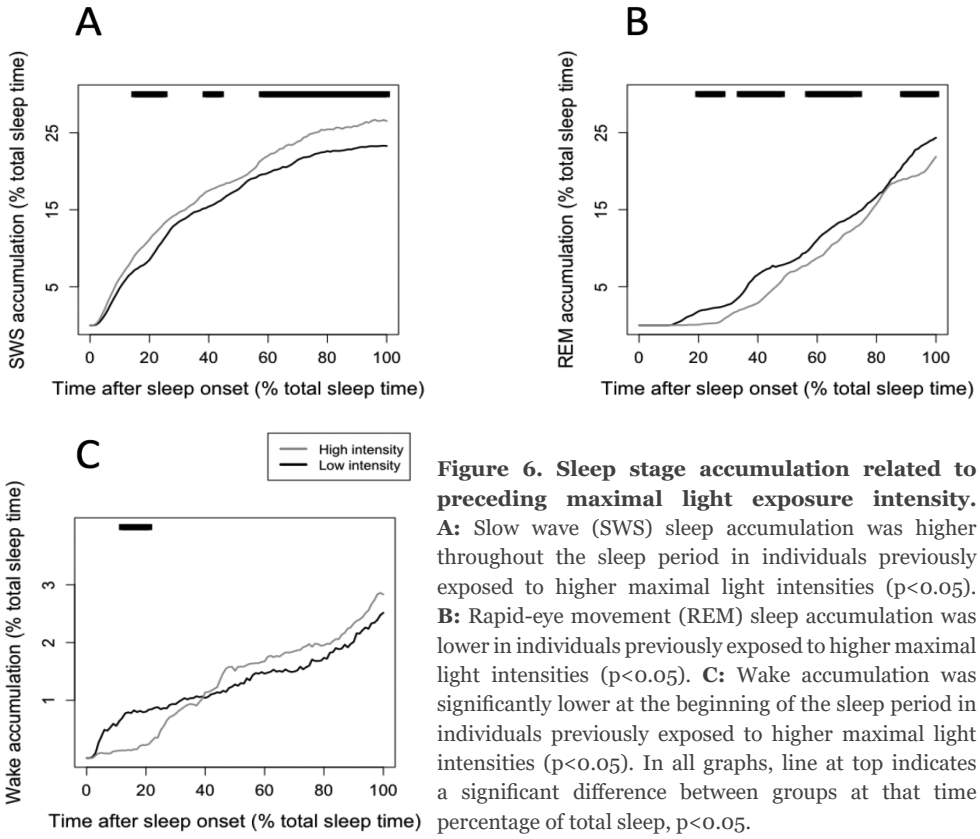

Figure 6. Sleep stage accumulation related to preceding maximal light exposure intensity. **A:** Slow wave (SWS) sleep accumulation was higher throughout the sleep period in individuals previously exposed to higher maximal light intensities ($p<0.05$). **B:** Rapid-eye movement (REM) sleep accumulation was lower in individuals previously exposed to higher maximal light intensities ($p<0.05$). **C:** Wake accumulation was significantly lower at the beginning of the sleep period in individuals previously exposed to higher maximal light intensities ($p<0.05$). In all graphs, line at top indicates a significant difference between groups at that time percentage of total sleep, $p<0.05$.

Discussion

Our data show that sleep timing, duration, structure and the number of sleep disturbances observed in the field objectively, for the first time, depended on aspects of preceding light exposure. In a sample of healthy 20 to 30 year olds, selected for a wide range of sleep timing (MSF), we observed large variation in clock phases (DLMO), which optimized the probability to find relationships with preceding light parameters within DLMO timing groups. DLMO was added to our models to assess the impact of clock phase and explain the variance in sleep architecture dependent on the circadian clock to allow for a better analysis of the effect of previous light on subsequent sleep[62]. We found that later endogenous clock timing was related to later timing and lower levels of light exposure. Later exposure to light has been observed experimentally to result in a later clock phase[3,10,39]. This finding confirms light interventions in the field[12,14,15] and the finding that manipulated reduction of blue light in the morning was associated with later clock phases[13]. Spectral light composition information would help to further elucidate this relationship.

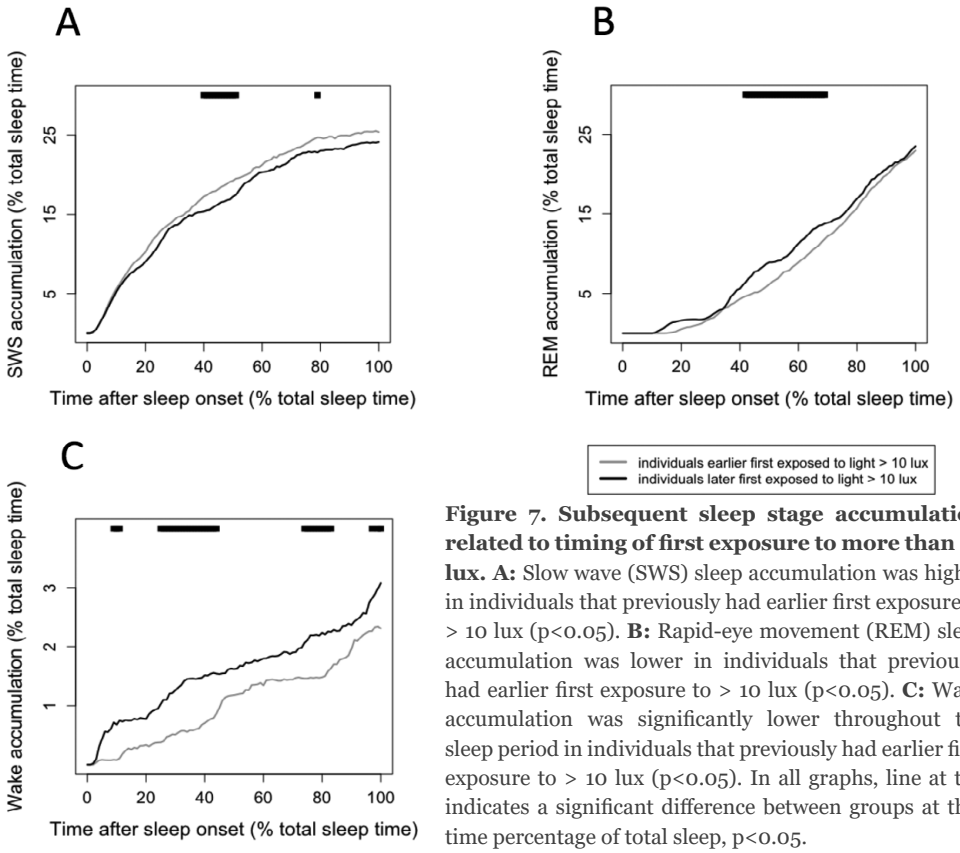

Figure 7. Subsequent sleep stage accumulation related to timing of first exposure to more than 10 lux. A: Slow wave (SWS) sleep accumulation was higher in individuals that previously had earlier first exposure to > 10 lux ($p<0.05$). **B:** Rapid-eye movement (REM) sleep accumulation was lower in individuals that previously had earlier first exposure to > 10 lux ($p<0.05$). **C:** Wake accumulation was significantly lower throughout the sleep period in individuals that previously had earlier first exposure to > 10 lux ($p<0.05$). In all graphs, line at top indicates a significant difference between groups at that time percentage of total sleep, $p<0.05$.

Despite the lack of intervention studies, field data indicate that later chronotypes are generally exposed to later light[33] and less time outdoors[32]. This likely results in lower light exposure[27,33], and probably a reduction in exposure to ~460-490 nm photons, which are important for entraining the circadian system[63]. In both our dataset and in previous studies, later sleep timing has been shown to be related later clock phase[54,55] and later preceding light exposure[33,34]. These relationships are most likely due to the influence of light on the entrainment of the circadian clock, which drives process C in sleep regulation, which in turn will shift the timing of sleep[6,7]. Because humans have on average an intrinsic circadian period longer than 24h (24.2h[64]), they need advancing (morning) light to entrain to the 24-h day. Exposure to lower light intensities indicate reduced *zeitgeber* strength and oscillatory theory predicts that this will result in a later (lagging) phase angle of entrainment[65,66] when intrinsic period is great than 24 hours. This later phase angle of entrainment may then be further amplified by artificial light in the evening. In addition, entrainment models would predict a bigger role for parametric entrainment in diurnal animals[67,68]. Moreover, according to Aschoff's rule, diurnal animals will lengthen intrinsic period with lower light intensity[69,70].

Although we only found that lower maximal light intensities were associated with subsequent longer rest durations, studies with high intensity light interventions have previously focused on the timing of the light[8,15], rather than the intensity itself. Despite that, shorter subsequent sleep duration has been related to brighter morning light[8] and exposure to artificial electric lighting[35]. In the current study, however, no relationship between light exposure and sleep duration was found. This is in line with the analysis of sleep behavior of three pre-industrial societies that indicated that there were no differences in sleep duration in societies without electric lighting as compared to our industrialized sleep habits[71] (but see also[72]). Because sleep onset and offset appear gated by the circadian system in a similar way, the reduction in the strength of light as the primary entrainment signal may only play a minimal role in the alteration of sleep duration.

Preceding light exposure, possibly through altering the balance of circadian and homeostatic regulation of sleep, appears to be associated with the amount of subsequent sleep disturbance. Later light was associated with more awakenings, in line with laboratory studies observing evening light being related to more arousals[39,73]. It is unclear why late DLMO correlates with less sleep transitions (Table S2), but the complex quadratic relationship of this correlation suggests that more data need to be collected to fully understand this. A clearer relationship was found between light parameters, DLMO and number of awakenings. Late first light exposure and late clock phase correlates with more awakenings (Figure 4A & B). We have described before, that people with a late clock phase sleep early relative to DLMO[51]. This may indicate that their sleep partially overlaps with the circadian drive for wakefulness, resulting in more awakenings[7].

The influence of the circadian drive for wake promotion on sleep offset timing has been reported to result in a reduction of REM sleep, with non-REM sleep appearing unaffected[8,25]. Sleep structure appears to be related to preceding light exposure in our dataset. Exposure to higher levels of maximal light was related to less REM in subsequent sleep. In the laboratory, higher levels of blue photons in evening light have been associated with a reduction in REM sleep duration[24,26]. Whereas light during sleep was associated with an increased prevalence of REM sleep[41]. Therefore, influence of light on REM sleep could be due to the circadian regulation of REM sleep. The timing of light during the daytime exposure in our subjects appears to be related also to the timing of the first REM episode. The finding that later light exposure was related to earlier first REM episodes indicates that the timing of light could modulate not only clock phase but in turn also the circadian regulated sleep architecture. There are two alternative explanations, either light is influencing sleep architecture through altering the rate of sleep pressure increase or through the shift of the sleep structure by a shift in the circadian-related drive for wakefulness (and REM sleep). What is known is that the alerting signal of the circadian system decreases throughout the night, rising just before sleep offset[7]. Based on forced desynchrony findings that REM sleep appears clock modulated[74], it can be hypothesized that the influence of later light extending the window for REM sleep episodes could be due to the altered phase of the circadian system and a reduced sleep load build up. Through the sleep stage accumulation analysis, it can be observed that

slow wave sleep (SWS) has a direct relationship with the timing and intensity of light. As REM sleep and wake accumulation show the opposite pattern to SWS it appears that light is influencing the homeostatic pressure shifting other sleep stages in accordance. Therefore, it appears that light, although known to affect the circadian system and in turn REM sleep, additionally increases the build-up of the homeostatic sleep pressure. To further assess the relationship of light exposure with subsequent sleep intensity, an analysis of delta power decay is required. This is beyond the scope of this current article due to the already complex nature of the included analyses. We hypothesize that the underlying biological mechanism for this is the direct light input observed from the retina to the ventrolateral preoptic nucleus, the sleep 'switch' alternating sleep stages[75]. Upon confirmation of interventional studies, this hypothesis could change the current understanding of the regulation of sleep.

Although there appears in our pilot analysis (in supplementary information) to be some influence of DLMO timing on the relationship between light and sleep structure, this influence needs to be further investigated, due to small sample size once participants were grouped by DLMO. In the main analyses of this study, despite the large amount of data obtained per participant, it is possible that this sample is not representative of the broader population. In addition, the majority of participants were university students, and therefore may have different lifestyles than the general working population. Although this might be a limitation, it must also be noted that the large variation present in our data (through participant selection based upon chronotype) provides the ability to assess the relationships in a statistically powerful way. Another possible limitation is the assumption that the subsequent sleep is related to the preceding light exposure rather than the sleep having an influence on future light exposure. Through correlational analysis, these relationships cannot be further elucidated here.

In general, our findings corroborate those observed in laboratory settings. Our observations support that despite lacking the many factors that influence sleep in real life, laboratory findings are transferable to how people sleep in naturalistic settings. Although light can be well controlled in the laboratory, it can be difficult to generalize laboratory findings to observations in the field where light quality and quantity shows large variation over the day. Our study is the first to assess sleep architecture in the field using ambulatory PSG in the context of chronobiological applications, showing its reliability with the new technological advances utilized here. This study provides further evidence for the link between light exposure and the timing, duration, structure and quality of subsequent sleep. Not only does this influence have implications for further strategies in the care for patients and those with sleep disturbances, but this study shows that light exposure shapes everyday life. Light technologies and those developing working schedules and living environments could greatly influence the sleep individuals have in real life and its subsequent effects on quality of life, health, productivity, mental performance, and safety. With confirmation from spectral analysis and interventional studies, this study could alter the current understanding of sleep regulation and the role of light history.

Acknowledgements

The authors would like to acknowledge students Heleen Rinsema and Robin Dennebos for their great assistance in the collection of data, and Moniek Geerdink for the melatonin radioimmunoassay analysis.

References

1. Daan S, Hut RA. Circadian Clock, Program, Oscillator, Pacemaker, Synchroniser? In: Honma K, Honma S, eds. *Circadian Clocks*. Hokkaido University Press; 2016:21-32.
2. Berson DM, Dunn F a, Takao M. Phototransduction by retinal ganglion cells that set the circadian clock. *Science*. 2002;295(5557):1070-1073.
3. Khalsa SBS, Jewett ME, Cajochen C, Czeisler C a. A phase response curve to single bright light pulses in human subjects. *J Physiol*. 2003;549(3):945-952.
4. Gooley JJ, Rajaratnam SMW, Brainard GC, Kronauer RE, Czeisler C a, Lockley SW. Spectral responses of the human circadian system depend on the irradiance and duration of exposure to light. *Sci Transl Med*. 2010;2(31):1-10.
5. Schmidt TM, Chen S-K, Hattar S. Intrinsically photosensitive retinal ganglion cells: many subtypes, diverse functions. *Trends Neurosci*. 2011;34(11):572-580.
6. Daan S, Beersma DG, Borbély a a. Timing of human sleep: recovery process gated by a circadian pacemaker. *Am J Physiol*. 1984;246(2 Pt 2):161-183.
7. Dijk D, Edgar DM. Circadian and homeostatic control of wakefulness and sleep. In: Turek F, Zee P, eds. *Regulation of Sleep and Wakefulness*. New York: Marcel Dekker, Inc.; 1999:111-147.
8. Dijk D-J, Visscher CA, Bloem GM, Beersma DG, Daan S. Reduction of human sleep duration after bright light exposure in the morning. *Neurosci Lett*. 1987;73(2):181-186.
9. Dijk D-J, Beersma DG, Daan S. EEG power density during nap sleep: reflection of an hourglass measuring the duration of prior wakefulness. *J Biol Rhythms*. 1987;2(3):207-219.
10. Gordijn MCM, Beersma DGM, Korte HJ, Van Den Hoofdakker RH. Effects of light exposure and sleep displacement on dim light melatonin onset. *J Sleep Res*. 1999;8(3):163-174.
11. Rüger M, Gordijn MCM, Beersma DGM, Vries B De, Daan S. Acute and Phase-Shifting Effects of Ocular and Extraocular Light in Human Circadian Physiology. 2003;18(5):409-419.
12. Figueiro MG, Plitnick B, Rea MS. The effects of chronotype, sleep schedule and light/dark pattern exposures on circadian phase. *Sleep Med*. 2014;15(12):1554-1564.
13. Figueiro MG, Rea MS. The effects of red and blue lights on circadian variations in cortisol, alpha amylase, and melatonin. *Int J Endocrinol*. 2010;2010(1):1-9.
14. Burgess HJ, Molina TA. Home lighting before usual bedtime impacts circadian timing: A field study. *Photochem Photobiol*. 2014;1(1):723-726.
15. Corbett RW, Middleton B, Arendt J. An hour of bright white light in the early morning improves performance and advances sleep and circadian phase during the Antarctic winter. *Neurosci Lett*. 2012;525(2):146-151.
16. Geerdink M, Walbeek TJ, Beersma DGM, Hommes V, Gordijn MCM. Short Blue Light Pulses (30 Min) in the Morning Support a Sleep-Advancing Protocol in a Home Setting. *J Biol Rhythms*. 2016;31(5):483-497.
17. Hut RA, Kronfeld-Schor N, van der Vinne V, de la Iglesia HO. In search of a temporal niche: environmental factors. *Prog Brain Res*. 2012;199:281-304.
18. Levy O, Dayan T, Kronfeld-Schor N. The relationship between the golden spiny mouse circadian system and its diurnal activity: an experimental field enclosures and laboratory study. *Chronobiol Int*. 2007;24(4):599-613.

19. Gattermann R, Johnston RE, Yigit N, et al. Golden hamsters are nocturnal in captivity but diurnal in nature. *Biol Lett*. 2008;4(3):253-255.
20. Tomotani BM, Flores DEFL, Tachinardi P, Paliza JD, Oda GA, Valentinuzzi VS. Field and laboratory studies provide insights into the meaning of day-time activity in a subterranean rodent (Ctenomys aff. knighti), the Tuco-Tuco. *PLoS One*. 2012;7(5):e37918.
21. Santhi N, Thorne HC, van der Veen DR, et al. The spectral composition of evening light and individual differences in the suppression of melatonin and delay of sleep in humans. *J Pineal Res*. 2012;53(1):47-59.
22. Komada Y, Tanaka H, Yamamoto Y, Shirakawa S, Yamazaki K. Effects of bright light pre-exposure on sleep onset process. *Psychiatry Clin Neurosci*. 2000;54(3):365-366.
23. Münch M, Scheuermaier KD, Zhang R, et al. Effects on subjective and objective alertness and sleep in response to evening light exposure in older subjects. *Behav Brain Res*. 2011;224(2):272-278.
24. Chang A-M, Aeschbach D, Duffy JF, Czeisler CA. Evening use of light-emitting eReaders negatively affects sleep, circadian timing, and next-morning alertness. *Proc Natl Acad Sci*. 2015;112(4):1232-1237.
25. Dijk DJ, Beersma DG, Daan S, Lewy a J. Bright morning light advances the human circadian system without affecting NREM sleep homeostasis. *Am J Physiol*. 1989;256(1 Pt. 2):106-111.
26. Münch M, Kobialka S, Steiner R, Oelhafen P, Wirz-Justice A, Cajochen C. Wavelength-dependent effects of evening light exposure on sleep architecture and sleep EEG power density in men. *Am J Physiol Regul Integr Comp Physiol*. 2006;290(5):1421-1428.
27. Goulet G, Mongrain V, Desrosiers C, Paquet J, Dumont M. Daily light exposure in morning-type and evening-type individuals. *J Biol Rhythms*. 2007;22(2):151-158.
28. Okudaira N, Kripke D, Webster J. Naturalistic studies of human light exposure. *Am J Physiol*. 1983;245(4):613-615.
29. Savides T, Messin S, Senger C, Kripke D. Natural light exposure of young adults. *Physiol Behav*. 1986;38(1):571-574.
30. Roenneberg T, Wirz-Justice A, Merrow M. Life between Clocks: Daily Temporal Patterns of Human Chronotypes. *J Biol Rhythms*. 2003;18(1):80-90.
31. Wright KP, McHill AW, Birks BR, Griffin BR, Rusterholz T, Chinoy ED. Entrainment of the human circadian clock to the natural light-dark cycle. *Curr Biol*. 2013;23(16):1554-1558.
32. Roenneberg T, Keller LK, Fischer D, Matera JL, Vetter C, Winnebeck EC. Human activity and rest in situ. *Methods Enzymol*. 2015;552(1):257-283.
33. Martin JS, Hébert M, Ledoux É, Gaudreault M, Laberge L. Relationship of Chronotype to Sleep, Light Exposure, and Work-Related Fatigue in Student Workers. *Chronobiol Int*. 2012;29(3):295-304.
34. Stebelová K, Molčan Ľ, Okuliarová M, et al. The influence of indoor lighting with low blue light dose on urine 6-sulphatoxymelatonin concentrations and sleep efficiency of healthy volunteers. *Biol Rhythm Res*. 2014;46(1):137-145.
35. de la Iglesia HO, Fernández-Duque E, Golombek DA, et al. Access to electric light is associated with shorter sleep duration in a traditionally hunter-gatherer community. *J Biol Rhythms*. 2015;30(4):342-350.
36. Boubekri M, Cheung I, Reid K, Wang C, Zee PC. Impact of Windows and Daylight Exposure on Overall Health and Sleep Quality of Office Workers : A Case-Control Pilot Study. *J Clin Sleep Med*. 2014;10(6):603-611.
37. Harb F, Hidalgo MP, Martau B. Lack of exposure to natural light in the workspace is associated with physiological, sleep and depressive symptoms. *Chronobiol Int*. 2014;1(1):1-8.
38. Leger D, Bayon V, Elbaz M, Philip P, Choudat D. Underexposure to light at work and its association to insomnia and sleepiness: a cross-sectional study of 13,296 workers of one transportation company. *J Psychosom Res*. 2011;70(1):29-36.
39. Carrier J, Dumont M. Sleep propensity and sleep architecture after bright light exposure at three different times of day. *J Sleep Res*. 1995;4(1):202-211.

40. Cajochen C, Di Biase R, Imai M. Interhemispheric EEG asymmetries during unilateral bright-light exposure and subsequent sleep in humans. *Am J Physiol Regul Integr Comp Physiol*. 2008;294(3):1053-1060.
41. Cho C, Lee H, Yoon H, et al. Exposure to dim light at night increases REM sleep and awakenings. *Sleep*. 2015;37(1):298-299.
42. Van Someren EJ, Kessler A, Mirmiran M, Swaab DF. Indirect bright light improves circadian rest-activity rhythm disturbances in demented patients. *Biol Psychiatry*. 1997;41(9):955-963.
43. Ancoli-Israel S, Gehrman P, Martin JL, et al. Increased Light Exposure Consolidates Sleep and Strengthens Circadian Rhythms in Severe Alzheimer's Disease Patients. *Behav Sleep Med*. 2003;1(1):37-53.
44. Cedernaes J, Schiöth HB, Benedict C. Determinants of shortened, disrupted, and mistimed sleep and associated metabolic health consequences in healthy humans. *Diabetes*. 2015;64(4):1073-1080.
45. Zavada A, Gordijn MCM, Beersma DGM, Daan S, Roenneberg T. Comparison of the Munich Chronotype Questionnaire with the Horne-Ostberg's Morningness-Eveningness Score. *Chronobiol Int*. 2005;22(2):267-278.
46. Buysse DJ, Reynolds CF, Monk TH, Berman SR, Kupfer DJ. The Pittsburgh Sleep Quality Index: a new instrument for psychiatric practice and research. *Psychiatry Res*. 1989;28(2):193-213.
47. Carroll BT, Kathol RG, Noyes R, Wald TG, Clamon GH. Screening for depression and anxiety in cancer patients using the Hospital Anxiety and Depression Scale. *Gen Hosp Psychiatry*. 1993;15(2):69-74.
48. Dozois DJA, Dobson KS, Ahnberg JL. A psychometric evaluation of the Beck Depression Inventory-II. *Psychol Assess*. 1998;10(2):83-89.
49. Clark J. The Ishihara test for color blindness. *Am J physiol Opt*. 1924;5:269-276.
50. Silber MH, Ancoli-Israel S, Bonnet MH, et al. The visual scoring of sleep in adults. *J Clin Sleep Med*. 2007;3(2):121-131.
51. Woelders T, Beersma DGM, Gordijn MCM, Hut RA, Wams EJ. Daily light exposure patterns reveal phase and period of the human circadian clock. *J Biol Rhythms*. 2017:online first.
52. Thapan K, Arendt J, Skene DJ. An action spectrum for melatonin suppression: evidence for a novel non-rod, non-cone photoreceptor system in humans. *J Physiol*. 2001;535(Pt 1):261-267.
53. Hut R a, Oklejewicz M, Rieux C, Cooper HM. Photic sensitivity ranges of hamster pupillary and circadian phase responses do not overlap. *J Biol Rhythms*. 2008;23(1):37-48.
54. Oster H, Damerow S, Hut RA, Eichele G. Transcriptional profiling in the adrenal gland reveals circadian regulation of hormone biosynthesis genes and nucleosome assembly genes. *J Biol Rhythms*. 2006;21:350-361.
55. Cleveland WS, Grosse E, Shyu WM. Local regression models. In: Chambers JM, Hastie TJ, eds. *Statistical Models in S*. Wadsworth & Brooks/Cole; 1992.
56. Obayashi K, Saeki K, Iwamoto J, Ikada Y, Kurumatani N. Association between light exposure at night and nighttime blood pressure in the elderly independent of nocturnal urinary melatonin excretion. *Chronobiol Int*. 2014;31(6):779-786.
57. Zeitzer JM, Khalsa SBS, Boivin DB, et al. Temporal dynamics of late-night photic stimulation of the human circadian timing system. *Am J Physiol Regul Integr Comp Physiol*. 2005;289(3):R839-R844.
58. Maechler M, Bates D. Design Issues in Matrix package Development. 2012;2008:1-5.
59. Johnson PC. Extension Nakagawa & Schielzeth's R_GLMM^2 to random slopes models. *Methods Ecol Evol*. 2014;5:44-46.
60. Bates D, Mächler M, Bolker B. Fitting linear mixed-effects models using lme4. *J Stat Softw*. 2012;51(1):1.
61. Hothorn T, Bretz F, Westfall P. Simultaneous inference in general parametric models. *Biometrical J*. 2008;50(3):346-363.
62. Dijk DJ, Czeisler CA. Contribution of the circadian pacemaker and the sleep homeostat to sleep propensity, sleep structure, electroencephalographic slow waves, and sleep spindle activity in humans. *J Neurosci*. 1995;15(5 Pt 1):3526-3538.

63. Gooley JJ, Ho Mien I, St Hilaire M a, et al. Melanopsin and rod-cone photoreceptors play different roles in mediating pupillary light responses during exposure to continuous light in humans. *J Neurosci*. 2012;32(41):14242-14253.
64. Duffy JF, Cain SW, Chang A-M, et al. Sex difference in the near-24-hour intrinsic period of the human circadian timing system. *Proc Natl Acad Sci U S A*. 2011;108 Suppl:15602-15608.
65. Daan S, Pittendrigh CS. A functional analysis of circadian pacemekrs in nocturnal rodents. *J Comp Physiol A*. 1976;106:253-266.
66. Floessner T, Hut RA. Basic principles underlying biological oscillations and their entrainment. In: Kumar V, ed. *Biological Timekeeping: Clocks, Rhythms and Behaviour*. India: Springer; 2017.
67. Beersma DG, Daan S, Hut R a. Accuracy of circadian entrainment under fluctuating light conditions: contributions of phase and period responses. *J Biol Rhythms*. 1999;14(4):320-329.
68. Roenneberg T, Hut R, Daan S, Merrow M. Entrainment concepts revisited. *J Biol Rhythms*. 2010;25(5):329-339.
69. Aschoff J. Exogenous and Endogenous Components in Circadian Rhythms. *Cold Spring Harb Symp Quant Biol*. 1960;25(1):11-28.
70. Daan S. The Colin S. Pittendrigh Lecture. Colin Pittendrigh, Jürgen Aschoff, and the natural entrainment of circadian systems. *J Biol Rhythms*. 2000;15(3):195-207.
71. Yetish G, Kaplan H, Gurven M, et al. Natural Sleep and Its Seasonal Variations in Three Pre-industrial Societies. *Curr Biol*. 2015;25(1):2862-2868.
72. de la Iglesia HO, Fernández-Duque E, Golombek DA, et al. Access to electric light is associated with shorter sleep duration in a traditionally hunter-gatherer community. *J Biol Rhythms*. 2015;30(4):342-350.
73. Cho JR, Joo EY, Koo DL, Hong SB. Let there be no light: The effect of bedside light on sleep quality and background electroencephalographic rhythms. *Sleep Med*. 2013;14(12):1422-1425.
74. Dijk D-J, Duffy JF, Riel E, Shanahan TL, Czeisler CA. Ageing and the circadian and homeostatic regulation of human sleep during forced desynchrony of rest, melatonin and temperature rhythms. *J Physiol*. 1999;516(Pt 2):611-627.
75. Hattar S, Kumar M, Park A, Tong P. Central Projections of Melanopsin-Expressing Retinal Ganglion Cells in the Mouse. *J Comp Neurol*. 2006;497(3):326-349.

Supplementary Information

Table S1. Coefficient information for significant regressions performed for rest-activity period.

Dependent Variable	Independent variable	Model Statistics [R^2 (df); Chi-square value (p-value)]
Raw average light intensity (log(lux))	DLMO (Hr; GMT+1)	n.s. (p>0.05)
Maximal light intensity (log(lux))	DLMO (Hr; GMT+1)	0.23 (2); 10.01 (0.0067)
Maximal light intensity (log(lux))	Rest duration (Hrs)	0.05 (1); 4.83 (0.0279)
Time of first exposure to >10lux (Hr; GMT+1)	DLMO (Hr; GMT+1)	0.14 (2); 9.82 (0.0074)
Time of first exposure to >10lux (Hr; GMT+1)	Activity onset (Hr; GMT+1)	0.43 (2); 28.32 (<0.0001)
Time of last exposure to >10lux (Hr; GMT+1)	DLMO (Hr; GMT+1)	0.07 (1); 4.24 (0.0394)
Time of last exposure to >10lux (Hr; GMT+1)	Activity offset (Hr; GMT+1)	0.45 (3); 44.75 (<0.0001)
Time of last exposure to >10lux (Hr; GMT+1)	Activity onset (Hr; GMT+1)	0.44 (3); 30.93 (<0.0001)
Time of maximal light exposure (Hr; GMT+1)	DLMO (Hr; GMT+1)	0.47 (3); 32.38 (<0.0001)
Time of maximal light exposure (Hr; GMT+1)	Activity onset (Hr; GMT+1)	0.49 (2); 37.92 (<0.0001)
Time of maximal light exposure (Hr; GMT+1)	Rest duration (Hrs)	0.05 (1); 4.82 (0.0281)
Activity offset (Hr; GMT+1)	DLMO (Hr; GMT+1)	0.27 (1); 12.76 (0.0004)
Activity onset (Hr; GMT+1)	DLMO (Hr; GMT+1)	0.50 (2); 37.02 (<0.0001)
Rest duration (Hrs)	DLMO (Hr; GMT+1)	0.08 (2); 8.19 (0.0166)

Possible dependent variables: raw average light intensity; maximal light intensity; time of first exposure to >10 lux; time of last exposure to >10 lux; time of maximal light exposure; activity offset; activity onset; rest duration. Possible independent variables: DLMO; activity offset; activity onset; rest duration. If not in table, regressions were not significant.

Independent Variable Coefficient Information [coefficient ±SE (p-value)]				
		Covariates		
Linear term	**Quadratic term**	**Daylength (Hr; GMT+1)**	**DLMO (Hr; GMT+1)**	**Time of maximal light Exposure (Hr; GMT+1)**
n.s. (0.1895)	n.s. (0.1019)	n.s. (0.8772)	-	-
1.26 ±0.63 (0.0565)	-0.03 ±0.01 (0.0341)	n.s. (0.4835)	-	-
-0.37 ±0.15 (0.0279)	n.s. (0.6759)	n.s. (0.6030)	n.s. (0.3746)	n.s. (0.178)
-3.80 ±1.76 (0.0408)	0.10 ±0.04 (0.0243)	n.s. (0.1308)	-	-
0.09 ±0.04 (0.0293)	n.s. (0.5560)	n.s. (0.7263)	0.49 ±0.08 (<0.001)	-
0.28 ±0.13 (0.0394)	n.s. (0.6472)	n.s. (0.3784)	-	-
-3.29 ±0.71 (<0.0001)	0.08 ±0.02 (<0.0001)	n.s. (0.6058)	0.34 ±0.08 (0.0003)	-
-1.72 ±0.85 (0.0470)	0.04 ±0.02 (0.0350)	n.s. (0.7308)	0.48 ±0.08 (<0.001)	-
-3.64 ±0.79 (0.0001)	0.10 ±0.02 (<0.0001)	-0.09 ±0.04 (0.0366)	-	-
0.33 ±0.08 (0.0002)	n.s. (0.8783)	n.s. (0.9205)	0.37 ±0.07 (<0.001)	-
0.16 ±0.07 (0.0281)	n.s. (0.9922)	n.s. (0.5568)	n.s. (0.6117)	-
0.41 ±0.10 (0.0004)	n.s. (0.3049)	-	-	-
-2.38 ±0.67 (0.0019)	0.07 ±0.02 (0.0003)	-	-	-
-1.59 ±0.69 (0.0322)	0.04 ±0.02 (0.0220)	-	-	-

Table S2. Coefficient information for significant regressions performed for PSG period.

Dependent Variable	Independent variable	Model Statistics [R^2 (df); Chi-square value (p-value)]
Raw average light intensity (log(lux))	% Slow-wave sleep (SWS; % of TST)	0.25 (2); 8.86 (0.0119)
Maximal light intensity (log(lux))	DLMO (Hr; GMT+1)	0.34 (1); 7.19 (0.0073)
Maximal light intensity (log(lux))	No. of awakenings	0.26 (2); 6.98 (0.0306)
Maximal light intensity (log(lux))	% Rapid-Eye Movement (REM) sleep (% of TST)	0.43 (2); 13.90 (0.0010)
Time of first exposure to >10lux (Hr; GMT+1)	DLMO (Hr; GMT+1)	0.56 (3); 13.03 (0.0046)
Time of first exposure to >10lux (Hr; GMT+1)	No. of awakenings	0.36 (2); 8.66 (0.0132)
Time of first exposure to >10lux (Hr; GMT+1)	Latency to first REM episode (Hrs)	0.21 (1); 5.77 (0.0163)
Time of last exposure to >10lux (Hr; GMT+1)	DLMO (Hr; GMT+1)	0.32 (2); 6.23 (0.0443)
Time of last exposure to >10lux (Hr; GMT+1)	Sleep onset (Hr; GMT+1)	0.68 (2); 22.09 (<0.0001)
Time of last exposure to >10lux (Hr; GMT+1)	Sleep offset (Hr; GMT+1)	0.68 (2); 20.39 (<0.0001)
Time of maximal light exposure (Hr; GMT+1)	DLMO (Hr; GMT+1)	0.58 (2); 19.39 (<0.0001)
Time of maximal light exposure (Hr; GMT+1)	Latency to first REM episode (Hrs)	0.36 (2); 11.17 (0.0038)
Sleep onset (Hr; GMT+1)	DLMO (Hr; GMT+1)	0.71 (1); 20.39 (<0.0001)
Sleep offset (Hr; GMT+1)	DLMO (Hr; GMT+1)	0.53 (1); 12.37 (0.0004)
No. of stage transitions	DLMO (Hr; GMT+1)	0.32 (2); 6.81 (0.0332)

Possible dependent variables: raw average light intensity; maximal light intensity; time of first exposure to >10 lux; time of last exposure to >10 lux; time of maximal light exposure; sleep onset; sleep offset; sleep duration; no. of awakenings; wake after sleep onset; % rapid-eye movement sleep; % slow-wave sleep; latency to first REM episode; latency to first SWS episode. Possible independent variables: DLMO; sleep onset; sleep offset; sleep duration; no. of awakenings; wake after sleep onset; % rapid-eye movement sleep; % slow-wave sleep; latency to first REM episode; latency to first SWS episode. If not in table, regressions were not significant.

Independent Variable Coefficient Information [coefficient ±SE (p-value)]				
		Covariates		
Linear term	**Quadratic term**	**Daylength (Hr; GMT+1)**	**DLMO (Hr; GMT+1)**	**Time of maximal light exposure (Hr; GMT+1)**
-72.54 ±26.34 (0.0072)	43.06 ± 14.72 (0.004)	n.s. (0.8418)	n.s. (0.7892)	n.s. (0.33)
-0.14 ±0.05 (0.0073)	n.s. (0.6180)	n.s. (0.4950)	-	-
2.83 ±1.38 (0.0368)	n.s. (0.3648)	n.s. (0.2363)	1.01 ±0.41 (0.0152)	n.s. (0.4393)
-5.90 ±1.45 (0.0002)	n.s. (0.4041)	n.s. (0.5752)	-0.74 ±0.33 (0.0220)	n.s. (0.9891)
-4.22 ±2.36 (0.0473)	0.11 ±0.05 (0.0313)	-0.23 ±0.13 (0.0421)	-	-
1.16 ±0.37 (0.0038)	n.s. (0.8473)	0.52 ±0.22 (0.0183)	n.s. (0.3902)	-
-0.15 ±0.06 (0.0163)	n.s. (0.4363)	n.s. (0.1374)	n.s. (0.8413)	-
-4.53 ±2.51 (0.0558)	0.11 ±0.06 (0.0422)	n.s. (0.6725)	-	-
-6.80 ±1.42 (<0.0001)	0.16 ±0.03 (<0.0001)	n.s. (0.1363)	n.s. (0.0618)	-
-5.03 ±1.16 (0.0002)	0.12 ±0.03 (<0.0001)	n.s. (0.7869)	n.s. (0.3641)	-
-3.73 ±1.34 (0.0061)	0.10 ±0.03 (0.0024)	n.s. (0.8589)	-	-
-1.89 ±0.88 (0.0291)	0.05 ±0.03 (0.0490)	n.s. (0.6795)	n.s. (0.6130)	-
0.49 ±0.08 (<0.0001)	n.s. (0.2034)	-	-	-
0.40 ±0.10 (0.0004)	n.s. (0.0625)	-	-	-
-110.33 ±41.33 (0.0092)	2.55 ±0.95 (0.0091)	-	-	-

Chapter 6

General discussion and conclusions

Tom Woelders

The work presented in this thesis aimed to explore the fundamental relationship between light, our biological clocks and sleep. The availability of light in the evening hours allows us to undertake activities that were otherwise not possible in darkness, and has led many companies to switch to a 24-hour working policy. Indeed, an efficient use of time is important in our society, but so is our health. We are still biological organisms that have evolved biological time keepers in our body and physiology that are influenced by light. There is a lot to be gained if we can understand how light impacts our physiology, and if we could use the power of light to synchronise and optimise social time with our biological time. Such advances will eventually prove useful in designing mathematical models that can predict how an individual's clock or sleep will be affected by different intensities, durations and colours of light.

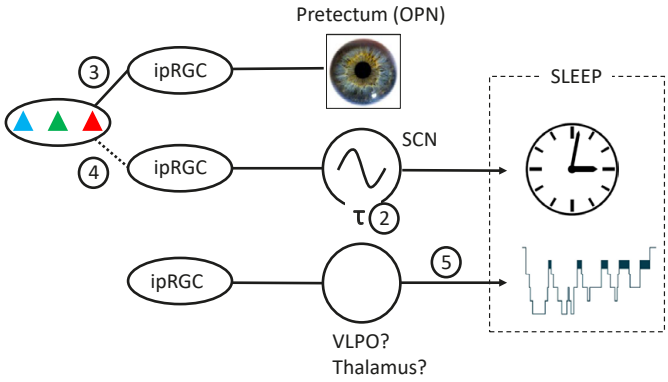

Figure 1. Graphical overview of the main results. IpRGCs relay light information to brain areas involved in nonvisual responses to light. Light exposure, via ipRGCs, causes pupil constriction (via the pretectum), indirectly modulates sleep timing (via the SCN) and might affect brain areas that are involved in sleep architecture and homeostasis (VLPO/thalamus). The coloured triangles correspond to the three cone-subtypes in the human retina. Numbers 2 to 5 indicate the main results from each chapter: 2) A method is presented that might be used to estimate the intrinsic period of the human pacemaker, using ambulatory collected light data and one clock-phase assessment. 3) IpRGCs that mediate the pupillary light response encode colour in a yellow-ON/blue-OFF and red-ON/green-OFF manner. 4) The SCN might benefit from an integration of intensity and colour information to maximize day-to-day stability in the *Zeitgeber* signal, irrespective of cloud cover. 5) Daytime light exposure may modulate sleep architecture, with higher daytime light exposure levels associated with more NREM sleep. A possible mechanism by which this effect may occur is by ipRGC projections to the VLPO and thalamus.

Such models may be of importance in 1) the treatment and diagnosis of sleep problems that are the consequence of misaligned circadian clocks, 2) predicting the effects of shift-work schedules or intercontinental traveling on the circadian system and sleep and 3) designing indoor lighting solutions tuned to obtain an ideal phase of entrainment and sufficient sleep, tailored to the needs of the individual, to name but a few examples. A quick overview of the main results presented in this thesis is presented in Figure 1.

As demonstrated in **chapter 2**, our current knowledge on the workings of the human circadian system may be sufficient in obtaining rough estimations of the intrinsic period of an individual, solely by measuring dim-light melatonin onset following a week of ambulatory collected light-exposure data. Although this method is yet to be validated in controlled laboratory conditions, the results so far are promising. As the intrinsic period of the circadian system is so difficult to measure, it is not surprising that research involving the intrinsic period of an individual's clock, especially in humans, is underrepresented in our scientific field. I hope that with the work presented in this chapter, we have introduced a novel technique in estimating the intrinsic period of an individual, to be used by scientists, clinicians or companies. Being able to estimate an individual's intrinsic period may open up an array of possible scientific and practical questions to be tackled. Can we alter the intrinsic period of an individual's circadian clock? If so, how flexible is the human clock period? What are possible factors that affect this period? Is the intrinsic period sensitive to certain changes in an individual's lifestyle? Can clinicians possibly treat sleep problems and reduce the delaying effects of evening light by shortening the intrinsic period of an individual? Does intrinsic period predict how well certain individuals will perform under a variety of shift-work schedules? Is our intrinsic period related to the severity of a jet lag after intercontinental flights? These are all valid questions that can be more easily studied when accessible tools to estimate circadian period become available. Finally, and perhaps most importantly, I want to stress the necessity of understanding how the human intrinsic period is altered by the light we expose ourselves to. From animal experiments, it is known that a short light pulse can result in long-lasting after-effects on circadian period, which has led researchers to construct τ-response curves in addition to phase-response curves for a number of species[1]. In fact, the human circadian pacemaker has also been shown to display such after-effects[2]. Humans, as well as many other species, may thus incorporate two very different (but perhaps ultimately linked) light-responses of the circadian clock that allow for entrainment to the light-dark cycle, where one is of phasic nature (as demonstrated by phase-response curves), and the other more tonic (as demonstrated by τ-response curves)[3,4]. In fact, both phasic and tonic effects may actually be the same process (light changing the velocity of the circadian pacemaker), but at different time scales. This is important, as Kronauer's model does not incorporate such tonic effects via modulations of its parameter describing intrinsic period, but only on the cycling rate of the clock during exposure to light. Perhaps incorporating human τ-responses in Kronauer's limit cycle oscillator model increases the accuracy by which this model describes how the human clock entrains to any light exposure pattern. Demonstrating long-lasting effects of any light-regime in the lab may prove difficult and costly, but until we stop ignoring this important feature of circadian pacemakers, we will never reach the point where our models reflect the true workings of any circadian system that incorporates both phasic and tonic responses to light. Hopefully such advances are more easy to achieve when tools of estimating intrinsic period become widely available, and are optimized in the process. Our proposed method may prove to provide at least a snapshot of an individual's

circadian period at one point in their lives. I hope that this method is an inspiration to the field, and that it provides our scientific field with the starting point necessary to start filling the substantial gap in our knowledge on arguably one of the most fundamental properties of how our clocks entrain to light.

Our proposed method to estimate intrinsic circadian period relies on the integrity of the mathematical model that is at the heart of this procedure: Kronauer's limit cycle oscillator model of the human circadian system[5,6]. Unfortunately, the majority of empirical data that was used to tune and optimise the model parameters, stems from a time when melanopsin was not yet discovered, and the presence of ipRGCs in the mammalian retina was unknown. The model was thus developed without specific knowledge on human retinal organisation involved in nonvisual responses to light. One of the main shortcomings of this model is therefore that light input is expressed in photopic lux. Photopic lux is based on psychophysiological experiments that rely on conscious perception of light stimuli, and is roughly speaking calculated by correcting a given light spectrum for the spectral sensitivity of our three-cone system. Light input in this model is thus tuned to the sensitivity of our visual system, but not to the sensitivity of the nonvisual function that the model aims to describe. A measure of light intensity for nonvisual functions has recently been proposed in which a given light spectrum is corrected for the spectral sensitivity of melanopsin (i.e. melanopic lux)[7]. The model may thus improve when light intensity is expressed in melanopic lux instead of photopic lux. However, as noted before, ipRGCs also receive input from cones. The most realistic metric of light intensity for nonvisual functions may therefore require an appreciation of both factors, and devices aimed to characterize light exposure for nonvisual functions should ideally incorporate at least four sensors showing the same spectral sensitivity as our three cone and melanopsin photopigments.

Before we can start thinking of modelling the effects of colour on our circadian system, the question should be answered as to whether signals from the outer retina (cones) indeed affect the output of ipRGC cells, and how. The results presented in **chapter 3** suggest they do. At least at the intensities and colours tested, it appears that increments in S-cone or M-cone signalling inhibit ipRGC output, while L-cones display an excitatory functionality. However, colour is not encoded at the level of the receptors themselves, and it is therefore necessary to evaluate these findings in the context of the bipolar and ganglion cells that relay information from the outer retina to the brain (see general introduction). There are strong indications that primate (also human) ipRGCs respond to colour in a blue-OFF/yellow-ON manner. This has been shown using the silent substitution paradigm, where S-cone or (L+M)-cone illumination was modulated selectively[8,9]. In these studies, S-cone increments dilate the pupil in humans and inhibit the ipRGC response in macacques, whereas (L+M) increments constrict the pupil in humans and increase the electrical output of the macacque ipRGC. IpRGCs in the primate retina have been shown to receive input from DB6 diffuse bipolar cells[10], which in turn receive the vast majority of their input from M- and L-cones[11]. Interestingly, S-cone OFF/(L+M)-cone ON ipRGCs show no center-surround organisation. One possible explanation

that unites all these findings is that ipRGCs receive input from blue-OFF bipolar cells (with a yellow-ON surround) and diffuse (DB6; L+M) yellow-ON bipolar cells (with a yellow-OFF surround). The yellow- OFF and yellow-ON surrounds would then cancel out, leaving only the blue-OFF and yellow-ON centers to mediate the spectrally opponent response of these ipRGC cells. If ipRGC responses would exclusively be modulated via a blue-OFF/yellow-ON circuit, M- and L-cone input would have to be relayed to ipRGCs via diffuse bipolar cells. Diffuse bipolar cells are insensitive to colour, as both center and surround are mediated by a mixture of M- and L-cones (see general introduction). Therefore, these cells should show responses of the same direction to increments in L- or M-cone activity, as both will lead to increments in the (L+M) channel. What we see, however, is a spectral opponency between L- and M-cone-mediated responses, strongly suggesting that ipRGCs receive input from red/green midget bipolar cells. Thus, these results combined with previous findings suggest that colour-coding in primate/human ipRGCs is mediated by yellow-ON/blue-OFF and red-ON/green-OFF channels, where the ON directions increase ipRGC output (Figure 2). The yellow-ON/blue-OFF channel may be mediated by S-cone OFF midget bipolar cells and (L+M)-ON diffuse bipolar cells, whereas the red-ON/green-OFF channel may be mediated by L-cone ON/M-cone OFF midget bipolar cells.

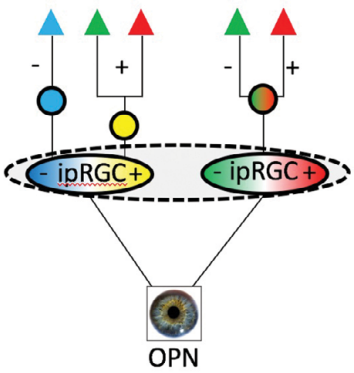

Figure 2. Hypothetical retinal wiring for colour-coding in human ipRGCs. Increasing the red:green ratio, either by decreasing M-cone or increasing L-cone stimulation, increases ipRGC output and constricts the pupil. Increasing the yellow:blue ratio by removing S-cone stimulation constricts the pupil. Adding L-cone stimulation increases ipRGC output via both pathways, which may explain the large-amplitude pupil constriction to L-cone increments. The presence of opposite-sign M-cone contributions in both pathways might explain the small pupil response to M-cone onsets, although the red-green mediated constriction to M-cone offset resulted in the largest constriction amplitude. Although presented as two separate pathways mediated by two distinct ipRGC subtypes, both pathways may in fact be integrated by assuming all bipolar cells project to the same ipRGC, as indicated by the grey shaded area.

Such interpretation of the results presented in this chapter needs to be taken with caution however, as we cannot be entirely sure that it is indeed solely the ipRGCs that mediate the pupillary light response in humans, or that other ganglion cells mediating visual colour-coding are involved as well. Certainly, literature showing a complete lack of pupillary light responses in mice after genetic ablation of ipRGCs does suggest that in the mammalian retina, ipRGCs indeed play a vital role in mediating this nonvisual response to light[12]. Of course, many more combinations of intensities and colours should be tested to understand the consistency of this type of color-coding in a variety of settings. Nevertheless, it is tempting to speculate on the functionality of this particular

colour-coding configuration from a circadian perspective. Our results suggest that switching from a long-wavelength-dominated light spectrum (L-cones) towards a short-wavelength-dominated spectrum (S- and M-cones) is encoded by our ipRGCs as a change from a bright to a relatively dark environment, as such a switch resulted in pupil dilation. From photographs of our planet taken from space, it can be appreciated that the materials present in the atmosphere let through mainly the long-wavelength photons, whereas the shorter wavelength photons are mostly scattered and reflected. Direct sunlight is thus not only brighter than sunlight that indirectly reaches our eyes, its spectrum contains relatively more power in the long-wavelength range of the visible spectrum. It could therefore be that a short-wavelength enriched spectrum is encoded as light that has already interacted with the atmosphere, as a consequence having lost much of its overall spectral power along the way. In addition, a human walking from an open field into a green forest experiences a long- to short-wavelength spectral change, which can serve as a signal to the circadian system that the decrease in light-intensity that was just experienced is the result of his or her own behaviour. The *Zeitgeber* signal driving our clocks should be minimally sensitive to such behaviour-induced noise, as any noise in the *Zeitgeber* signal is expected to consequentially result in day-to-day noise in our phase-angle of entrainment. The colour of the spectrum may thus provide our circadian system with an indication of whether or not (and to what degree) the light it was exposed to was unobstructed daylight. With this information, our circadian system may be buffered against any abrupt decrease in *Zeitgeber* strength that is accompanied by a relative increase in short-wavelength photons, for example by increasing its sensitivity to light when the spectrum deviates from that of unobstructed daylight. Practically, our retinas would then consistently be sending a signal of intensity to our circadian clocks that is as close as possible to the intensity of unobstructed daylight. Such noise-filtering properties are beneficial for any circadian clock, as intensity of unobstructed daylight is intimately related to the position of the sun, therefore being the most reliable *Zeitgeber* thinkable for life on earth. This hypothesis would suggest that short-wavelength light potentiates the sensitivity of ipRGC cells and increases their firing rate, which is not in line with our results concerning the pupillary light response where increments in the short-wavelength part of the spectrum appear to cause a decrease in ipRGC firing rate. When ipRGCs decrease their firing rate when we enter a forest, the behaviour-induced effect on our *Zeitgeber* signal would not be compensated, but instead exaggerated. Although, given its main functionality of controlling the light that enters our eyes, it makes sense for the pupil to dilate when we enter a forest, the effect should be opposite for a *Zeitgeber* signal that should be buffered against such behaviour-induced decrements in light intensity. Indeed, the spiking rate of the majority of mouse SCN cells is increased with increments in short-wavelength (UV) cone activity[13]. Similarly, human melatonin suppression is biased towards the short-wavelength part of the spectrum[14,15] indicating an excitatory role for S-cones in clock-related nonvisual responses. It is therefore unclear whether the blue/green-OFF red-ON colour-coding ipRGCs we suggest to be present in the retina project also to the SCN, or whether these cells are exclusively involved in the pupillary

light response pathway. It may be possible that ipRGC cells projecting to the SCN are of a different class that exhibit the exact opposite color-coding, namely blue/green-on and red-off, although such ipRGC cells have thus far not been located in the primate retina. In the mouse retina, a subset of M1 cells expresses the Brn3b transcription factor, which allows for a functional distinction between M1 cells that project to the SCN (which are Brn3b-negative) and M1 cells projecting to the OPN (which are Brn3b-positive)[16]. It will be interesting to see whether these subtypes of M1 cells are also present in the human retina, and whether colour-coding is different in these M1 subtypes. Alternatively, a higher-level form of colour processing may occur at the level of the hypothalamus (or even the SCN), where signals originating from a subset of ipRGCs are inverted (possibly cells that are mainly sensitive to colour and express little melanopsin). This alternative hypothesis would suggest that the hypothalamus, just like our visual cortex, comprises a network of higher-order processing of low-level input signals originating from the retina. It will be important to work out at what point in the nonvisual phototransduction cascade the clock- and pupillary light response-pathways diverge in terms of colour-coding.

Yet another mechanism by which colour-coding may affect photoentrainment is that effects of colour modulations on the pupil itself gate the amount of light entering the eye, which may indirectly affect circadian photoentrainment. However, the pupil responses we show are very small (<1 mm) compared to the range of diameters an average human pupil can achieve (~1.5 – 8 mm)[17]. A maximal constriction from 8 mm to 1.5 mm in diameter would allow for a ~30-fold decrease in pupil surface area, resulting in a 1.5 log-unit change in retinal irradiance that is maximally achievable. The small pupil responses to colour modulations can therefore in theory modulate retinal irradiance only to a minor extent. In fact, the pupil serves many more functions than solely gating retinal irradiance, such as refraction, optical aberrations and depth of focus, all affecting image quality[17]. The small pupil dilations and constrictions to short- and long-wavelength spectral changes respectively may thus be more important in retaining an optimal visual acuity under such conditions than allowing more light to enter the eye. Thus, although the pupil reponses we show here reveal retinal circuitry for colour-coding by ipRGCs that may be important for vision, these responses by themselves may not be biologically relevant for circadian photoentrainment. This makes direct spectral modulation of ipRGC cells projecting to the SCN a more parsimonious candidate for colour-effects on circadian photoentrainment than indirect effects mediated by the pupil.

What we have thus learned so far is that it is very likely that ipRGCs in the human retina exhibit a means of color-coding, and whether or not these ipRGC cells are involved in mediating the pupillary light response, melatonin suppression effects, effects on the clock, or perhaps a subset of these responses remains to be studied. To obtain more knowledge on how our circadian system incorporates irradiance and colour information, it would be interesting to construct dose-response curves, and perhaps phase-response curves, using different combinations of irradiance (melanopic lux) and colour (as encoded by our three-cone system), thus employing a similar strategy as we have chosen for revealing the nature of cone-input to the pupillary light response. What would for example two

dose response curves look like when two light sources are employed exhibiting identical melanopic lux but different relative cone excitations? Based on the hypotheses discussed in this paragraph we may expect that visually-perceived blue spectra display a half-maximal response dose at lower intensities than red spectra with an identical melanopic lux. Additionally, phase-response curves constructed using such spectra would provide us with information necessary to conclude whether effects of colour on the circadian pacemaker are modulated by circadian phase.

So far, I have speculated that colour-coding by ipRGCs may be a feature that has evolved to allow our circadian systems for buffering the *Zeitgeber* signal strength against behaviour-induced changes. There can be other functions for this colour-coding. It has been proposed that recurrent changes in the spectrum of daylight are perhaps more reliable predictors of time of day than irradiance (i.e. melanopsin-signalling) itself [8,13,18–20]. Especially at twilight transitions, the gradual shift from short- to long-wavelength dominated skies (i.e. low to high solar angles relative to the horizon respectively) is often proposed to be a more reliable *Zeitgeber* at these times of day than the intensity of daylight. Congruently, it has been proposed that cloud cover elicits a relatively large impact on the perceived irradiance of daylight, but little on the colour of daylight[20]. Our data in **chapter 4** suggest otherwise; especially at lower solar angles, it appears that not irradiance, but the colour of the sky is largely affected by different degrees of cloud cover. What we were able to show, however, is that an integration of colour and intensity information provides the most reliable indication of time of day over intensity alone. This means that even though colour in itself may not be a more stable *Zeitgeber* signal than light intensity, not even during twilight transitions, colour does contain enough unique information on solar time for our circadian system to potentially correct for the effects of cloud cover on our intensity-dependent *Zeitgeber* signal. The functional explanations of chapters 3 and 4 that I propose therefore display a substantial amount of overlap. Both hypotheses suggest that circadian colour-coding may have evolved to provide our circadian system with a means of filtering noise in the *Zeitgeber* signal. This noise may be induced by our own behaviour as a diurnal species, but also by environmental factors we have no control over such as weather conditions. It has already been established that our circadian system possesses many more noise-filtering properties, as discussed in the discussion of chapter 4, a list which I propose may be extended by adding colour-processing as an additional noise-filtering property. When we know exactly how the shape of the light spectrum influences our nonvisual responses to light, we may be able to more efficiently counter jet lag, delayed sleep phase syndrome, or a delayed sleep phase in general. This work has added to our knowledge regarding the fundamental properties of nonvisual processing of light, which may be of use in ultimately reaching such goals.

Although much of this discussion thus far concerns effects of light on our biological clocks, direct effects of light on our sleep should not be ignored as both processes are intimately linked. A recent model developed by Phillips and colleagues[21,22] effectively captures the intimate relationship between our circadian pacemaker and our sleep-wake cycle. It describes how the timing of our sleep is influenced by the light we choose

to expose ourselves to, by incorporating both homeostatic (i.e. time since waking up) and circadian (24-hour rhythmicity in wake-promoting signals, the timing of which is affected by light) influences on sleepiness, and hence the likelihood or ease with which we will (or can) fall asleep at a certain time. Our novel ambulatory polysomnography findings presented in **chapter 5** are the first to demonstrate the direct relationship between light and subsequent sleep in an ambulatory setting, combining knowledge of homeostatic and circadian regulation by light. Interestingly, our data suggest that effects of light on sleep need not be solely clock-regulated, but may be mediated by altering the homeostatic regulation of sleep. What the results in chapter 5 suggest, is that more light exposure during wakefulness increases the time spent in slow-wave sleep at the expense of time spent in REM sleep. We hypothesize this may be due to effects of light on the VLPO, which contains neurons that are essential for promoting NREM sleep[23]. It is also possible that direct effects of light on the thalamus can explain these findings, as there are strong indications that intact thalamocortical connections are required for the generation of slow waves during sleep[24]. Light may impact this circuit, with ipRGC projections to the thalamus[25]. Whatever the exact pathway, such knowledge on the impact of light on slow-wave sleep may in the future be incorporated into existing models of sleep regulation. Such advances may open up the possibility to predict not only the timing of sleep, but also more qualitative aspects of sleep such as time spent in slow-wave and REM sleep.

I see a bright future for mathematical models describing the intimate relationship between light, our circadian system and sleep, not only because I am convinced that such models will be of great importance in the treatment of sleep disorders related to a disturbed circadian rhythm, but also because such models provide a comprehensive framework that incorporates all knowledge on the human circadian system we have gathered over the course of the past century. It has been an honour to share my obtained knowledge with this scientific community, and I hope it will bring us closer to our goal of obtaining a complete understanding on how light affects our subconscious brains.

References

1. Daan, S. Colin Pittendrigh, Jürgen Aschoff, and the Natural Entrainment of Circadian Systems. *J. Biol. Rhythms* **15,** 195–207 (2000).
2. Scheer, F. A. J. L., Wright, K. P., Kronauer, R. E. & Czeisler, C. A. Plasticity of the intrinsic period of the human circadian timing system. *PLoS One* **2,** (2007).
3. Hut, R. A. Natural entrainment of circadian systems: A study in the diurnal ground squirrel, Spermophilus citellus Groningen : s.n. (2001).
4. Beersma, D. G., Daan, S. & Hut, R. A. Accuracy of circadian entrainment under fluctuating light conditions: contributions of phase and period responses. *J. Biol. Rhythms* **14,** 320–329 (1999).
5. Jewett, M. E., Forger, D. B. & Kronauer, R. E. Revised Limit Cycle Oscillator Model of Human Circadian Pacemaker. **14,** (1999).
6. Hilaire, M. A. S., Klerman, E. B., Khalsa, S. B. S., Wright, K. P., Czeisler, C. A. & Kronauer, R. E. Addition of a non-photic component to a light-based mathematical model of the human circadian pacemaker. *J. Theor. Biol.* **247,** 583–599 (2007).
7. Lucas, R. J., Peirson, S. N., Berson, D. M., Brown, T. M., Cooper, H. M., Czeisler, C. a, Figueiro, M. G., Gamlin, P. D., Lockley, S. W., O'Hagan, J. B., Price, L. L. a, Provencio, I., Skene, D. J. & Brainard, G. C. Measuring and using light in the melanopsin age. *Trends Neurosci.* **37,** 1–9 (2014).
8. Dacey, D. M., Liao, H.-W., Peterson, B. B., Robinson, F. R., Smith, V. C., Pokorny, J., Yau, K.-W. & Gamlin, P. D. Melanopsin-expressing ganglion cells in primate retina signal colour and irradiance and project to the LGN. *Nature* **433,** 749–754 (2005).
9. Spitschan, M., Jain, S., Brainard, D. H. & Aguirre, G. K. Opponent melanopsin and S-cone signals in the human pupillary light response. *Proc. Natl. Acad. Sci.* **2014,** 15568–15572 (2014).
10. Liao, H. W., Ren, X., Peterson, B. B., Marshak, D. W., Yau, K. W., Gamlin, P. D. & Dacey, D. M. Melanopsin-expressing ganglion cells on macaque and human retinas form two morphologically distinct populations. *J. Comp. Neurol.* **524,** 2845–2872 (2016).
11. Tsukamoto, Y. & Omi, N. ON Bipolar Cells in Macaque Retina: Type-Specific Synaptic Connectivity with Special Reference to OFF Counterparts. *Front. Neuroanat.* **10,** (2016).
12. Hatori, M., Hiep, L., Vollmers, C., Keding, S. R., Tanaka, N., Schmedt, C., Jegla, T. & Panda, S. Inducible Ablation of Melanopsin-Expressing Retinal Ganglion Cells Reveals Their Central Role in Non-Image Forming Visual Responses. *PLoS One* **3,** e2451 (2008).
13. Walmsley, L., Hanna, L., Mouland, J., Martial, F., West, A., Smedley, A. R., Bechtold, D. a., Webb, A. R., Lucas, R. J. & Brown, T. M. Colour As a Signal for Entraining the Mammalian Circadian Clock. *PLOS Biol.* **13,** e1002127 (2015).
14. Thapan, K., Arendt, J. & Skene, D. J. An action spectrum for melatonin suppression: evidence for a novel non-rod, non-cone photoreceptor system in humans. *J. Physiol.* **535,** 261–267 (2001).
15. Brainard, G. C., Hanifin, J. P., Greeson, J. M., Byrne, B., Glickman, G., Gerner, E. & Rollag, M. D. Action spectrum for melatonin regulation in humans: evidence for a novel circadian photoreceptor. *J. Neurosci.* **21,** 6405–6412 (2001).
16. Chen, S.-K., Badea, T. C. & Hattar, S. Photoentrainment and pupillary light reflex are mediated by distinct populations of ipRGCs. *Nature* **476,** 92–95 (2011).
17. Gamlin, P. D. R. & McDougal, D. H. Pupil. in *Ocular Periphery and Disorders* (eds. Dartt, D. A., Bex, P., D'Amore, P., Dana, R., Mcloon, L. & Niederkorn, J.) 487–493 (2011).
18. Krüll, F., Demmelmeyer, H. & Remmert, H. On the circadian rhythm of animals in high polar latitudes. *Naturwissenschaften* **72,** 197–203 (1985).
19. Roenneberg, T. & Foster, R. G. Invited Review Twilight Times: Light and the Circadian System. *Photochem. Photobiol.* **66,** 549–561 (1997).
20. Brown, T. M. Using light to tell the time of day: sensory coding in the mammalian circadian visual network. *J. Exp. Biol.* **219,** 1779–1792 (2016).

21. Phillips, A. J. K., Chen, P. Y. & Robinson, P. A. Probing the mechanisms of chronotype using quantitative modeling. *J. Biol. Rhythms* **25,** 217–227 (2010).
22. Skeldon, A. C., Phillips, A. J. K. & Dijk, D.-J. The effects of self-selected light-dark cycles and social constraints on human sleep and circadian timing: a modeling approach. *Sci. Rep*. **7,** 45158 (2017).
23. Scammell, T. E., Arrigoni, E. & Lipton, J. O. Neural Circuitry of Wakefulness and Sleep. *Neuron* **93,** 747–765 (2017).
24. Crunelli, V., David, F., Lorincz, M. L. & Hughes, S. W. The thalamocortical network as a single slow wave-generating unit. *Curr. Opin. Neurobiol.* **31,** 72–80 (2015).
25. Hattar, S., Kumar, M., Park, A. & Tong, P. Central Projections of Melanopsin-Expressing Retinal Ganglion Cells in the Mouse. **497,** 326–349 (2006).

Samenvatting

Het onderzoek dat is gepresenteerd in dit proefschrift heeft geleid tot een aantal nieuwe bevindingen, welke nu kort zullen worden samengevat.

In **hoofdstuk 2** wordt een nieuwe methode beschreven om de intrinsieke periode van de menselijke biologische klok te kunnen voorspellen aan de hand van lichtblootstelling-data verzameld gedurende een week, onder ambulante omstandigheden, gevolgd door een klokfase-meting in het lab. Dit soort methodes zijn cruciaal voor ons begrip met betrekking tot circadiane ritmiek op individueel niveau. Dit soort ontwikkelingen zouden belangrijk kunnen zijn bij individuele chronotherapie en zouden bijvoorbeeld gebruikt kunnen worden om te voorspellen hoe het circadiane ritme van een individu reageert op verschillende dagelijkse lichtblootstellingspatronen.

De analyses in **hoofdstuk 3** suggereren dat menselijk ipRGCs die de pupilrespons regelen (en waarschijnlijk de circadiane klok) kleurgevoelig zijn. Deze ipRGCs lijken te reageren op kleurveranderingen op zowel een rood-groen en geel-blauw as, op een rood-AAN/groen-UIT en geel-AAN/blauw-UIT manier. Afhankelijk van de toepassing, is het n zeker mate van belang om controle te kunnen uitoefenen over de grootte van klokverschuivingen veroorzaakt door een gegeven lichtspectrum. Wanneer we de effecten van jetlag willen verkleinen, is het wenselijk om de klok snel te kunnen verschuiven om ons gewenste gedrag snel overeen te kunnen laten komen met de nieuwe dag/nacht cyclus na een intercontinentale vlucht. Voor dagelijks gebruik van led schermen en andere soorten kunstlicht, is het daarentegen juist van belang dat onze biologische klok minimaal wordt beïnvloed om het dagelijks heen en weer schuiven van de biologische klok te voorkomen. Onze data suggereren dat naast het veranderen van de lichtintensiteit, kleurveranderingen een extra vrijheidsgraad toe kunnen voegen om dit soort doelen efficiënt te kunnen bewerkstelligen.

Nu het duidelijk begint te worden dat menselijke ipRGCs gevoelig zijn voor kleur, wordt het steeds belangrijker om te weten te komen waarom onze biologische klok gevoelig is voor kleur, en waarom dit evolutionair gezien voordelig is voor de mens. Hier zijn allereerst testbare hypotheses voor nodig, waarvan wij er een voorstellen in **hoofdstuk 4**. Dit werk laat zien dat lichtintensiteit en kleur samen meer informatie bevatten over de tijd van de dag dan intensiteit of kleur alleen. Een combinatie van beide factoren is dan ook de meest stabiele tijdsindicatie die onze biologische klok uit zonlicht kan halen. Dit zou de reden kunnen zijn dat ook de menselijke biologische klok beide daglicht componenten integreert.

In **hoofdstuk 5** laten we zien dat de intensiteit van daglicht blootstelling niet alleen de timing van slaap beïnvloedt, maar ook de opbouw en kwaliteit van slaap. Dit soort bevindingen zijn belangrijk, en zouden uiteindelijk geïntegreerd kunnen worden in bestaande slaapmodellen, om niet alleen de timing maar ook meer kwalitatieve aspecten van slaap te kunnen voorspellen.

Acknowledgements

“Dag Tom,

Ik sprak net Johan en ik vertelde dat je was aangenomen in Groningen en dat je nog twijfelt over Manchester. Ja zei hij toen, anders kan hij toch hier beginnen en als hij het niet leuk vindt over een half jaar gewoon weggaan? Ik vertelde hem dat dat niet slim is bij een Phd, dat moet je afmaken anders is je CV bijzonder slecht geworden(toch?) Nou zei hij toen, als die professor in Manchester een beroemdheid is en je CV wordt subliem als je daar promoveert, tja, dat is wel mooi natuurlijk. Nou zei ik, een beroemdheid is het niet, alleen Tom vindt het onderzoek wat ze daar doen erg leuk en een buitenlandervaring moet hij toch een keer opdoen. Toen vertelde ik hem over de situatie in Groningen. De twee begeleiders hebben jou een 9 gegeven voor je afstudeeropdracht. Je stond unaniem met stip bovenaan in de sollicitatieprocedure. Je mag van het pad afwijken eventueel omdat ze je ideeën zo creatief vinden. Ze zien je helemaal zitten en wat niet geheel onbelangrijk is, jij kunt goed met hen overweg en twijfelt er niet aan dat je onderzoek daar zal gaan lukken. Bovendien mag je vandaag nog beginnen als je wilt en in Manchester moet je wachten tot oktober. Daarop volgde Johan zijn befaamde schaterende vette lach en hij zei dat het dan wel duidelijk is wat je moet doen. Daar dacht ik niet meer over na zei hij, meteen beginnen. Nou zit Johan natuurlijk niet in de wetenschappelijke wereld, maar een nuchtere kijk heeft hij wel. Ik vind dat hij gelijk heeft. Natuurlijk snap ik dat jij je ook nog wel vereerd voelt dat wildvreemde professoren jouw onderzoeksvoorstel heel goed vinden en je misschien een Phd aanbieden, maar je kunt het ook zo zien Tom. Jij bent vet goed, dat hebben ze je in Groningen ook al verteld. Je komt er wel. Zorg dat je een prima promotie doet hier en ga dan weer de markt op. Tegen die tijd weet Roos misschien ook beter welke kant ze op wil en gaan jullie echt weg samen. Ik wilde je niet meteen een advies geven vorige week, omdat ik echt niet weet wat beter is. Maar nu ik langer heb nagedacht, is dit wat ik ervan denk.

Kus mama”

M.G. Woelders-Eman (18-01-2012)

Lieve **Mama**, dit mailtje stuurde je me toen ik de keuze moest maken tussen een PhD doen in Manchester of in Groningen. Ook al had je achteraf in alles gelijk, ik moest er destijds niets van weten, want ik wilde zelf de keuze maken, eigenwijs als ik ben. Ook al heb ik het idee dat ik dat uiteindelijk ook gedaan heb, weet ik tegelijkertijd dat alle keuzes die ik in mijn leven heb gemaakt en zal maken gekleurd zijn en zullen worden door jou. Want je bent Mama, en daarom ben je bij me, nu en voor altijd. Ik zal het nu zonder je (ongevraagde) adviezen moeten doen, al weet ik zeker dat je me dit keer niet zou afraden om naar Manchester te gaan. Mama, ik hou van je en ik mis je; ik zou er de wereld voor over hebben om nu je lachende gezicht en trotse twinkelende oogjes te kunnen zien, ook al zie ik ze nog steeds. Dankjewel voor alles wat je me gegeven hebt. Kus en knuffel, je aller knapste zoon.

After my mom, there is only one person who truly deserves to receive my very first words of gratitude, namely my favourite person in the world. **Roos**, bb lievelings, I cannot describe within a few sentences how much you have helped me to be where and who I am now. The challenges of living with someone who is pursuing a career in academia are significant ($p < 0.05$), especially when that person is a workaholic, extremely late (occasionally free-running) daydreaming scientist and you yourself could not care less about science in general. Yet, we have discovered a common ground that cannot be captured by words, which makes us an awesome couple with a beautiful relationship that we are genuinely proud of. Thank you for your life lessons and (non-science related) discussions and for all your understanding, honesty, patience, support, advice, comfort, beautiful evenings of listening to music, fights, make ups, tears, laughs, sharing disappointments, celebrations, hugs and kisses. Thank you for always being there for us and for me, in both the good and the bad times.

Papa, **Lineke** and **Jan**. When I overthink my years as a PhD student, beautiful memories are mixed with not so good ones. You are the only people, together with Roos, who share the most difficult memories with me (and also some beautiful ones of course!), and that makes me feel not so alone. Being family, you guys are the most important persons in my life, and you have helped me through tough times during my PhD, just by being there. Thank you for that. On a less dramatic note, I am looking forward to the next sushi binge eating fest to celebrate joyful things, starting with me having finished this thesis!

Then I want to thank all of my (ex-)colleagues, especially **Domien, Marijke, Roelof, Emma, Serge, Menno, Martha, Peter, Robbert, Maan, Igor, Jasper, Margien, Maria, Kees, Vincent, Kim, Thomas, Moniek, Sjaak, Renske, Giulia, Theresa, Lauren, Laura, Sjoerd, Pleunie, Maria, Wanda, Bonnie** and **Gerard.** First I want to thank the chronos in general, for being such a respectful, intellectual, kind and social group, where everyone is always happy to help one another, where you can speak your mind and where independence, creativity and cooperation are encouraged. Thank you for everything, it has been a pleasure working with you! Then, a number of important people in particular, starting of course with my diverse and complementary

team of supervisors. **Domien**, you are the reason I loved chronobiology from the start (finally having a scientific excuse for being late all the time had nothing to do with it, I promise). There I was, starting with the "Timing of Behaviour" course you organised, ignorant about even the existence of something like a biological clock. Your teaching has played a major part in motivating me to pursue a PhD in chronobiology, and it has been of invaluable use during that PhD. You were also the perfect mentor for me; I very much admired the patient and respectful way in which you let your students be absolutely free to discover their own interests and strengths. Thank you for being such a responsive professor, I enjoyed our discussions a lot! **Marijke,** thank you for further introducing me into the topic of human chronobiology by supervising my second Master's thesis and later also my PhD. You have always been a very involved supervisor and it was you, together with Domien, who provided me the opportunity to develop myself as a scientist. I cannot thank you enough for not only that, but also for the high level of mentoring I received from you, it was a pleasure! **Emma**, I had the luxury of having you as my private day-to-day supervisor. You always had time to discuss ideas, to design experiments, to help out with the practical work, to drink beers and to have my back at all times (including conferences where you forced me to talk with a lot of scary people!). It has been a pleasure working with you, I really think you contributed greatly to the quality of this work. Finally, **Roelof**, who has by now become more of a friend than a boss. Who would have thought that putting together our two personalities would lead to such a healthy mix of creativity, originality, fun, (relative) organization and (if I may do say so myself) quality. It has truly been an honour; I hope you enjoyed working with me as much as I did working with you. I loved our weekly Thursday 11 o'clock meetings, but I loved the spontaneous meetings even more;) Then, my closest PhD buddies! **Moniek**, my favourite drinking and conference partner in crime! You are by far the most sociable person I have ever met; you truly are an amazing person. Thank you for all the social time and for being my RIA guru! Sorry that I made fun of your gullibility at times, but those "Moniekjes" made my day every time ;) **Sjaak**, thanks for the football-related evenings and for being such a good scientific sparring partner; you may not realize but I have learned so much from you by just picking your brain at times. Both of you, I am honoured that you are my paranimphs! **Giulia** and **Renske**, thank you for the social drinks at unconventional times. Also, thanks for not disregarding my *R* advice; your graphs and random effects models look awesome! Subset for life;) **Theresa**, social time with you was always interesting and fun! Never change, stay honest.

Kenny, thank you so much for the famous "chill avondjes". How good it was to alternate PhD stress with hours of Mario Kart, playing chess, binge watching series and cycling towards beautiful views. Those moments were really something for me to look forward to every time. We figured out how to chill in the most efficient way possible and I consider myself truly lucky for having such a very special friend. **Yoeri, Nico, Stefan** and **Steven**, my dear friends, thank you for the welcome talking-, beer- (and tea, Steven), music- and gaming-related distractions! Being around you guys has always been a lot of

fun! **Paul (8), Sanne, Koen, Wytske, Daan, Frederike** and **Paul (26)**, my brothers and sisters from the 4th floor! When I moved to Groningen I got you guys for free. It was the best trade deal in the history of trade deals, maybe ever. I love it that we transitioned from a group of house mates into a group of friends who still meet on a regular basis after all those years. Being around you guys still feels like being home to me. For all of you, I hope our friendship will continue for a very long time, and that it will provide us with many more good and memorable moments!

Then, my students: **Rick, Timo, Karl, Jacqueline** and **Thomas.** Being your Master's thesis supervisor has truly been a lot of fun. Thank you for all your help in collecting some beautiful data, and for producing such high-quality reports which were the best compliments a supervisor can get. I hope you learned as much from our cooperation as I did!

I finally want to thank the **boys and girls who participated in my experiments**. Thank you so much for your willingness to cooperate in the experiments. Your professional attitude played a crucial role in maximizing the quality of the data presented in this thesis.

Curriculum Vitae

Tom Woelders was born on the 3rd of May 1986 in Enschede, the Netherlands. He obtained his Bachelor's degree in psychology in 2009, and successfully obtained his behavioural and cognitive neuroscience Master's degree in 2011, both at the University of Groningen, the Netherlands. During his Master's programme, he was first introduced to the field of chronobiology by Prof. Domien Beersma and instantly became passionate about this rich scientific field because of its many biological layers and societal importance. In 2012 he started his PhD under the supervision of Prof. Domien Beersma and Dr. Marijke Gordijn (later succeeded by Prof. Roelof Hut and Dr. Emma Wams). His PhD work involved the nonvisual effects of light (and the importance of melanopsin-expressing retinal ganglion cells in nonvisual effects of light) including sleep, photoentrainment and pupil constriction. For his PhD work, Tom won several awards, including two poster prizes (SCNi chronobiology summer school in Oxford, UK, 2014 and the Society for Research on Biological Rhythms meeting in Florida, US, 2018) and the J Chris Gillin young investigator award of the Society for Light Treatment and Biological Rhythms in Berlin, Germany, 2017). While finishing his PhD, he worked as a research associate in the lab of Prof. Roelof Hut in Groningen for two years during which he, together with Renske Lok, designed and performed the first bright light human forced-desynchrony study to explore clock-gated effects of light on a wide array of (psycho)physiological parameters, including sleep, alertness and metabolism. Tom will continue to apply his obtained knowledge on melanopsin-expressing retinal ganglion cells in a novel context to explore their contribution to visual perception, as a research associate in the lab of Prof. Robert Lucas in Manchester, UK.

Publications

Peer-reviewed

Woelders, T., Leenheers, T., Gordijn, M. C. M., Hut, R. A., Beersma, D. G. M., & Wams, E. J. (2018). Melanopsin- and L-cone–induced pupil constriction is inhibited by S- and M-cones in humans. Proc. Natl. Acad. Sci., 115(9).

Wams, E. J., Woelders, T., Marring, I., Van Rosmalen, L., Beersma, D. G. M., Gordijn, M. C. M., & Hut, R. A. (2017). Linking light exposure and subsequent sleep: A field polysomnography study in humans. Sleep, 40(12).

Woelders, T., Beersma, D. G. M., Gordijn, M. C. M., Hut, R. A., & Wams, E. J. (2017). Daily Light Exposure Patterns Reveal Phase and Period of the Human Circadian Clock. J. Biol. Rhythms, 32(3), 274–286.

Lok, R., Woelders, T., Gordijn, M.C.M., Hut, R.A. & Beersma, D.G.M. (2018). White light during daytime does not improve alertness in well-rested individuals. J. Biol. Rhythms [Epub ahead of print].

Woelders, T., Wams, E.J., Gordijn, M.C.M., Beersma, D.G.M. & Hut, R.A. (2018). Integration of color and intensity increases time signal stability for the human circadian system when sunlight is obscured by clouds. Sci. Rep. 8, 15214.

Submitted

Spitschan, M. & Woelders, T. The method of silent substitution for examining melanopsin contributions to pupil control

In preparation

Lok, R., Woelders, T., Gordijn, M.C.M., Hut, R.A. & Beersma, D.G.M. A bright light forced-desynchrony study: effects of light on alertness

Woelders, T., Lok, R., Gordijn, M.C.M., Hut, R.A. & Beersma, D.G.M. A bright light forced-desynchrony study: effects of light on sleep architecture